ADDIS ABABA UNIVERSITY
COLLEGE OF NATURAL SCIENCES
SCHOOL OF EARTH SCIENCES

GEOLOGCAL AND GEOMORHOLOGICAL CHARACTERIZATION OF THE DENDI CALDERA, WEST CENTRAL ETHIOPIA: IMPLICATIONS FOR PALEO-ENVIRONMENTAL RECONSTRUCTION USING LAKE SEDIMENT CORES

A THESIS SUBMITTED TO THE SCHOOL OF GRADUATE STUDIES OF ADDIS ABABA UNIVERSITY IN PARTIAL FULFILLMENT OF THE REQUIREMENTS FOR THE DEGREE OF MASTER OF SCIENCE IN EARTH SCIENCES (PETROLOGY).

BAHRU ZINAYE

Addis Ababa. May 2014

GEOLOGCAL AND GEOMORHOLOGICAL CHARACTERIZATION OF THE DENDI CALDERA, WEST CENTRAL ETHIOPIA: IMPLICATIONS FOR PALEO-ENVIRONMENTAL RECONSTRUCTION USING LAKE SEDIMENT CORES

A THESIS SUBMITTED TO THE SCHOOL OF GRADUATE STUDIES OF ADDIS ABABA UNIVERSITY IN PARTIAL FULFILLMENT OF THE REQUIREMENTS FOR THE DEGREE OF MASTER OF SCIENCE IN EARTH SCIENCES (PETROLOGY).

BY: BAHRU ZINAYE

MAY 2014

ADVISOR: ASFAWOSSEN ASRAT (PHD)

ADDIS ABABA UNIVERSITY
COLLEGE OF NATURAL SCIENCES
SCHOOL OF EARTH SCIENCES

GEOLOGCAL AND GEOMORHOLOGICAL CHARACTERIZATION OF THE DENDI CALDERA, WEST CENTRAL ETHIOPIA: IMPLICATIONS FOR PALEO-ENVIRONMENTAL RECONSTRUCTION USING LAKE SEDIMENT CORES

By: **BAHRU ZINAYE**

College of Natural Sciences
School of Earth Sciences
Petrology stream

Approved by board of Examiners

Dr. Balemwal Atnafu _____

(Chairman)

Dr. Asfawossen Asrat _____

(Advisor)

Dr. Dereje Ayalew _____

(Examiner)

Prof. Gezahegn Yirgu _____

(Examiner)

ACKNOWLEDGEMENT

Above all I am honored when I thank and glorify the Almighty God, the creator of Earth and Heaven, who helped me throughout my life and the ultimate means of my success.

My special thanks go to my supervisor, Dr. Asfawossen Asrat for his sound-full guidance, constructive criticism, constant encouragements and reviewing the thesis and providing useful comments since the beginning and throughout the research.

I am thankful to Addis Ababa University, Madawalabu University and Geological Survey of Ethiopia, for the assistance I have received during my studies and/or research of the Master's Program. I am also thankful to the Ginchi Woreda and Boda kebele of Oromiya Riginal State and the friendly people who live in the Dendi caldera.

I am highly indebted to the CRC project, especially Prof. Dr. Frank Schaebitz, for hosting me in the University Of Cologne for the analysis of the sediment core and cover my expenses during my thesis work. I appreciate the help of Tsige Kassa, Jonathan Heinze, and Nicole Mantke during my stay in the University. I am also thankful to the Aachen University (Prof. Dr. Frank Lehmkhul) for the XRF analysis on the rock samples. I thank all those who accompany me during my field work especially Dr. Ralf Vogelsang, Dr. Tamrat Endale, Meklit Yadeta and Zenebe Yirgalem.

At last, I would like to express my deepest gratitude to all my family, my mother (Meseret Seifu), my brothers and sisters (Kaleb Hintsaye, Kidus Hintsaye, Wude Aredo, Tigist Zinaye, Gosaye Mokonnen, Rahel Worku and Lewi Basazinew) and my Aunts (Mekdes Seifu and Yeshimebet Worku). Without you, I am not who I am. And many thanks are also for all other family and friends who constantly encouraged, helped and sustained me in prayer for my success. I love you all.

Table of Contents

List of Figures

Page

List of Tables & Annexes

Pages

List of Acronyms

a.s.l ➔ Above Sea Level

AFC ➔ Assimilation Fractional Crystallization

ANS ➔ Arabian Nubian Shield

CRC ➔ Collaborative Research Centre

FC ➔ Fractional Crystallization

ITCZ ➔ Intertropical Convergence Zone

MB ➔ Mozambique Belt

MER ➔ Main Ethiopian Rift

MORB ➔ Mid-Oceanic Ridge Basalt

MS ➔ Magnetic Susceptibility

PM ➔ Partial Melting

PPL ➔ Plane Polarized Light

SSTA ➔ Sea Surface Temperature Anomalies

XPL ➔ Crossed Polarized Light

XRF ➔ X-Ray Fluorescence

ABSTRACT

The Dendi Caldera is located on the West Central Ethiopian Plateau, approximately 120 kilometers to West of Addis Ababa. It is located between $08^0 48^1 00^{11}$ - $08^0 52^1 00^{11}$ North latitude and $37^0 58^1 00^{11}$ - $38^0 04^1 00^{11}$ East longitude in Dendi kebele, Ginchi woreda, western showa zone, Oromiya regional state of Ethiopia. The caldera has almost elliptical shape with about 8.5 km diameter in its longest direction and 6.5 km in the shortest direction. There are two crater lakes making the shape of '8' within this caldera, each with a circumference and an area of about 7.5 km and 4 sq. km respectively. The altitude varies between 2830m - 3270 m a.s.l..

The main objective of this research work is to study the geology, geochemistry and petrology of the Dendi caldera rocks, to construct the geological evolution of the caldera and to study the effect of the geology on the composition of the lake sediments in order to help reconstruct the paleoclimate using lake sediment core.

The methods involved to achieve the objectives are desk studies about the area, fieldwork for mapping and sampling, petrographic studies, XRF analysis both on the lake sediment and rock samples, analysis and interpretation of data using different computer softwares.

The caldera comprises different felsic volcanic products including trachyte, rhyolite and obsidian overlain by the pyroclastic deposits ignimbrite, volcanic surge and tuff. The rhyolite and trachyte are formed both as lava flow and lava dome. In some areas they show columnar joints. The surge deposit shows sedimentary structures like bedding and X-bedding. In thin section, the rhyolite, trachyte and ignimbrite has aphanitic and porpyritic aphanitic textures with alkali feldspar phenocrysts. The Trachyte also shows trachytic texture.

On TAS diagram, the lavas are rhyolitic and trachytes/trachydacite and the pyroclastics are trachyandesite and basaltic andesite. In the spider diagrams (MORB normalized), Ba, Sr, P, Ti and Cr shows strong negative anomaly which verifies fractionation. The lava shows high Th and Nb with very low Sr. Rb/Nb and La/Nb ratios are very low while Rb/Sr ratio is very high in the Dendi volcanic products. These conditions show the only possible mechanism for the formation of the Dendi caldera is fractional crystallization of basaltic magma with limited or no crustal contamination.

Five different sections have been identified based on the variation of different chemical and physical parameters applied on the lake sediment core. Section 4, with high grain size, MS, K, Si/Ti and Mn and low inc/coh, Sr/Ca, Zr/Rb and Rb/K, shows the driest period in the stratigraphy while section 2 shows the most humid period in the stratigraphy. The remaining sections spans between these two extremes.

Key words: Dendi, Caldera, volcanic, felsic, fractional crystallization, paleoclimate

CHAPTER ONE
1. INTRODUCTION

1.1. Background of the study

This research project is conducted in the Dendi caldera with the aim of characterizing the rocks that constitute the caldera and to reconstruct the geological evolution of this caldera. Moreover, a geomorphological assessment of the catchment has been conducted in order to characterize the sediment input to the Dendi Lake. The contribution of the geological and geomorphological setting of the caldera on the type and rate of sediment input to the Dendi Lake is also studied on a sediment core collected from Dendi Lake under the CRC project, which aims at reconstructing the paleoclimatic and paleoenvirnmental history of the area.

The Dendi Caldera is located on the Ethiopian Plateau, approximately 120 kilometers to the west of Addis Ababa. A caldera is a geological feature formed by the near-total eruption of magma from beneath a volcano, leading to collapse of the volcanic structure into the now-empty magma chamber. This collapse typically leaves a crater or depression where the volcano stood, and later volcanic activity can fill the caldera with younger lavas, ash, pyroclastic rocks and sediments. A crater lake can be formed, if the caldera is later filled with water.

The Dendi caldera and the surrounding areas were studied before under regional level and the map produced was at small scale. The previous studies were not detailed and lack lots of information about the caldera. There have not been any detailed geological works conducted in the Dendi caldera. The area was only mapped as part of the Ethiopian plateau volcanic and regionally mapped in small scale with the surrounding areas.

The current study aims at investigating the Dendi caldera and surrounding in order to characterize the geological and geomorphologic evolution of the caldera and to characterize the sediment input into the crater lakes within the caldera, in order to help in interpretation of the paleoenvironmental and paleoclimatic records in the sediment cores recovered from the lakes.

Geochemistry of lake deposits

Geochemical data from lake sediments is one major archive of paleoenvironmental changes. Climate variations are one of the factors that influence the sedimentation processes in lakes. Geochemical data provides information about the source region of clastic material and about in

situ deposition within the water column. Changes in the geochemistry along sediment records can be read in terms of variations in local climate pattern. For the interpretation of geochemical data it is more advantageous to use element ratios instead of the distribution of single elements (Weltje & Tjallingii 2008). Furthermore, the accuracy of the gathered data increases with a good understanding of the pre-depositional and diagenetic processes that affect the sedimentation. Lake sediments are generally composed of a limited number of elements representing the chemical composition of the earth crust. The abundance or limited amount of these elements, other trace elements and ratios among some of these elements are used to tell about the paleoclimate of an area. Also the grain size variation of the sediments and changes in the magnetic susceptibility of the sediments are useful indicators of paleoclimatic changes.

The geochemistry of the lake sediment is highly dependent on the geology of the Caldera. All sediment inputs to the lake have to come from the caldera because the catchment of the Dendi lake is restricted to the highest pick of the caldera. The minerals that constitute the caldera determine which element has higher/lower concentration in the lake sediment. For example, we do not expect high concentration of Mg/Fe in the Dendi caldera where the caldera is predominantly constituted by felsic volcanic rocks. The high altitude contrast (steep slope) of the area gives advantage to the increase in the sedimentation rate. But both the sedimentation rate and geochemistry of the lake sediments are somehow dependent on the climate of the area. For e.g. during arid environment, where the situation is dry and there is little or no water, the sedimentation rate is very low and weathering of minerals decrease due to lack of the main agent of weathering i.e. water. During humid conditions, in contrast, the rate of sedimentation is very high plus we will have high amount accumulation of sediments.

1.2. General and specific objectives

1.2.1. General Objective

The general objective of this project is to study the geology, geochemistry and petrology of the Dendi caldera rocks, to construct the geological evolution of the caldera and to study the effect of the geology on the composition of the lake sediments in order to help reconstruct the paleoclimate using lake sediment core.

1.2.2. Specific Objectives

The specific objectives of this thesis work are:

- To produce the geological map and geologic cross-section of the Dendi Caldera
- To characterize the petrology and geochemistry of the rocks constituting the caldera
- To reconstruct the stratigraphy of the area
- To reconstruct the petrogenesis and geologic evolution of the caldera
- To study the effect of the geology of the area on the composition of the Dendi lake sediments in order to help interpret their paleoclimatic records.
- To compile and characterize the modern climate and hydrologic setting of the Dendi catchment.

1.3. Location and access

The project area is the Dendi caldera, which is found in the Ethiopian plateau, located along the road from Addis Ababa – Ginchi – Boda - Dendi at a distance of approximately 120km West of Addis Ababa. The Dendi caldera is located between $08^{0}48^{1}00^{11}$ - $08^{0}52^{1}00^{11}$ North latitude and $37^{0}58^{1}00^{11}$ - $38^{0}04^{1}00^{11}$ East longitude in Dendi kebele, Ginchi woreda, western showa zone, Oromiya regional state of Ethiopia. It falls in the eastern margin of Agere Hiywet sheet and the western margin of Boda sheet of the Ethiopian Mapping agency topo sheet. The nearest town is Boda about 11 km away from the caldera. The caldera has almost elliptical shape with about 8.5 km diameter in its longest direction and 6.5 km in the shortest direction. There are two crater lakes making the shape of '8' each with a circumference and an area of about 7.5 km and 4 sq. km respectively within this caldera.

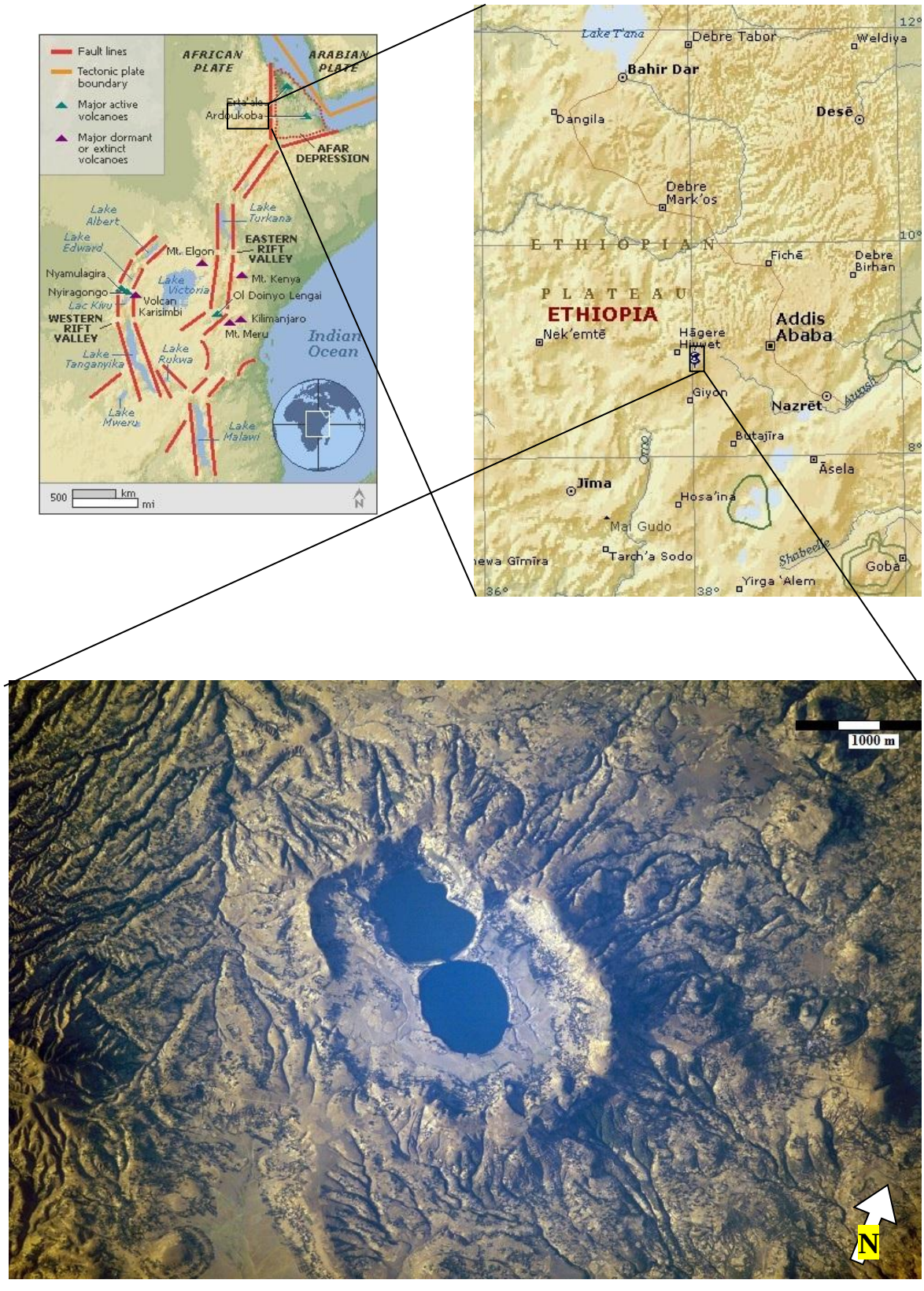

Fig. 1.1: Location map

1.4. Physiography and drainage

Physiographically, the Dendi caldera is found partly in the Central Lava Highlands and Massifs within the Western Highland Plateaus. The study area is featured by varied topography ranging from plain lands and steep slope areas to vertical cliffs. The area is situated in a topographically elevated area with the lowest point, at the lake level, is 2830m a.s.l., while the highest point, at the top of the mountain in the North East side of the caldera, is 3270 m a.s.l..

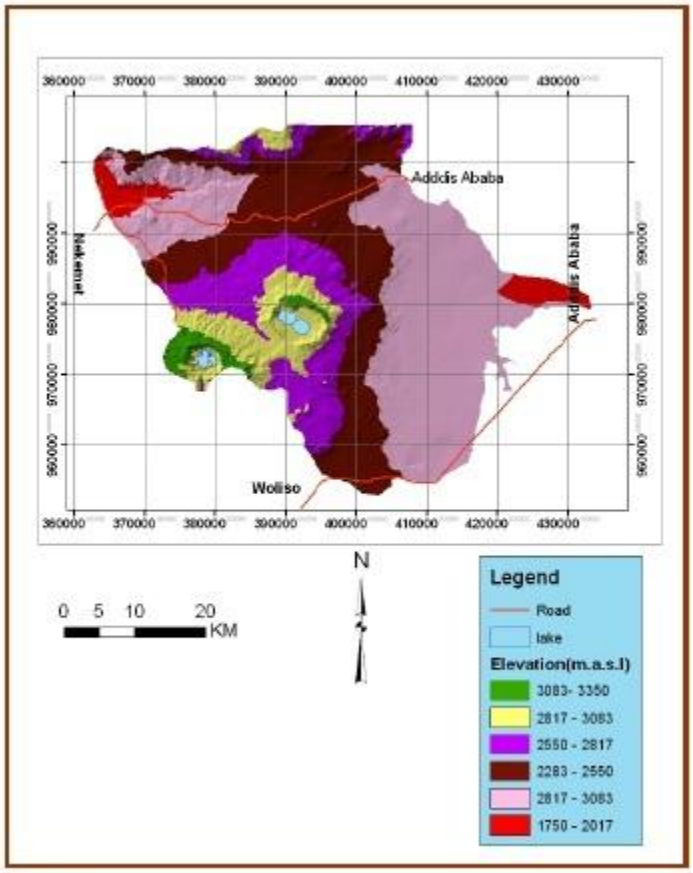

Fig. 1.2: Relief Setting of Dendi and the surrounding area (after Abenezer Kefeni, 2007)

There are many springs located mostly in the steep slope areas and flows as streams towards the lake with the exception of tributaries of Huluka River which flows away from the caldera and join the Blue Nile (Abay) basin. Some of the streams flow throughout the year while the others flow only during rainy seasons.

The geomorphology of the area can be grouped into four geomorphic units: The flat lands at the top of the mountains, the vertical cliffs, the steep slope areas, the gentle slope areas and the flat

land surrounding the lake. A brief description of each unit is given in the unit which describes the geomorphology of the area.

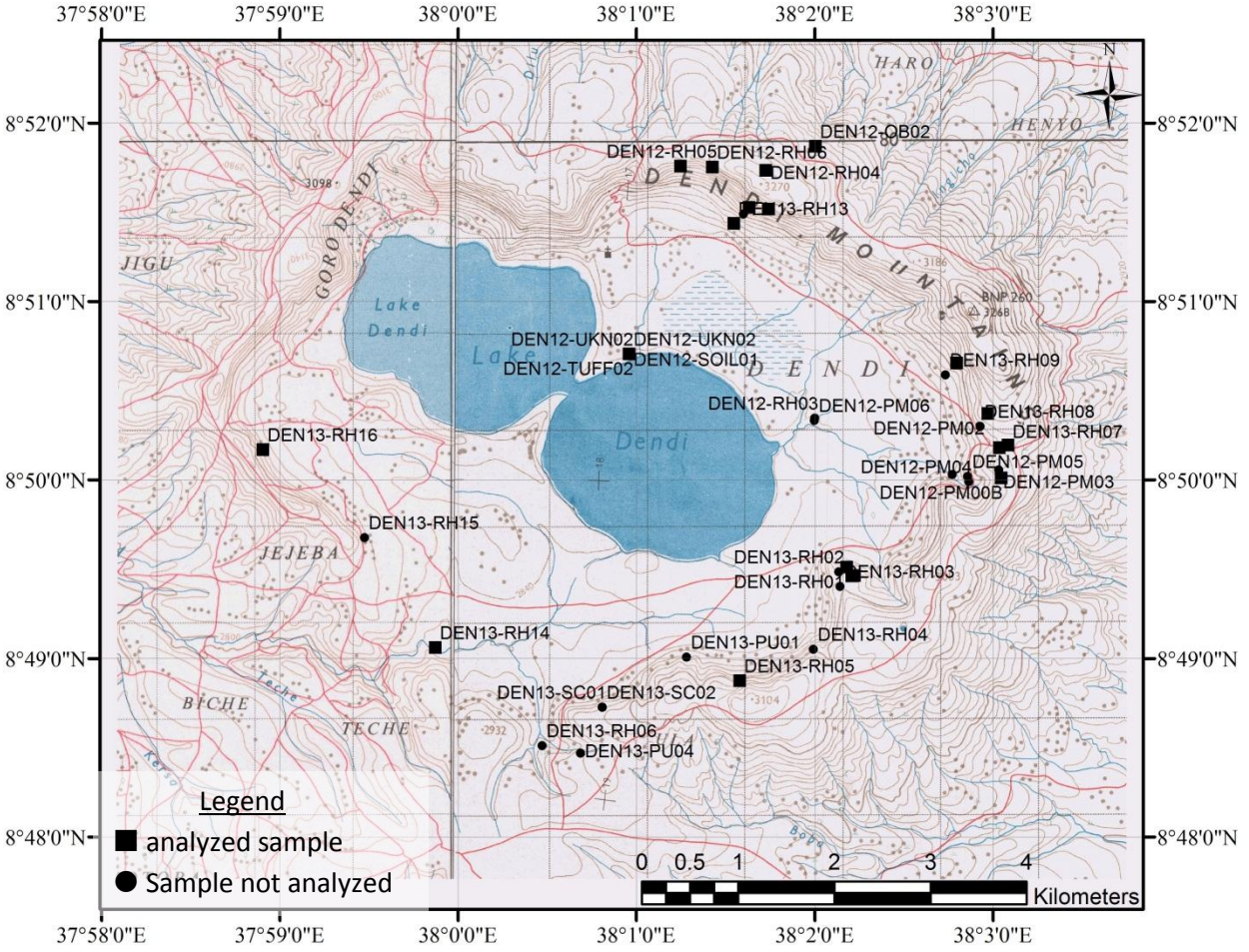

Fig 1.3: Topographic map of the study area with collected samples.

1.5. Climate

Ethiopia has complex topography, with altitudes ranging from hundreds of meters below sea level in the northeast (Afar depression) to over 4000 m above sea level in the northern highlands. As a result of its latitude and altitude variation, Ethiopian rainfall exhibits high variability both spatially and temporally (Degefu, 1987; Bekele, 1997). Three main rainfall regimes are commonly identified as shown in Figure 1.4 (Diro et al. 2009). Regime A in the western part of the country has a monomodal rainfall pattern (February to November). Regime B (comprising central and eastern parts) has two consecutive rainy periods: Belg (February to May) followed by Kiremt (June to September) with the dry season Bega (October to January). Regime C in the

south and southeast has two distinct rainy periods which are separated by two dry periods: March to May (long) and October to November (short).

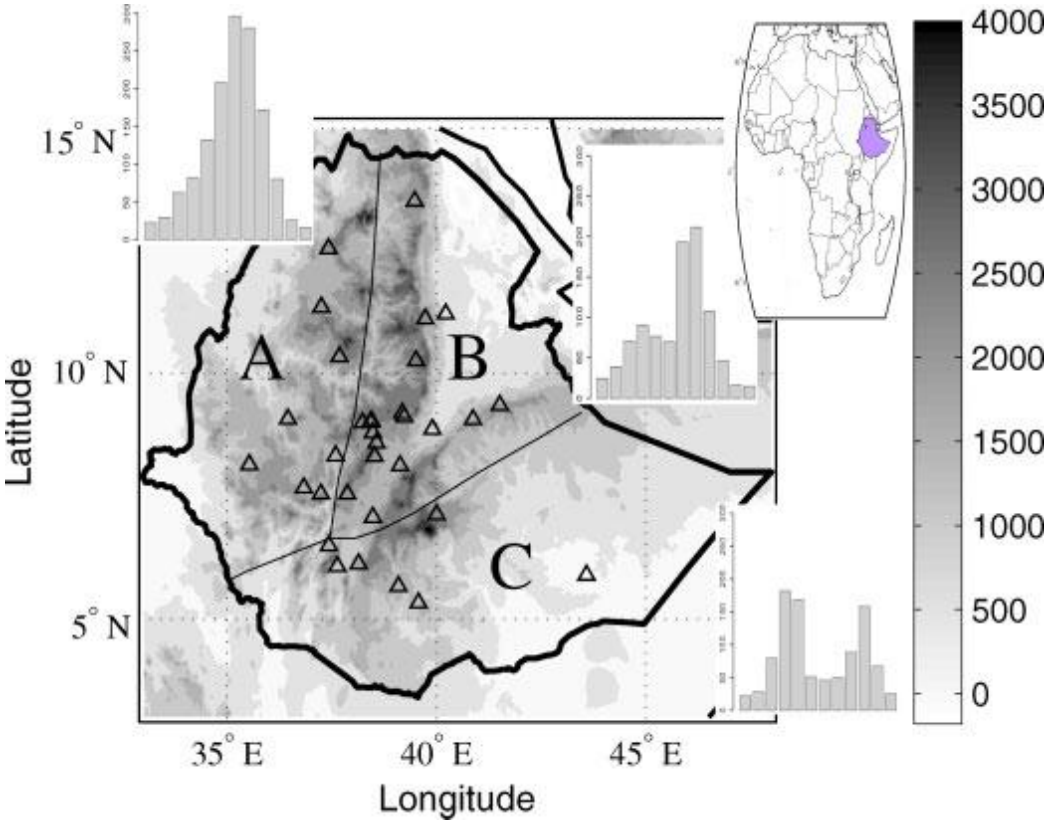

Figure 1.4: Location, topography (in meters) and rainfall regimes in Ethiopia. The histograms are climatological monthly rainfall (January to December) averaged over the rainfall regimes A, B and C. (after Diro et al., 2009)

Ethiopia is located in the tropics and variations in altitude have produced a variety of microclimates. Mean annual rainfall ranges from 2000-mm over some pocket areas in the southwest highlands, and less than 250-mm in the lowlands. In general, annual precipitation ranges from 800 to 2200-mm in the highlands (>1500 meters) and varies from less than 200 to 800-mm in the lowlands (<1500 meters). Rainfall also decreases northwards and eastwards from the high rainfall pocket area in the southwest (Bekele F., 1992)

In Central Ethiopia there are three seasons based on climatological mean of rainfall and temperature namely Bega, Belg and Kiremt (Bekele F., 1992). Bega (dry season) is from October to January. It is characterized by dry and cool period. Belg (small rainy season) is from February to May. It is characterized by varying dry and wet days. Kiremt (main rainy season) is from June

to September violent thunderstorms in the highlands are common in late June.

The study area is located in the central plateau, its relief is very essential in controlling the climatological condition. Considerable rainfall is received in the study area due to High Point Mountains that poses orographic influence.

The main features that affect the climate of East Africa, specifically Ethiopia, are: the Inter tropical Convergence Zone (ITCZ), the positions and strengths of the nearby subtropical high-pressure systems, upper-level jet streams and tropical cyclones (Diro et al., 2009). In Africa, the ITCZ oscillates annually between an extreme northward location of 15 °N in July and an extreme southward location of 15 °S in January (Asnani, 2005). This gives rise to the bimodal rainfall pattern in southern Ethiopia and the monomodal pattern in northern Ethiopia. In addition, the rainfall in East Africa is affected by a meridional arm of the ITCZ, which arises because of the difference in heat capacity of the land surface and the Indian Ocean, thus producing rainfall over the southwest of Ethiopia in February/March even though the main ITCZ is still in the southern hemisphere (Kassahun, 1987).

Upper-level features affecting Ethiopian rainfall is affected by upper-level features including the Tropical Easterly Jet (TEJ) and African Easterly Jet (AEJ) during the Kiremt season and the Subtropical Westerly Jet (STWJ) during Belg. The location and strength of these jets modulate convection and consequently rainfall (e.g. Camberlin and Philippon (2002); Nicholson and Grist (2003); Segele and Lamb (2005)). The subtropical high-pressure zones in the vicinity of Africa influence moisture fluxes followed by rainfall over Ethiopia. The low-level moisture sources during the Kiremt rainy season are the Atlantic and the Indian Ocean and the flux of moisture depends on the intensity and position of the St Helena and Mascarene highs (Kassahun, 1987). Several studies (Ininda et al. 1987; Bekele, 1997; Camberlin, 1995) show that there is a relationship between Ethiopian rainfall and sea surface temperature anomalies (SSTA) over the Indian Ocean. They also suggest that SSTAs over the eastern Pacific may affect the rainy seasons in Ethiopia. Positive SSTAs in the eastern Pacific are associated with severe and widespread rainfall deficits in the main (Kiremt) rainy season and excess rainfall in the short (Belg) rainy season.

The altitude of the Dendi area varies between 2,830 and 3,270 meters above sea level. The whole area, lying in a tropical climate, classified as wet, humid region with a mean annual rainfall of

1137.35mm. There are two seasons of rainfall. The first rainy season spans from late May to late September and the second from mid of March to mid of April. The total amount of rainfall and its seasonal distribution is fairly adequate for crop production. The main cropping season extends from June through January. The mean maximum temperature is 19.6^0C and the mean minimum temperature is 17.2^0C. The warmest months are April, May and June whereas the coldest months are July to October.

To characterize the hydrologic property of the area different hydrometerological parameters are incorporated. These include; precipitation, sunshine duration, relative humidity, evaporation, wind speed and temperature data are obtained from Ethiopian Metrology Service Agency. These selected seven stations are located surrounding the study area, where Ambo, Asgori, Busa and Ginchi stations are more nearer to the study area.

- Ambo
- Asgori
- Wolonkomi
- Ginchi
- Tulubolo
- Woliso
- Busa

Two prominent climatical conditions prevail in the study area: wet season (June to September) and dry season October to May with slight Belg rainfall from April and May. Hydrometerological data obtained from National Meteorological Service Agency (NMSA) are analyzed to understand the hydrometerological nature of the area and presented in the following manner by AbenezerKefeni (2007) and inherited in this thesis work.

1.5.1. Temperature

Air temperature is a measure of the average speed at which air molecules are moving; higher temperature is achieved by high speed of air molecules and vice versa. The Temperature variation in the study area is negligible when considered on yearly basis (see table 1.1 and figure 1.5 below). The maximum temperature record is about 19.6^0C during April while July is with the minimum temperature, 17.2^0C. Annual mean temperature is 18.1^0C.

1.5.2. Relative Humidity

Relative humidity is defined as the ratio of the partial pressure of water vapor in a gaseous mixture of air and water to the saturated vapor pressure of water at a given temperature. Relative humidity is expressed as a percentage and is calculated in the following manner:

$$RH = \frac{P(H_2O)}{P^*(H_2O)} X100\%$$

Where:

RH: The relative humidity of the gas mixture being considered.

$P(H_2O)$: The partial pressure of water vapor in the gas mixture; and

$P^*(H_2O)$: The saturation vapor pressure of water at the temperature of the gas mixture.

The relative humidity of a system is dependent not only on the temperature but also on the absolute pressure of the system of interest. Therefore, a change in relative humidity can be explained by a change in system temperature, a change in the absolute pressure of the system, or change in both of these system properties.

The relative humidity data are obtained from two stations, Ambo and Woliso. The maximum (79.4%) and minimum (44.3%) relative humidity are during August and February respectively. This result is acceptable since, August is the month characterized by low temperature and high rainfall that enhances relative humidity. Generally, the relative humidity is above 50% on monthly basis. The annual mean relative humidity is about 59.5% implies the partial pressure of water vapor in the gas mixture is greater.

1.5.3. Wind Speed

Wind is air in motion. It is caused by horizontal variations in air pressure. The speed of movement of air relative to a fixed point on the Earth defines wind speed.

Wind speeds usually mean the movement of air in an outside environment, but the speed of movement of air inside is important in many areas, including weather forecasting, hydrological cycle, aircraft and maritime operations, building, civil engineering. High wind speeds can cause unpleasant side effects. Technically, wind speed is given by

$$/V/= \sqrt{u^2 + v^2 + w^2}$$

Where u, v, and w: are zonal, meridional and vertical components of wind velocity. Except in unusual circumstances (e.g. in cumulus updrafts), the vertical component of the velocity is much smaller than the horizontal components.

As it's shown in Fig 1.5 and Table 1.1, the wind speed is low from May to September while the other months experience relatively higher wind speed. The maximum wind speed of the area is about 3.3m/s, which is recorded during the month December, computed minimum wind speed is 0.9m/s in August.

1.5.4. Sunshine Hours

The maximum sunshine duration is about 10 hours recorded in December and the minimum sunshine hour is about 4 hours recorded during August whereas the average sunshine of the year in the study area is about 7 hours.

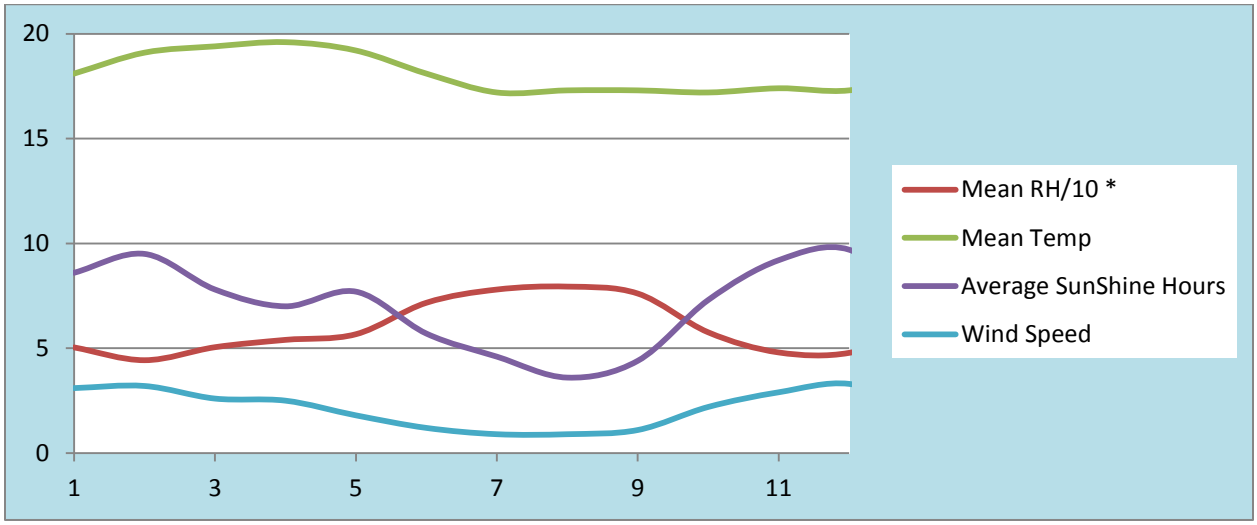

Fig 1.5: Meteorological parameter graph showing mean monthly temperature, average sunshine hours, wind speed and Monthly Relative Humidity of the study area.

* The mean relative humidity in the graph is divided by ten in order to show it in this graph without affecting the peak pattern of the others.

1.5.5. Precipitation

Precipitation is the process of deposition of any form of water (either liquid or solid) that falls from the atmosphere and reaches the ground, such as rain, snow, or hail. As a tropical area, however, the major portion of precipitation is obtained from rainfall. Rainfall is the main component of hydrologic cycle which varies with space and time. The distribution of water on the Earth surface is governed by evaporation and precipitation, which in turn depends on:

Physical factors (geographical conditions) and Meteorological factors (wind speed, temperature, sunshine, etc.)

Precipitation amount of a given area is obtained by determining the average of rainfall records over a given period of time. The Arithmetical mean is the common method used to compute the average. Arithmetical average is given by the equation:

$$\overline{P} = \frac{\sum_i^n P_i}{n}$$

Where:

P: mean precipitation P_i: rainfall records n: is number of stations

The rainfall recording stations are located in the North and South border of the Ambo-Woliso area except Busa station situated near Goro-Dendi, more near to the study area, where orographic control is significant. The arithmetic mean rainfall of the area is given in table 1.2. Busa station with 1431.8 mm of rainfall records the highest rainfall showing that the Dendi area receives higher rainfall than the surrounding area. The highest rainfall is recorded from June to September while the driest months in the Dendi area are from November to January.

Meteorological parameters	Jan	Feb	Mar	Apr	May	Jun	Jul	Aug	Sep	Oct	Nov	Dec	Annual Average
Mean RH	50.4	44.3	50.5	54	56.7	71.7	78	79.4	76.1	57.6	48	47.8	54.60
Mean Temp	18.1	19.1	19.4	19.6	19.2	18.1	17.2	17.3	17.3	17.2	17.4	17.3	18.92
Wind Speed	3.1	3.2	2.6	2.5	1.8	1.2	0.9	0.9	1.1	2.2	2.9	3.3	2.40
Average SunShine Hours	8.6	9.5	7.8	7	7.7	5.7	4.6	3.6	4.4	7.3	9.2	9.7	7.72

Table1.1: Mean monthly temperature, average sunshine hours, wind speed and Monthly Relative Humidity of the study area.

Station	Jan	Feb	Mar	Apr	May	Jun	Jul	Aug	Sep	Oct	Nov	Dec	Total
Tulubolo	18.30	18.60	54.20	67.80	78.40	192.90	287.50	277.70	90.60	24.60	7.40	7.00	1125.00
Asgori	18.50	32.80	53.60	83.60	67.90	128.10	242.50	239.40	102.20	25.70	6.90	5.30	1006.50
Woliso	23.90	27.40	66.50	84.80	122.80	190.90	271.90	257.30	130.50	40.40	7.60	5.30	1229.30
Busa	21.30	59.00	55.90	73.70	84.40	179.80	358.20	372.50	164.90	43.00	10.00	9.10	1431.80
Wolonkomi	22.80	29.20	66.10	72.40	77.90	154.40	240.00	234.40	133.70	36.00	12.20	6.60	1085.70
Ambo	31.87	15.27	52.76	74.65	73.18	149.87	177.20	163.20	87.71	45.83	9.22	11.30	892.06
Ginchi	33.91	65.93	84.38	105.10	87.46	148.68	238.70	224.30	150.60	32.04	4.00	16.00	1191.10
Arithmetic Mean	24.37	35.46	61.92	80.29	84.58	163.52	259.43	252.69	122.89	35.37	8.19	8.66	1137.35

Table 1.2: The arithmetic mean rainfall of the areas surrounding Dendi; annual mean is 1137.35mm

1.6. Vegetation and Socio-Economy

The area is vegetated by different types of natural and planted vegetation. The major vegetation is: savanna grass, bamboo forest, eucalyptus and other varieties. There are several scattered settlements and villages inhabited by the local people who support their life by rain feed subsistence agriculture and products of their cattle. The main crops cultivated in the area include: barley, wheat, enset, potato and cabbage with other minor cultivations. Barley and enset are the most dominant one among these agricultural products.

The agricultural activity is still traditional. It depends on animal. The most important livestock breeds of the region include cattle, sheep, goats, equine (horses, mules, and donkeys) and poultry. The livestock resource is mainly indigenous with some number of improved animals introduced in the region. Livestock are bred for the source of power for plough, milk and meat production, hided and skins production, fuel manure and prestige.

The Dendi caldera is sparsely populated. Afan Oromo language, the official language of the Oromiya regional state, is the dominant language in the study area while, some people communicate with Amharic, the official language of the country. Meaningful resource degradation is continuously occurring due to the increasing number of human population pressure and improper farming practices that by now severely causing and aggravating deforestation, land degradation, soil erosion, and loss of habitat for wildlife and loss of wildlife. In general, loss of forest resources, land degradation from agriculture and loss of habitat and biodiversity are the results of high population density and growth rates in the region.

The marketing of firewood and forest products (e.g. eucalyptus trees), very small number of cottage industries (e.g. weavers, carpenters, potters, blacksmiths, charcoal makers and tanners) supply the indigenous people with very small amount of extra cash income. Some of the local people are used to work as daily laborers in the newly planned real state which will build in the Dendi caldera by Egyptian investors.

1.7. Methods and techniques

1.7.1. Desk study and image processing techniques

Acquisition of background geological, geomorphological and paleoclimatic information and relevant data of the previous prospects, begin with a literature study and review of open file

materials available and collected from different sources. Landsat ETM+ image was used and the data analysis and processing were carried out with ERDAS IMAGINE 9.2. Similarly mapping, geographic analysis, data editing and compilation were carried out with ArcGIS 10.1software package

1.7.2. Surface geological mapping and sampling methods

Geological mapping was done on the interpretation of satellite imagery. A field trip was conducted in order to collect rock samples and structural data and to prepare a geologic map of the study area at the scale of 1:25,000. Standard geological mapping techniques, including traversing and detailed description of exposed units, were conducted. In addition, a geomorphological mapping of the catchment was conducted in order to characterize the impact of landforms on sediment transport to the lake.

The following materials were used during the field work activity: base map (topographic maps at the scale of 1:50,000 and satellite images), GPS, Digital camera, Sample bag, Geological hammer, Hand lenses, Compass, and Stationary materials.

A 14.5m long sediment core was recovered from the Dendi Lake which is used for the paleoclimatic reconstruction. One 63 cm long short core and seven 2m long cores were drilled with an overlap of ~ 50 cm to reach a depth of 10.2m down from the surface of the bottom of the lake.

1.7.3. Analytical methods

1.7.3.1. The core sediment

The recovered core sediments are split into two halves, the working half and the archive half. Then the working half is well described in terms of color, texture, structure, organic matter and other materials that might be present in the sediment core. Consequently, the sediment core is photographed under a high resolution core scanning camera before it loses its original color as a result of oxidation.

XRF measurements of the core sediments in order to get the geochemistry of the sediments were analyzed under the high resolution ITRAX core scanner. XRF core scanner technology allows a rapid, non-destructive acquisition of geochemical and X radiographic data from sediment cores. To determine the geophysical parameter Magnetic susceptibility (MS) a high resolution core

logger (Geotek MSCL) with point sensor, which is suitable for continuous measurement of split half core, was used.

After these analyses, subsampling of the sediment cores by using U-channels for paleomagnetic studies and subsampling the whole sediment core in every 2 cm interval for further analyses was done. The whole analyses on the core sediments were undergone in the University of Cologne

The rock samples

Two methods of sample preparation were employed to know the elemental concentrations and mineralogical composition of the various samples. The methods are:

Petrography study

Fresh outcrops of representative rock samples were collected to investigate the mineralogical composition, texture, degree of alteration and variation of lithologic units. Eight representative thin-sections were prepared at the Central Laboratory of the Geological Survey of Ethiopia by splitting each specimen with various diamond blades. They are prepared by mounting a small cut and polished sample of rock, using a strong adhesive onto a plate of glass (usually27x46 mm in size) and then the exposed surface of the rock is gradually ground or 'lapped' down to 0.03 mm thickness to be examined under a petrographic microscope using transmitted light in the mineralogy-petrology laboratory of the school of Earth Sciences of Addis Ababa University

X-ray fluorescence (XRF)

The rock and soil samples collected were dried and powdered, and then a pellet is formed from each sample to be scanned under XRF and to produce elemental composition of the samples. Each sample is scanned twice to get rid out of analytical error. Values for major oxides are recalculated from the major elemental values. The XRF analysis is done in the Aachen University, Germany.

Principles of XRF analysis

X-ray fluorescence (XRF) is the emission of characteristic "secondary" (or fluorescent) X-rays from a material that has been excited by bombarding with high-energy X-rays or gamma rays. It is a powerful quantitative and qualitative analytical tool for elemental analysis of materials. The method is fast, accurate, non-destructive, and usually requires only minimal sample preparation.

When elements in a sample are exposed to a source of high intensity X-rays, fluorescent X-rays will be emitted from the sample at energy levels unique to those elements.

The basic concept for all XRF spectrometers is a source, a sample, and a detection system. The source irradiates the sample and a detector measures the fluorescence radiation emitted from the sample. In most cases for XRF, the source is an X-ray tube. Alternatives are a radioactive source or a synchrotron.

The analysis of major and trace elements in geological materials by x-ray fluorescence is made possible by the behavior of atoms when they interact with radiation. When materials are excited with high-energy, short wavelength radiation (e.g., X-rays), they can become ionized. If the energy of the radiation is sufficient to dislodge a tightly-held inner electron, the atom becomes unstable and an outer electron replaces the missing inner electron. When this happens, energy is released due to the decreased binding energy of the inner electron orbital compared with an outer one. The emitted radiation is of lower energy than the primary incident X-rays and is termed fluorescent radiation. Because the energy of the emitted photon is characteristic of a transition between specific electron orbitals in a particular element, the resulting fluorescent X-rays can be used to detect the abundances of elements that are present in the sample.

XRF analyzers determine the chemistry of a sample by measuring the spectrum of the characteristic x-ray emitted by the different elements in the sample when it is illuminated by X-rays. These X-rays are emitted either from a miniaturized x-ray tube, or from a small, sealed capsule of radioactive material.

- ✓ A fluorescent x-ray is created when an x-ray of sufficient energy strikes an atom in the sample, dislodging an electron from one of the atom's inner orbital shells.
- ✓ The atom regains stability, filling the vacancy left in the inner orbital shell with an electron from one of the atom's higher energy orbital shells.
- ✓ The electron drops to the lower energy state by releasing a fluorescent x-ray, and the energy of this x-ray is equal to the specific difference in energy between two quantum states of the electron.

When a sample is measured using XRF, each element present in the sample emits its own unique fluorescent x-ray energy spectrum which helps to discriminate between each element

Strengths

X-Ray fluorescence is particularly well-suited for investigations that involve:

- ✓ Bulk chemical analyses of major elements (Si, Ti, Al, Fe, Mn, Mg, Ca, Na, K, P) in rock and sediment
- ✓ bulk chemical analyses of trace elements (>1 ppm; Ba, Ce, Co, Cr, Cu, Ga, La, Nb, Ni, Rb, Sc, Sr, Rh, U, V, Y, Zr, Zn) in rock and sediment

Limitations

In theory the XRF has the ability to detect X-ray emission from virtually all elements, depending on the wavelength and intensity of incident x-rays. However,

- ✓ In practice, most commercially available instruments are very limited in their ability to precisely and accurately measure the abundances of elements with Z<11 in most natural earth materials.
- ✓ XRF analyses cannot distinguish variations among isotopes of an element, so these analyses are routinely done with other instruments (see TIMS and SIMS).
- ✓ XRF analyses cannot distinguish ions of the same element in different valence states, so these analyses of rocks and minerals are done with techniques such as wet chemical analysis or Mossbauer spectroscopy.

1.7.4. Data processing and presentation

For satellite image analysis, Landsat ETM+ image was used and the data analysis and processing were carried out with ERDAS IMAGINE 9.2. Similarly mapping, geographic analysis, data editing and compilation were carried out with ArcGIS 10.1, and Global Mapper 7 software packages. For geochemical data plotting and interpretation MS-Excel and Petrograph2beta softwares were used.

CHAPTER TWO

2. REGIONAL GEOLOGIC SETTING

2.1. Summary of The Geology of Ethiopia

The main lithostratigraphic successions that crop out in Ethiopia are: the proterozoic crystalline basement, the late paleozoic to mesozoic continental and marine sedimentary rocks, and the Cenozoic basic and acidic volcanics and associated volcano-sedimentary and volcanoclastic rocks. Volcanic rocks are predominant in the central Ethiopia whereas the crystalline basement and the sedimentary rocks are locally exposed by erosional processes and faulting.

The precambrian rocks of Ethiopia contain a wide variety of sedimentary, volcanic and plutonic rocks which have been subjected to varying degrees of metamorphism and deformation. Earlier studies by Kazmin et al. (1978) suggested a three-fold lithotectonic sequence consisting, the upper, middle and lower complex. However, recent geochronological and isotopic studies shows that, the precambrian basement of Ethiopia is composed of the low grade metasedimentary and metavolcanics complex of the Arabian Nubian Shield (ANS) and the high grade gneiss dominating Mozambique Belt (MB) associated syn to post tectonic plutonic rocks which are the results of a contemporaneous event during Neoproterozoic (Alene et al., 2000; Asrat et al., 2001; Ayalew et al., 1990; Teklay et al., 1998). These rock units are mainly exposed in the northern (Tigray), western (around Wollega), southern (around Adola) and Eastern (Harar) periphery of the country and covers about 23% of the total surface area of the country.

The paleozoic Era is marked by a regional unconformity due to long period of denudation resulting in near peneplanation of the ancient precambrian basement. This era is also considered as a time of glacial deposits of that of the Enticho sandstone and the EdagaArbi glacials (Kazmin 1972; Mohr 1971).

The transgression-regression of the Indian Ocean is the main event that occurred during the Mesozoic Era in Ethiopia. During this time, the sedimentary sequence formation is generally continental (e.g. Adigrat sandstone?) ==> Transitional (e.g. Gohatsion formation) ==> marine (e.g. antalo limestone) ==> transitional (e.g. mugher mudstone/shale) ==> continental (e.g. Debre libanos sandstone) sedimentary deposits. Recent studies are suggesting that the Adigrat sandstone is a shallow marine deposit.

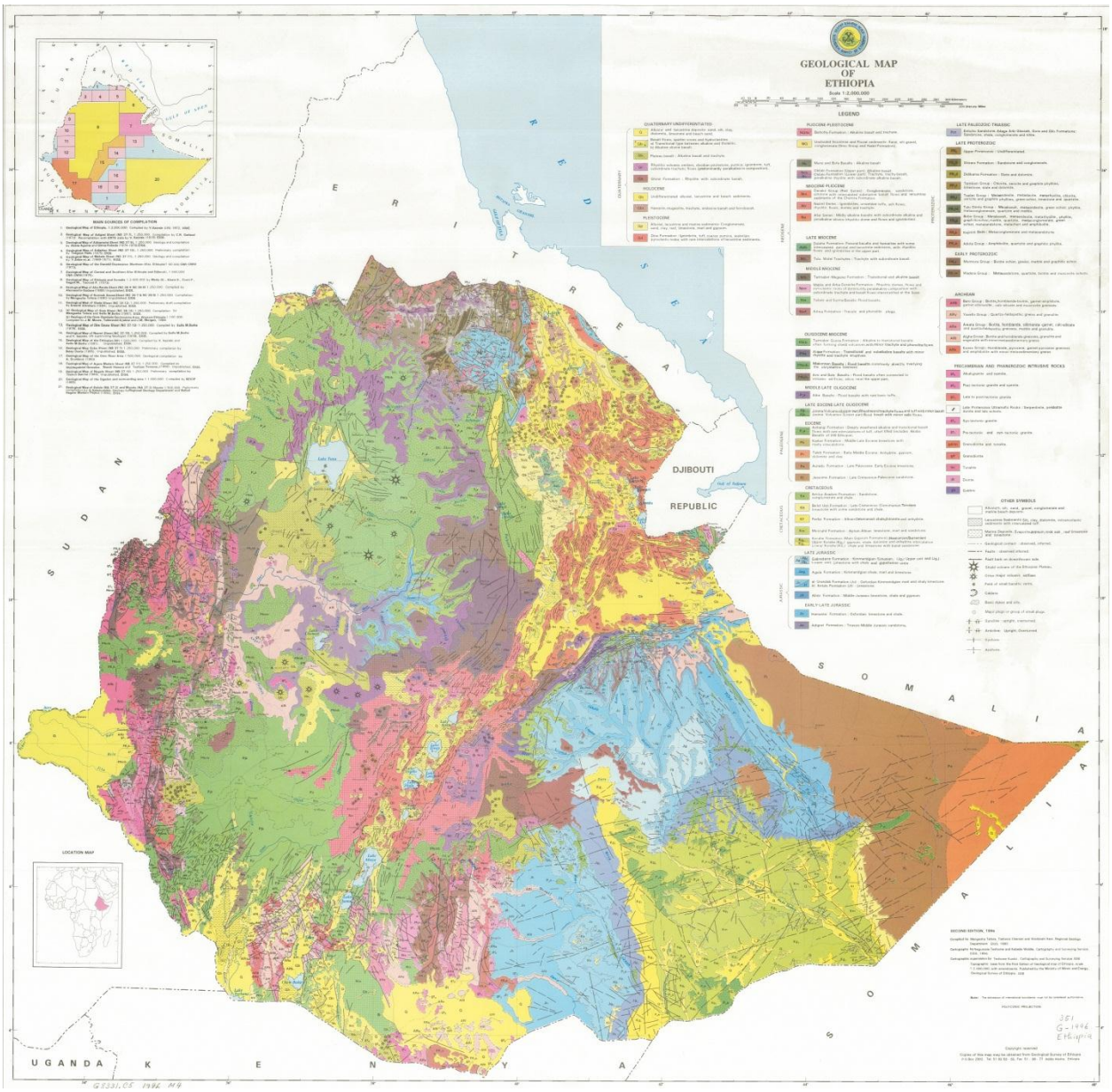

Fig. 2.1: Geological map of Ethiopia

These very thick sedimentary formations are resulted from the transgression-regression of the Indian Ocean. These rock units cover the whole of the Eastern lowlands (Ogaden basin), the upper valleys of the Blue Nile and its tributaries in central Ethiopia (Blue Nile basin), large areas of Northern Ethiopia (Mekele outlier) and covers about 25% of the total surface area of the country. (Getaneh, 1991)

The Cenozoic volcanic rocks are associated with the formation of the Main Ethiopian Rift (MER), Afar Depression and highland volcanics (trap series) which is the earliest and most extensive group of volcanic rocks. The rock units are crop out in the eastern and western Ethiopian highlands and within the Main Ethiopian Rift (MER) and the Afar depression. These rock units represent more than half, about 52%, of the surface of the country. Cenozoic sedimentary rocks are also reported in eastern Ogaden, the Danakil depression and the lower Omo Valley. (Kazmin 1972; Mohr and Zanettin 1988; Tefera et al 1996)

2.2. Regional Geology

Widespread Cenozoic volcanism in Africa is almost exclusively restricted to areas of the continent affected by the Pan-African tectono-thermal event. This non-random distribution suggests that during the Cenozoic the large-scale structure of the lithosphere has exerted a control on the location of volcanic areas.

The Ethiopian Highlands are a rugged mass of mountains in Ethiopia, Eritrea and northern Somalia in the Horn of Africa. The Ethiopian Highlands form the largest continuous area of its altitude in the whole continent, with little of its surface falling below 1500 m, while the summits reach heights of up to 4550 m. It is sometimes called the Roof of Africa due to its height and large area. The Ethiopian Highlands began to rise 75 million years ago, as magma from the Earth's mantle uplifted a broad dome of the ancient rocks of the African Craton.

According to Hofmann et al. (1997), most of the Ethiopian flood basalts erupted 30Myr ago, during a short 1Myr period, to form a vast volcanic plateau. Immediately after this peak of activity, a number of large shield volcanoes developed on the surface of the volcanic plateau, after which subsequent volcanism was largely confined to regions of rifting (Mohr, 1983; Mohr & Zanettin, 1988). The rift that opened along the Red Sea and Gulf of Aden separated the Arabian and African continents, and isolated a small portion of the volcanic plateau in Yemen

and Saudi Arabia (Baker et al., 1996). Volcanic activity continues to the present day along the Ethiopian and Afar rifts.

The Ethiopian flood basalts (or traps) cover an area of about 600, 000 km^2 with a layer of basaltic and felsic volcanic rocks (Fig. 2.1). The thickness of this layer is highly variable but reaches 2 km in some regions. The total volume of volcanic and shallow intrusive rocks has been estimated by Mohr (1983) and Mohr & Zanettin (1988) at about 350,000 km^3.

In Ethiopian igneous province during Miocene –Pliocene there was uplift, rifting and building of basaltic shields with associated rhyolites and phonolites. About 10ma is marked by one of the major episodes of rifting (Kazmin et al., 1980).

The presence of rift – related volcanics on the plateaus can be explained by the possibility that the Afar plume material may have been channeled to adjacent favorable fracture systems allowing 'fissure type' volcanic eruption to take place away from hotspot.

The Ethiopian plateau is made up of several distinct volcanic centers of different ages and magmatic affinities (Bruno K. et.al. 2004). Two sequences have been recognized in the volcanic succession. The lower volcanic sequence (Oligocene to Lower Miocene), consists of flood basalts with associated trachyte to phonolite domes and necks, is considered to belong to the uplifted Ethiopian Volcanic Plateau. The upper volcanic sequence, which is late miocene to recent in age, consists mainly of several central volcanoes such as Dendi, Wenchi, Konchi, etc and associated small domes and cones (Abebe T. et.al., 2005).

The study area is made of volcanic rocks that belong to the upper volcanic sequence. much of the volcanic rock around the study area and its surrounding is comprised of basalt erupted as part of the opening of the East African Rift, more silica-rich rock types like rhyolites and trachytes (characterized by minerals such as quartz and feldspar) are also present.

The approximately7.5 kilometers wide Dendi Caldera includes some of this silica-rich volcanic rock -- the rim of the caldera is comprised mainly of poorly-consolidated ash erupted during the quaternary period (Abebe T. et al., 1998). K-Ar dating result on trachyte sample from the adjacent Wenchi caldera gives an age estimate of <0.1 Ma age.

A notable feature of the Dendi Caldera is the presence of two shallow lakes formed within the central depression (center). The image in the location map highlights a radial drainage pattern

surrounding the remnants of the Dendi volcanic cone. Such patterns typically form around volcanoes, as rainfall has equal potential to move downslope on all sides of the cone and incise channels.

No historical volcanic eruptions of Dendi are recorded; however the Wenchi Caldera 13 kilometers to the southwest of Dendi caldera may have been active as "recently" as A.D. 550. The distal pyroclastic products of these central volcanoes might exist in the Dendi caldera. Therefore, dating the pyroclastic products, especially the volcanic ash, might not give the actual age of the Dendi volcanics. Even more distal pyroclastic products might deposit from the Main Ethiopian Rift and Afar Depression volcanoes.

The geochemical analysis, not only the geochronology, results of the lithologic units from these areas show differing composition. The rock units from the Wenchi caldera are compositionally trachytic while the Dendi caldera constituted by both trachytic and rhyolitic volcanic rocks (Abebe T., 1998).

According to the report of Geological Survey of Ethiopia which is compiled by Efrem Beshawered (2010), the present study area falls in the Akaki-Beseka area which is bounded between $\mathbf{8^0 00^1}$ and $\mathbf{9^0 00^1}$ north latitude and $\mathbf{37^0 30^1}$ and$\mathbf{39^0 00^1}$ east longitude. This is a wide area covering almost the whole lithostratigraphic sequence that crop out in Ethiopia since Proterozoic. The report has forwarded the presence of:

1. Pre-Rift Units: constituting high grade metamorphic rock (biotite gneiss); Mesozoic sedimentary rocks comprising Adigrat-Sandstone, shales and marls, and Antalo-Limestone; and Oligocene to Late Miocene plateau flood (Jimma, Amba-Alaje, Makonnen, Tarmaber-Megezez, Guraghe-Anchar, and Addis Ababa) basalts;
2. Syn-Rift Units: constituting Upper Miocene-Quaternary products of Nazret pyroclastic rocks of welded to partially welded pyroclastic flows with rhyoliticandtrachytic lava domes;
3. Main Rift Units: comprising Quaternary-Holocene young central volcanoes of Gash Megal rhyolites and Wechacha trachytes, ChefeDonsa pyroclastic deposits, scoria fall out and phyric basaltic lava flows of Akaki, Zikwala trachytes, rhyolitic domes, obsidian lava flow, pyroclastics and pumice fall deposits of Bora-Bericha, lacustrine sediments, and phreatomagmatic, scoria cones and fallout deposits of Wonji basalts; and
4. Quaternary alluvial deposits.

According to this report and references therein the general stratigraphy of the Akaki-Beseka area is as given in table 2.1.

The wechecha trachyte in the main rift unit is found surrounding the Dendi Wenchi pyroclastics with an age estimate of 3.3-4 Ma. Therefore, the Dendi Wenchi volcanic centers cannot have an age older than this unit. The products of Dendi and Wenchi volcanoes have ages less than 3.3Ma. The age of the Wenchi products might be much younger than that of Dendi as it's known to be historically active. The age of products of Wenchi volcanics (<0.1Ma) might not tell us the actual age of Dendi volcanics, but they don't seem to have that much time difference.

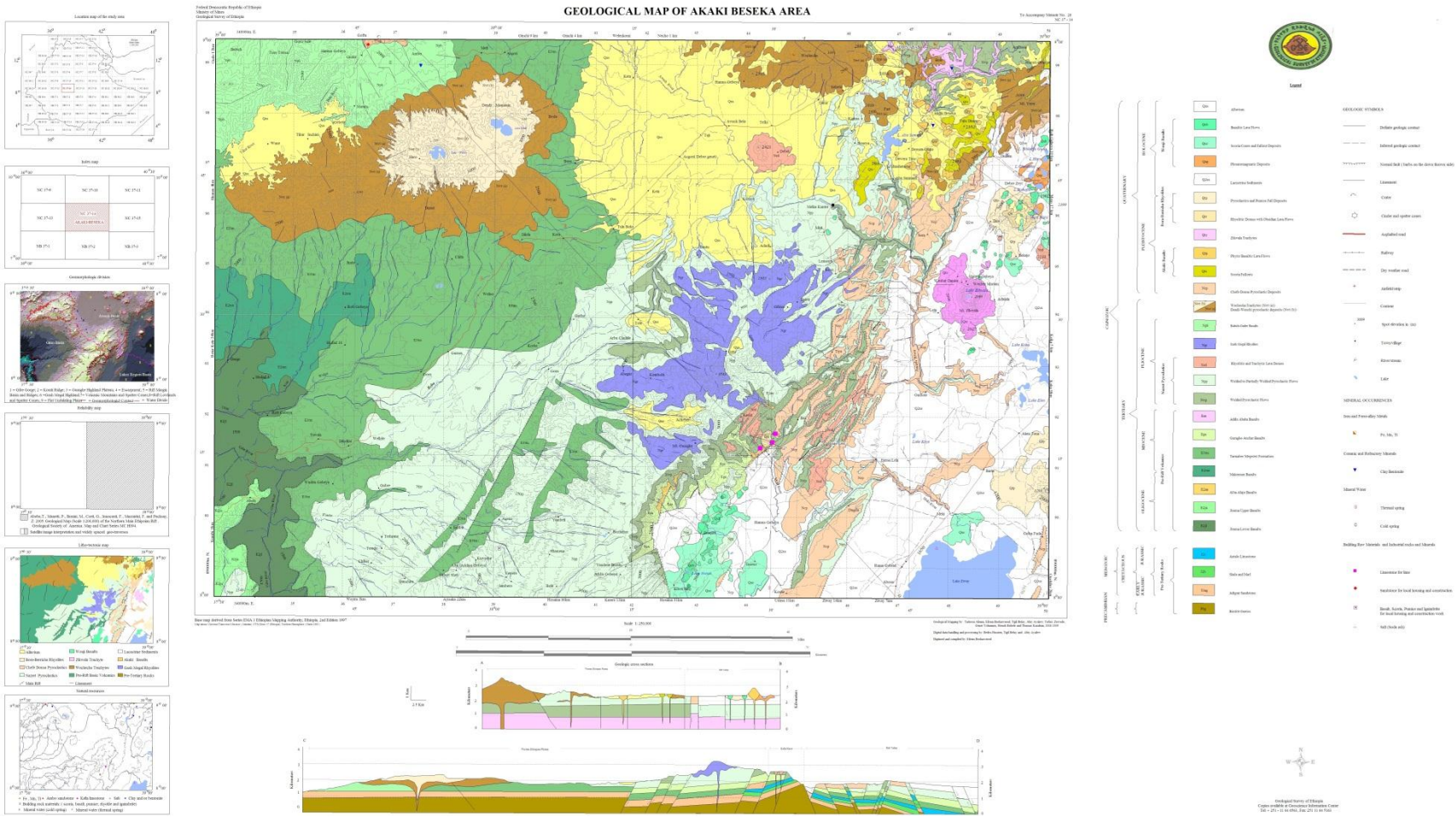

Fig2.2: Geological map of Akaki-Beseka area (after Efrem Beshawered, 2010)

Thickness (m)	Lithology	Description	Abebe et al., 2005		
			Age (Ma)	Category	Lithologic unit
> 0.5		Alluvium: reworked materials of volcanic origin	Holocene		Alluvial Cover
10		Lacustrine sediments: sand, silt, clay, diatomites, limestone, and beach sand	< 0.5	Main Rift	Lacustrine Sediments
		Basaltic lava flows: porphyritic to aphyric alkali- and/or olivine basalts	< 1.6		Wonji Basalts
		Scoria cones and fallout deposits: reddish or black in color			
60		Phreatomagmatic deposits: maar deposits intercalated with lacustrine sediments and distal silicic volcanic ashes			
200		Pyroclastics and pumice fall deposits: pumice falls with intercalation of fine ash and lacustrine deposits	< 0.9		Bora Bericha Rhyolites
50		Rhyolitic domes with obsidian lava flows:			
		Zikwala trachytes: dark gray, porphyritic trachytes with intercalation of pyroclastic material	1.28-0.85		Zikwala Trachytes
5		Phyric basaltic flows: pyroxene and olivine -phyric basalts with microcrysts of plagioclase and opaque minerals	2.9-2.0		Akaki Basalts
		Scoria fallouts:			
40		Chefe Donsa pyroclastic deposits: unwelded to poorly welded, fine volcanic ash flow and fall deposits	2.54-1.7		Chefe Donsa pyroclastic deposits
		Wechacha trachytes: short, thick trachytic lava flows and domes with minor pyroclastic materials	4.6-3.3		Wechacha trachytes
		Guder Basalt: aphanitic basalt with coumnar joint	?		?
		Gash Megal rhyolites: fine-grained to alkali-feldspar phyric lava flows with interbedded basaltic lava flows	<5	Main Rift	Gash Megal Rhyolites
50		Rhyolitic and trachytic lava domes: rhyolitic and trachytic quartz, sanidine, anorthoclase-phyric lava domes	5.2-2.6	Syn-Rift	Nazret Pyroclastic Rocks
700		Welded to partially welded pyroclastic flows: ignimbrite			
150		Welded pyroclastic flows: ignimbrite with minor intercalated basaltic lava flows			
60		Addis Ababa basalts: fine grained to olivine phyric alkali basalts, olivine basalt and trachybasalt lava flows	7.5-5	Pre-Rift	Addis Ababa Basalts
300		Guraghe-Anchar basalts:aphyric to plagioclase and pyroxene phyric basalts intercalated with rhyolitic tuffs	10.6-8.3		Guraghe-Anchar Basalts
		Tarmaber-Megezez Formation: transitional alkaline basalt	M. Miocene		?
		Makonnen basalts: flood basalt	Oligo-Mio.		?
150		Aiba-Alaje basalts: weakly altered, tilted basalt with intercalation of pyroclstic rocks	32-29		Aiba-Alaje Basalts
		Jimma upper basalts: rhyolite, trachyte and tuffs with minor basalt	L.Eocene - L.Oli		?
		Jimma lower basalts: flood basalt with minor salic flows			?
25		Antalo Limestone :yellowish gray fossiliferous	Jurassic	Pre-Rift	Antalo-Adigrat Sedimentary Rocks
30		Shales and marls: interbedded marl and shale			
150		Adigrat Sandstone:variegated in color, medium to coarse grained, crossbedded and laminated	Triassic		
150		Biotite gneiss: strongly weathered, yellowish, coarse grained often cut by pegmatite veins	Precambrian		Kella Metamorphic Rocks

Table 2.1: General stratigraphy of the Akaki-Beseka area (after Efrem Beshawered, 2010)

CHAPTER THREE

3. GEOLOGY OF THE STUDY AREA

3.1. Introduction

The Dendi Caldera is one of the volcanic centers on western central Ethiopian Plateau. It is found 13 kilometers east of the recently active Wenchi volcano in the Akaki-Beseka sheet of the Geological survey of Ethiopia. It's located in the south-east of Ambo town and south-west of Ginchi town.

The volcanic caldera has a diameter of about 8.5km in E-W and 6.5 km in N-S directions, it covers an estimated area of about 40 km^2. The altitude varies from about 2830m at the base (lake level) to 3270m at the peak. There are two adjacent crater lakes in the caldera forming a shape that looks like the number '8'. Each of the lakes has a circumference of about 7.5 km.

The caldera comprises different felsic lava flows/dome overlain by different volcanoclastics and alluvial deposits. The lithological units that crop out in the area are the lava flows/domes which consists rhyolite, trachyte and obsidian and pyroclastic deposits including ignimbrite, volcanic ash/pumice and surge deposit. The distribution of these rock units is shown in the geological map of the Dendi caldera. The field description of each unit is summarized here along with the petrographic description of the rocks.

3.2. Volcanic Successions

The stratigraphy of the Dendi caldera is shown in Table 3.1 below, including rhyolite/trachyte lava and the pyroclastic deposits (from bottom to top).

Thickness	Lith. symbol	Lithologic units	Sub units	Description
~90 m		Pyroclastic deposits	Volcanic ash Surge deposit Ignimbrite	The major unit is the surge deposit, while the remaining totally doesn't occupy a single contour
>350m		Rhyolite/trachyte lava flow/dome	Obsidian flow Rhyolite/trachye	There is an obsidian flow at the top of the rhyolite/trachyte flow/dome

Table 3.1 volcanic successions of the Dendi caldera

3.3. The lava flows/domes

These rocks are crop out in the area by making a steep slope/ vertical cliffs and occupy the elevated areas of the caldera. These units have an outcrop thickness of about 350m and their lateral extent covers the whole ridge in the caldera. The lithological units include:

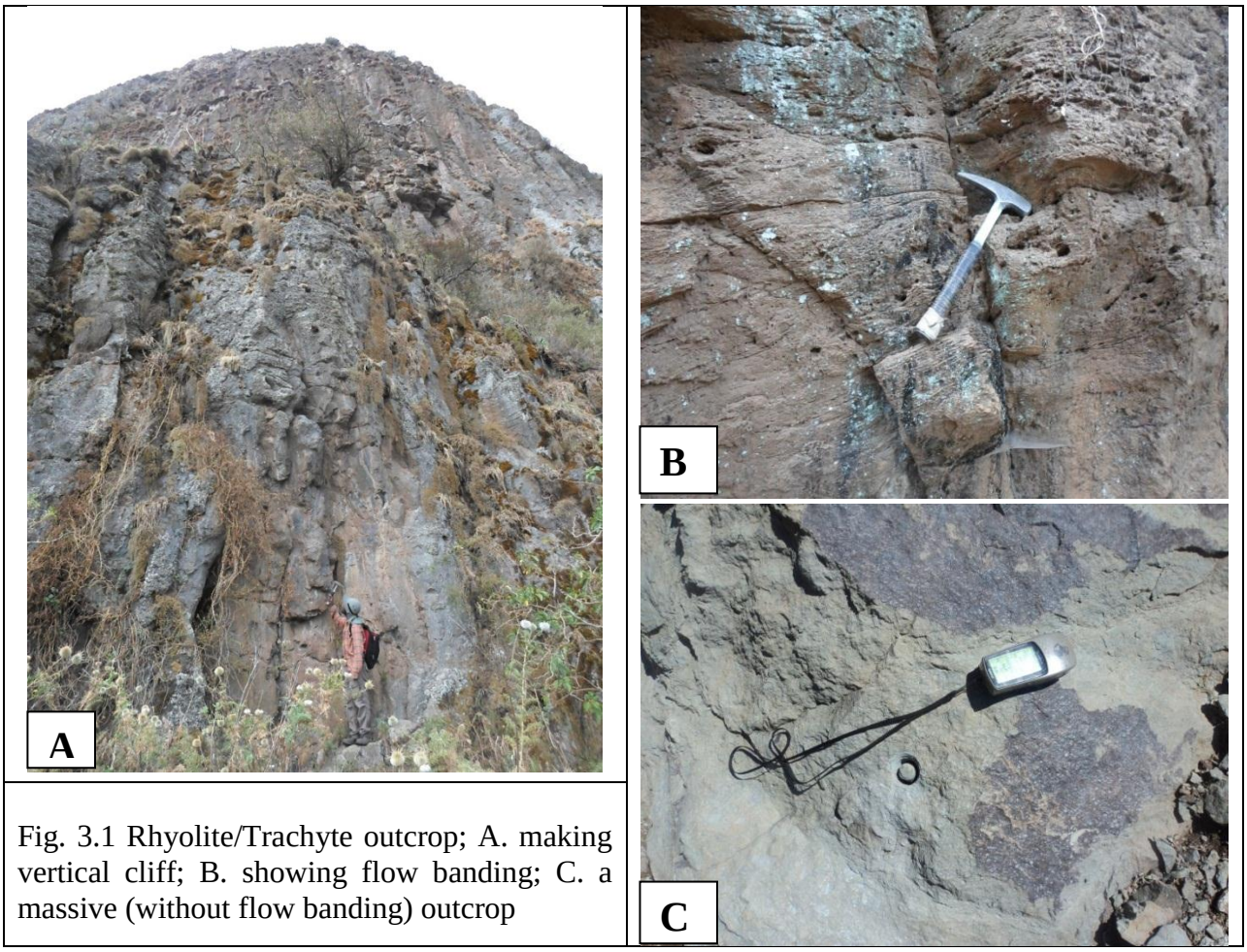

Fig. 3.1 Rhyolite/Trachyte outcrop; A. making vertical cliff; B. showing flow banding; C. a massive (without flow banding) outcrop

3.3.1. Rhyolite

Rhyolite is a felsic extrusive (volcanic) igneous rock. This type of rock is compositionally felsic/acidic, i.e. high percentage of silica, and crystallizes from silicate minerals at relatively low temperatures. Its mineral constituents crystallize at the last stage of (low temperature extreme) of the Bowen's reaction series (magmatic differentiation).

Rhyolite has light color (in comparison with basalt which is black). This is because of its composition which is felsic. And it is fine grained which is a result of solidification at or near the

surface. Texturally, it is classified as aphanitic (fine grained). But, early crystallized minerals might exist forming the phenocrysts of a porphyritic texture. It frequently contains voids and glassy fragments, evidence of having formed in a surface environment with rapid cooling.

This is one of the rock types exposed in the steep slope area and making the cliffs. In hand specimen, its texture is fine grained and its color is generally light gray but due to alterations its color is changed to light brownish, yellowish, dark grayish. In the field, it was difficult to discriminate it from trachyte, because they have similar appearances. Its texture is very fine. It's impossible to identify individual minerals by a naked eye or by using hand lens.

The rhyolite cliff in the north western section of the caldera shows columnar joint structure. Part of the cliff is also broken, a little bit transported and rotated to some angle. The columnar joints have a general orientation of $70^0 \rightarrow 140^0$. In the south eastern section of the caldera, the rhyolite lava flow shows flow banding structure which is a concrete evidence for having lava flow.

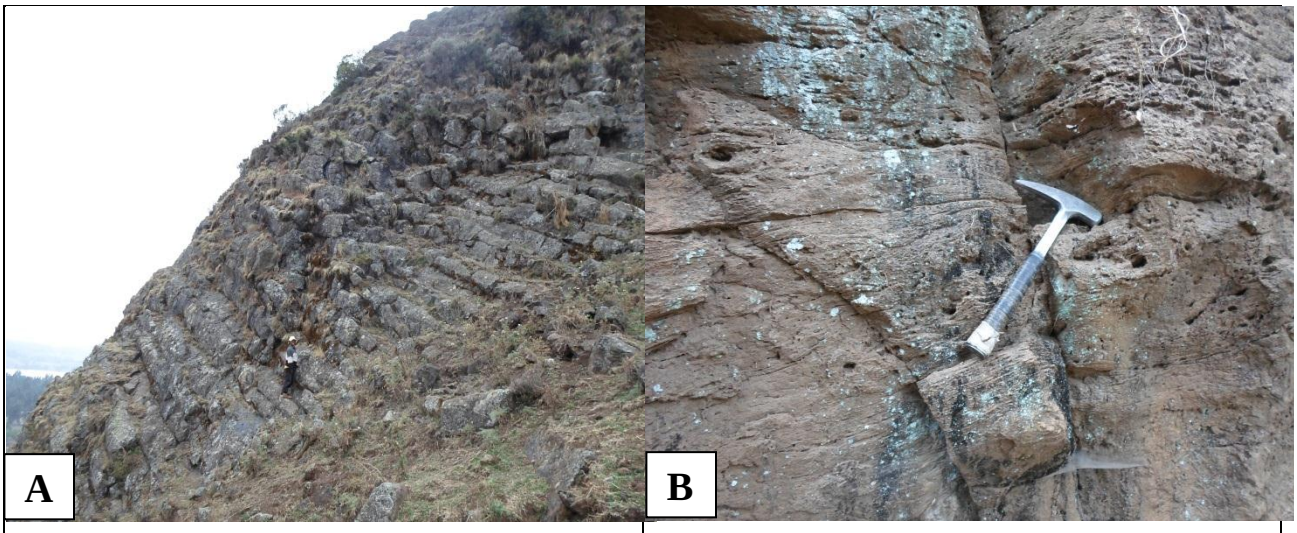

Fig. 3.2: rhyolite lava flow showing: A, Columnar joint; B, flow banding.

Under petrographic microscope, the rhyolite is fine grained having aphanitic or porphyritic texture with phenocrysts of dominantly alkali feldspar (sanidine). It's generally colorless under PPL. These conditions show that rhyolite is composed of felsic minerals and formed at the surface i.e. it's a volcanic rock. There are minor amounts of hornblende in some of the thin section. It's not easier to differentiate between the rhyolite and trachyte. The absence of quartz grain in the rhyolite makes the identification difficult. But geochemical data helped a lot for the rhyolite identification. The presence of trachytic texture (euhedral phenocrysts set in a ground

mass of smaller feldspar laths) also helped a lot to identify the trachyte. The feldspar laths are oriented by the lava flow. The thin-section description is given below.

Color	Generally color less, Colorless phenocrysts, muddy and brownish ground mass. And in some thin-sections there's a s small amount of green colored mineral ➔ Felsic	
Texture	Aphanitic, Porphyritic ➔ Volcanic	
Minerals present & description	Phenocrysts (0-30%)	Alkali feldspar (sanidine and/or orthoclase)(0-25%) – generally around 15%
		Opaques and glassy (0-10%) generally around 3 %
	Ground mass (70-100%)	Feldspars (0-10%)
		Hornblende – it's found in some of the thin-sections and it's concentration is ~6%
		Opaques, glassy and other felsic minerals (not well visible) (30-70%). They are generally ~ 50%
Rock name	Rhyolite	

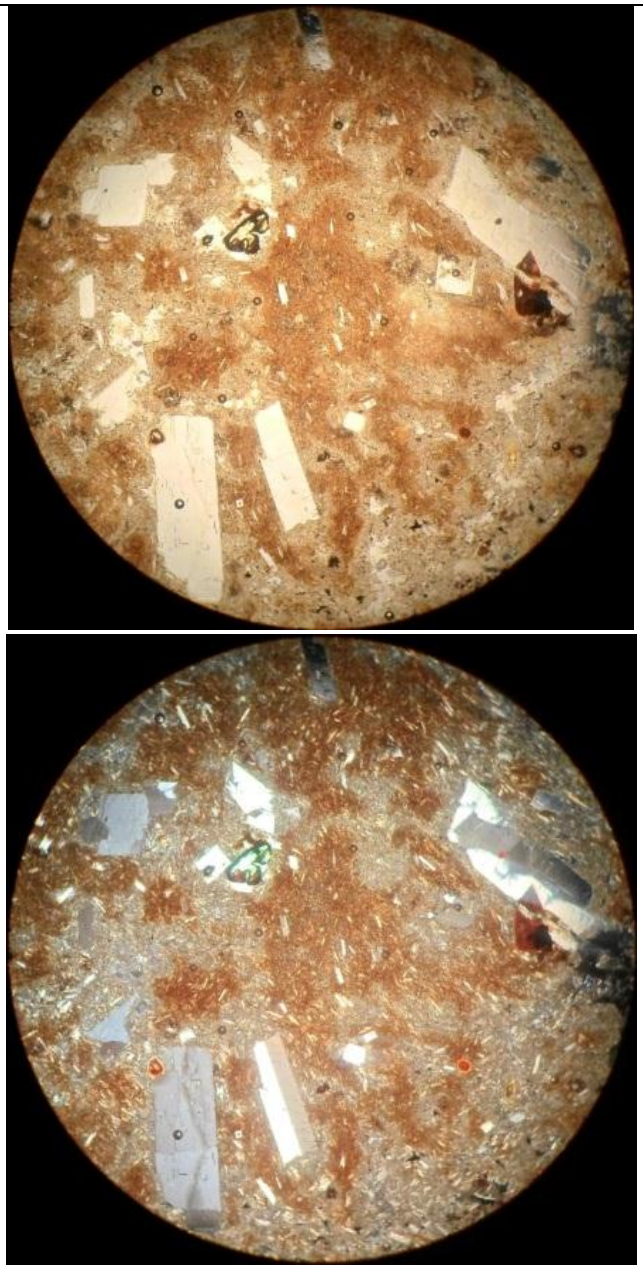

Fig. 3.3: Representative hotomicrograph of of rhyolitic thin-section (objective – 4X). The top is under PPL and the bottom is under XPL. The alkali feldspar phenocrysts are well visible.

Table 3.3: petrographic description of rhyolite

3.3.2. Trachyte

Trachyte is a volcanic rock, generally gray in color, which is dominated by alkali feldspar. The Trachyte is exposed along with the rhyolite in the steep slope/ vertical cliff/ area. In hand specimen, it has similar characteristics with the rhyolite. Its texture is fine grained and its color is

generally light gray but due to alterations its color is changed to light brownish, yellowish or dark grayish. It's the dominant among the lava flows. This implies the cliffs and steep slope areas are dominantly made of Trachyte. As mentioned earlier, it has a similar appearance with rhyolite. But, it's distinguished easily under petrographic microscope.

Color	Generally color less, Colorless phenocrysts, fine dark and muddy ground mass with the color less ones. ➔ Felsic	
Texture	• Aphanitic to medium grained, Porphyritic (the ground mass is generally medium grained) ➔ Volcanic • Euhedralphenocrysts (generally alkali feldspars) set in a ground mass of smaller feldspar laths showing trachytic structure	
Minerals present & description	Phenocrysts (5-20%)	Alkali feldspar (5-20%) – generally around 15%
		Opaques and glassy (0-10%) generally around 5 %
	Ground mass (80-95%)	Feldspars (20-50%). It's dominant among the ground mass.
		Opaques, glassy and other felsic minerals (not well visible) (20-50%). They are generally ~ 30%
Rock name	Trachyte	

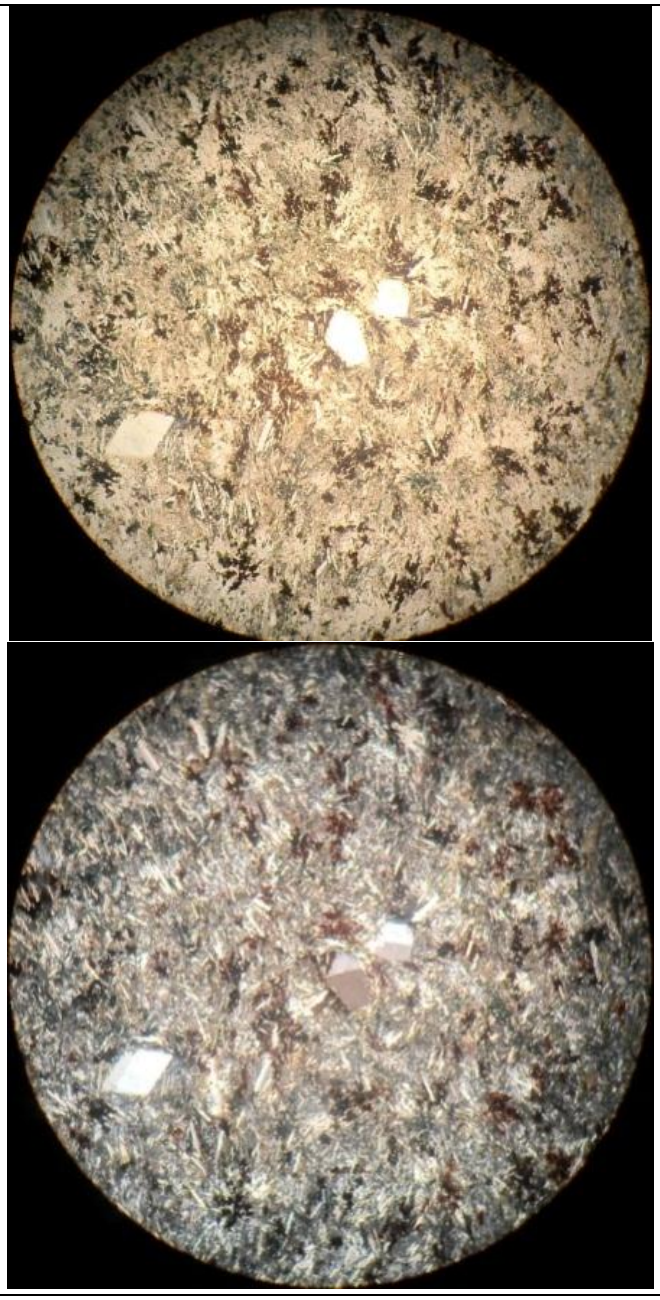

Fig. 3.4: Representative photomicrograph of trachyte thin-section (objective – 4X). The top is under PPL and the bottom is under XPL.

Table 3.4: petrographic description of the trachyte

Under petrographic microscope, the trachyte is fine grained having aphanitic (medium grained) or porphyritic texture with most of the phenocrysts are alkali feldspar with some opaque and

glassy materials. Its texture reveals that trachyte is a volcanic rock. It shows generally colorless minerals under PPL telling us its composition is felsic. It's much easier to identify the trachyte than rhyolite. This is because of the presence of trachytic texture (euhedral phenocrysts set in a ground mass of smaller feldspar laths). The feldspars laths are oriented by the lava flow. The thin-section description is given below. All the trachyte show trachytic texture. Most of the feldspar laths are alkali feldspars. But, it's difficult to identify every component/ composition of the feldspar laths.

The trachyte/rhyolite flow is followed by an obsidian flow at the top. Obsidian is a volcanic glass which results from a very rapid cooling of magma. Compositionally it's similar with rhyolite and granite but it's very rapid of cooling makes it a volcanic glass where there was no enough time to form minerals at the time of emplacement.

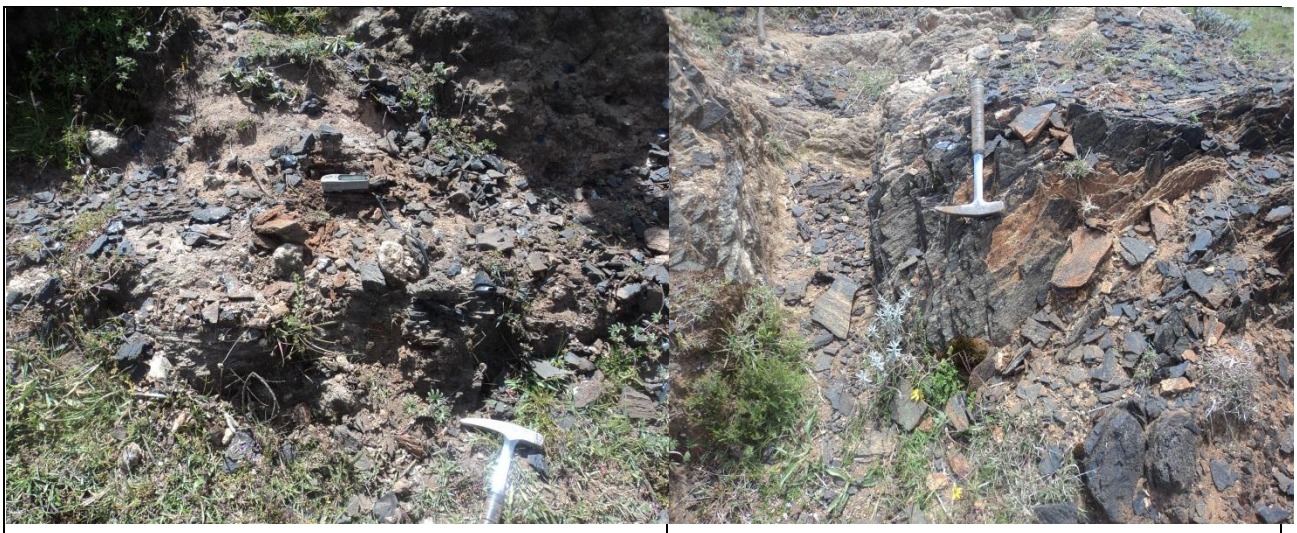

Fig. 3.5: Obsidian flow cropping out in the area; the left is from the north-northeastern section while the right is from the south-eastern section.

The Obsidian is exposed sandwiched within the rhyolite lava flow in the ridges located southeastern and north-northeastern part of the caldera. In some areas it's intercalated with the rhyolite flow. Its thickness reaches a maximum of 1m. In hand specimen, It has a glassy texture (i.e. it is a volcanic glass) which shows a very rapid cooling of magma where there was no enough time to form a mineral during its crystallization. Its color is black, but this doesn't tell us the composition of the rock, because, its color is dependent in trace amount of minerals and its composition is felsic, similar with the rhyolite.

There seems to be a baking effect around the obsidian layer where a dark brownish/reddish material is present. It's useless to see obsidian under petrographic microscope, because there are no or little minerals formed/crystallized.

3.4. The pyroclastic deposits

Volcanic Pyroclasic deposits are results of high gas content magma. When magma with high gas content erupted it becomes energetic. Therefore, instead of a lava flow, it results in fragmental deposit of volcanic origin. These fragments might be welded usually due to its own pressure and temperature or by overlaying pressure to form coherent seem rock like ignimbrite. Otherwise, it's easier to discriminate this kind of rocks, since they are fragmented, from those which are formed from effusive magma, which are coherent. This unit covers the whole of the floor of the caldera and thin ash deposit is found also on the ridges.

The pyroclastic rocks are classified by using their grain size and shape ranging from volcanic ash to agglomerate. And for ignimbrite by its welding which makes it similar with that of rhyolite and trachyte. The volcanic succession of the pyroclastic deposits is given in the following table.

Thickness	Lithologic units	Sub units	Description
1m - 7m	Volcanic ash		Very recent deposit overlaying the rhyolite/trachyte ridges even, in some places, above alluvial deposits.
~90m	Surge deposit	Volcanic ash	Bright white colored ash with pumice clasts immediately overlying the lapilli tuff.
		Lapilli tuff	Bedding, X-bedding showing layer with lapilli size
		Agglomerate	Very big rounded fragments underlying the lapilli tuff.
5m	Ignimbrite		Massive lava flow seeming deposit

Table 3.4: stratigraphy of the pyroclastic deposits

3.4.1. Ignimbrite

Ignimbrite is a volcanic rock formed when pyroclastic deposits are welded to form a coherent rock which sometimes resembles the lava flows ignimbrite/trachyte. But, the presence of rock fragments and fiamme (an elongated/stretched glassy material due to welding) clearly shows it's formed from a pyroclastic deposit (not a lava flow).

This unit is exposed in the western side of the caldera. It resembles the rhyolite, and in some cases it was difficult to identify weather it's an Ignimbrite or Rhyolite. But the presence of some rock fragments helped a lot. Its thickness reaches up to 5m.

Color	Colorless phenocrysts, muddy ground mass+ opaque brown materials ➔ Felsic	
Texture	• Porphyritic (v.fine grained ground mass) ➔ Volcanic • It shows a primary foliation (Eutaxitic texture) • Euhedral phenocrysts (generally alkali feldspars)	
Minerals present & description	Phenocrysts (20%)	Alkali feldspar (5-14%) – generally around 13%
		Rock fragments (3-5%)
		Opaques and glassy (3-5%) generally around 5 %
	Ground mass (80%)	There seems to be a feldspar lath, glassy & opaque material. But difficult to identify individual minerals.
Rock name	Ignimbrite	

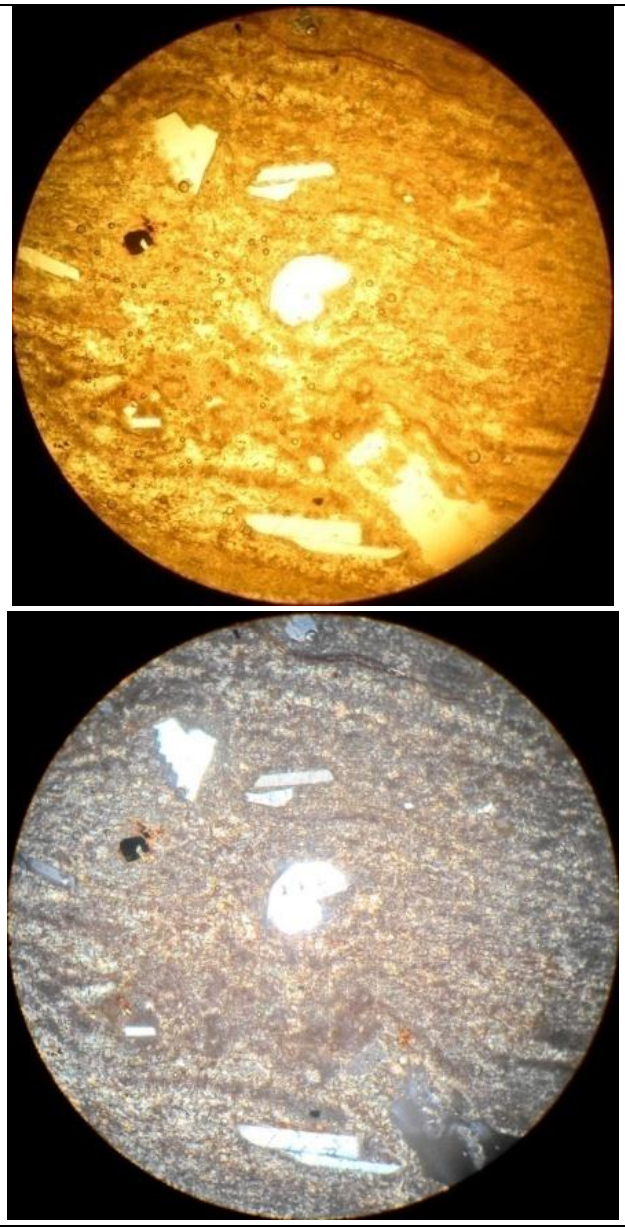

Fig. 3.6: representative photomicrograph of Ignimbrite thin-section (objective – 4X). The top is under PPL and the bottom is under XPL.

Table 3.5: petrographic description of the Ignimbrite

In hand specimen, its texture is fine grained and its color is generally light gray, light brownish, yellowish having similar appearance with the rhyolite. Its texture is fine grained with no visible mineral except some rock fragments in some samples. This condition shows the ignimbite is not sorted. The highly welded ignimbrite is difficult to break resembling rhyolite in appearance.

Under petrographic microscope, the ignimbrite is fine grained having aphanitic or porphyritic texture with phenocrysts of dominantly alkali feldspar (sanidine) and rock fragments, showing the unsorted characteristics of this rock. It's, generally color less & muddy under PPL. Its texture and light colored (color less) telling us that this rock is a felsic volcanic rock with the presence of rock fragments it will fulfill the criteria of being Ignimbrite. The ignimbrite also shows eutaxitic texture, a planar foliation texture formed principally by the welding compaction of pumice and glass shards. The feldspar phenocrysts represent the crystals in the ignimbrite, the rock fragments represent the lithics from the surrounding while the fine ground mass making the eutaxitic texture represents the juvenile magma. The thin-section description is given in Table 3.5 above.

3.4.2. The Pyroclastic Surge deposit

The floor of the caldera (flat land immediate to the lake) is composed of the pyroclastic surge deposits, which shows sedimentary structures like bedding and X-bedding. These are typical characteristics of surge deposits. This unit is also exposed in a little bit elevated area at the western side of the caldera. Its size ranges from fine ash at the top to very big bombs (~15cm diameter) at the bottom. The description given below is mainly based on their size difference starting from the big bombs dominated the agglomerate deposit at the bottom upwards to the fine ones consisting the volcanic ash deposit at the top.

The Agglomerate

The Agglomerate/lappillistone is found at the bottom of the ridge just below the sand sized surge deposit and above the ignimbrite deposit. Most of the pyroclastic fragments are rounded, i.e. they are bombs which are rhyolitic in composition. This unit is exposed in the western side of the caldera just below the sand sized deposits. Fine material (ash) is found between the bombs used as a cementing material. It has a total thickness of about 1 meter. Half of it at the top is dominated by the bombs while the bottom half is dominated by fine materials of ash and the big pyroclastic fragments are more of angular, i.e. they are blocks.

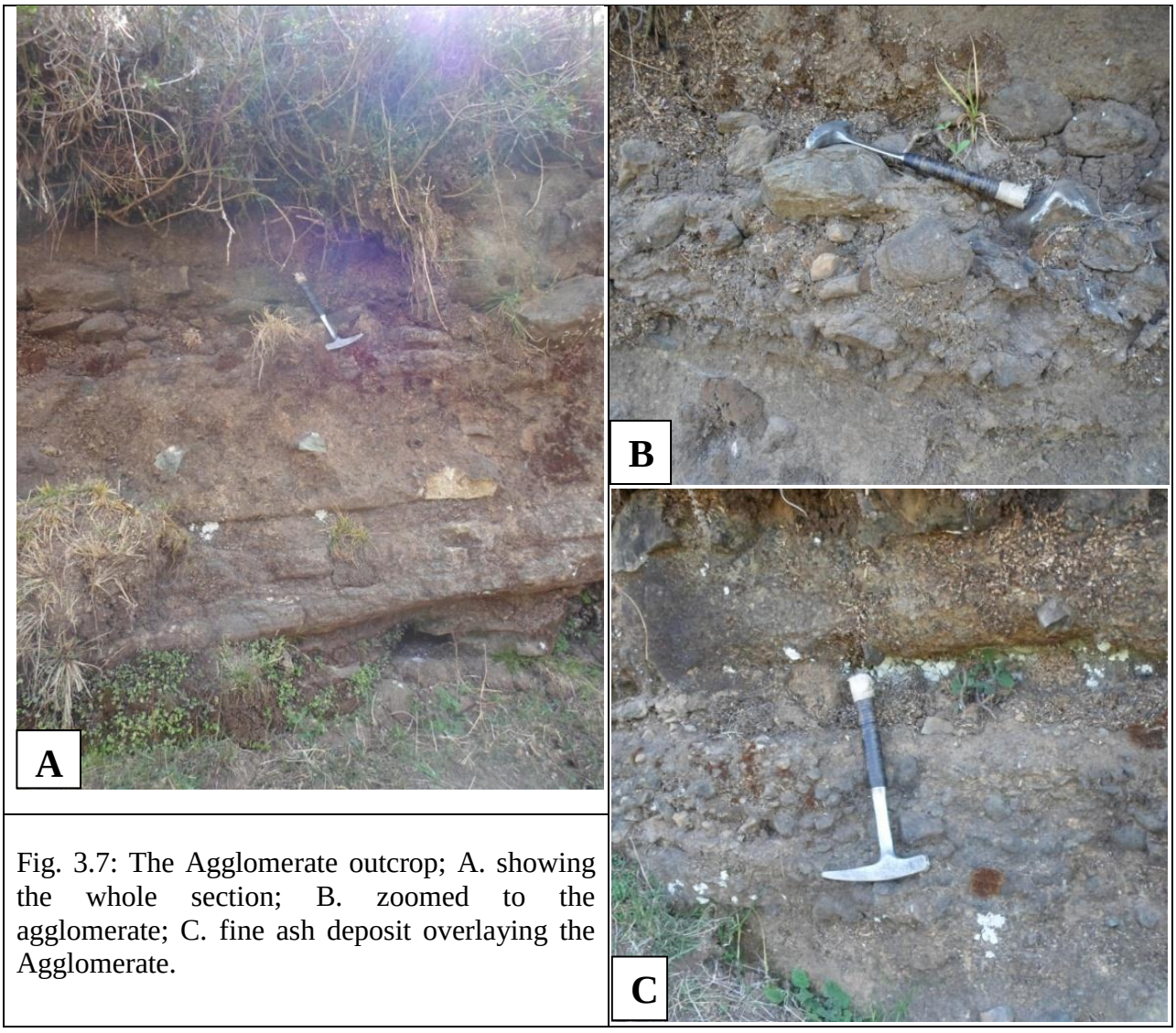

Fig. 3.7: The Agglomerate outcrop; A. showing the whole section; B. zoomed to the agglomerate; C. fine ash deposit overlaying the Agglomerate.

The Lapilli-Tuff

This is the main unit that totally constitutes the low land immediate to the lake (the floor of the Caldera). It's also exposed in the western ridge just above the previous aglomerate. In this part, it's underlain by this aglomerate while in the flat land/ the floor of the lake it's invisible what's found beneath it. But, in one of the caves a soil like deposit is found just below this unit. In some parts, it's overlain by volcanic ash/pumice deposit while most of this unit is covered by only alluvial deposits. The grain size of this unit varies from fine ash to fine lapilli.

This unit shows sedimentary structures like bedding, X-bedding and even leaf casts are in some cases visible at the bottom of this unit. This structures show the presence of water during its

deposition. It also forms caves near the lake, may be due to its interaction with the lake water. These caves were modified by humans and were used as shelters in earlier times. It has a maximum thickness of 90m.

Fig.3.8 lapilli-Tuff (Surge deposit) outcrop; A. showing the section with bedding and X-bedding structure; B. one of the caves. It also shows the sedimentary structures (at the bottom soil like deposit); C. leaf cast on the lappili-tuff.

3.4.3. Volcanic ash/pumice deposits

This unit is widely spread in the area where it's exposed at the top of the steep slope areas (rhyolite) in the gentle slope area and also at the top of the pyroclastic surge deposits.

In the middle of the lowland at the top of the pyroclastic surge deposit there is a bright white colored volcanic ash deposit with pumice clasts. It is most probably formed just following the pyroclastic surge deposit. This unit has a maximum thickness of 4 meters.

In the gentle slope areas below the rhyolite ridges, it shows lareritization, accumulation of black colored material in circular shaped openings. The materials that fill these openings are more wet clayey materials and they have higher magnesium and aluminum content. This deposit is also wetter than the other volcanic ash deposits and its color is more light brownish. It's well sorted suggesting it most probably is an ash fall. Its thickness ranges from 2 meters up to a maximum of 8 meters. This unit is bedded (laminated) ash. In most cases the bed is horizontal. But, in some areas it's inclined; the strike and dip in average is $10^0 \rightarrow 205^0$.

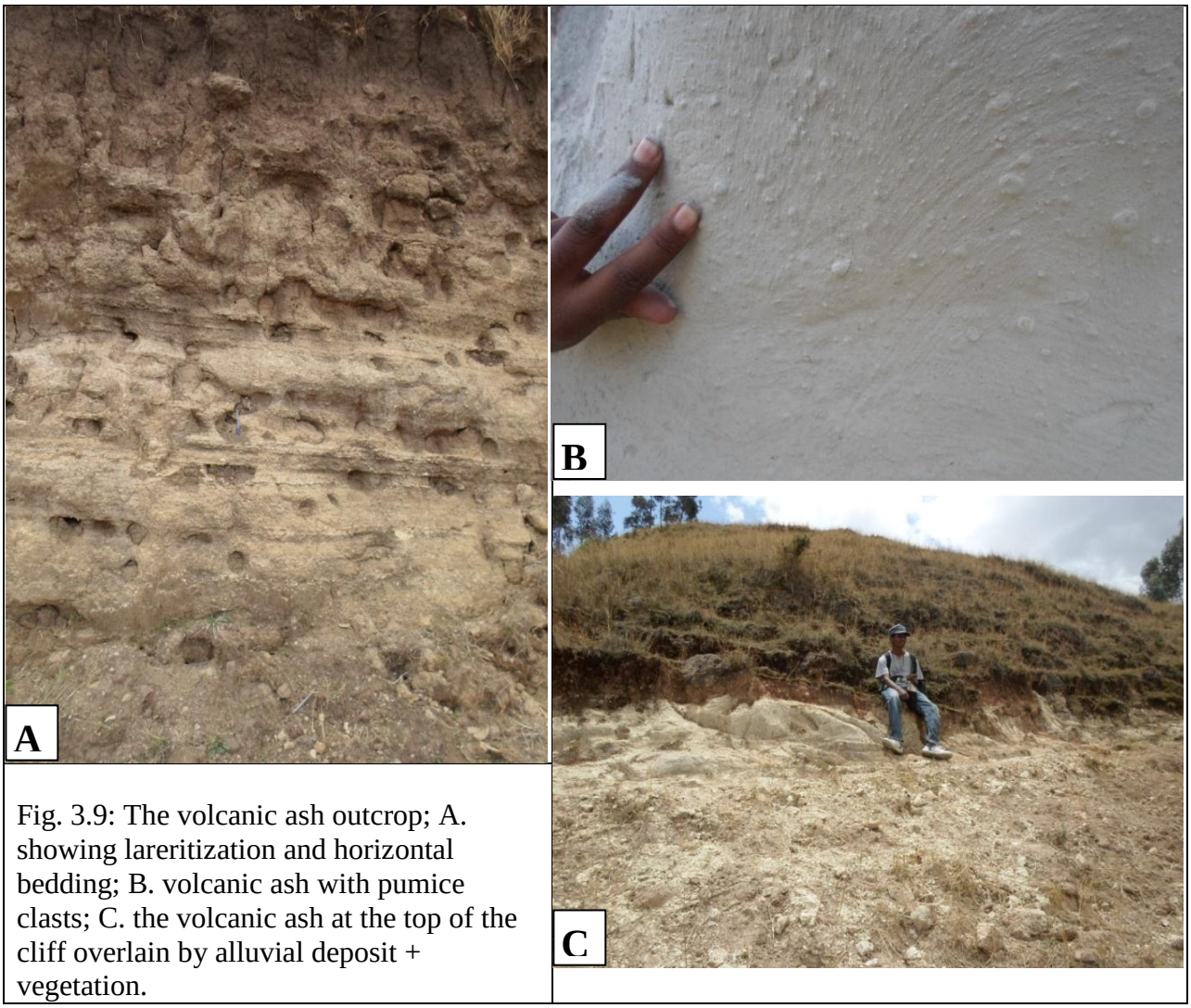

Fig. 3.9: The volcanic ash outcrop; A. showing lareritization and horizontal bedding; B. volcanic ash with pumice clasts; C. the volcanic ash at the top of the cliff overlain by alluvial deposit + vegetation.

The volcanic ash deposit at the top of the rhyolite/trachyte ridges has a different appearance than the previous two. In this area its exposure is found also above a soil deposit and even intercalated with soil (see fig. 10). This shows the presence of a recent volcanic deposit, may be from the

nearby volcanic centers, for e.g., Wenchi crater. The thickness varies from place to place in some areas it's almost absent and in other areas it has a maximum thickness of 2 meters. Its color also varies from place to place (may be due to weathering) from white, light brown to light gray. It's well sorted and it maintains similar local thickness across the area. These conditions show that this ash is an ash fall deposit rather than an ash flow deposit. This unit is dipping towards the lake with varying degree reaching a maximum of 25^0.

Fig. 3.10 Volcanic Ash deposit locally intercalated with soil

3.5. Structural Features

Dendi caldera has almost elliptical shape with about 8.5 km diameter in its longest direction (NW-SE) and 6.5 km in the shortest direction (NE-SW). The total area covered by the caldera is about 44sq. km with a maximum altitude difference of 440m.

Dendi caldera is not that much affected by tectonic structures like fault. As a collapse caldera there has to be a location where the actual volcanic collapse occurs and the actual subsidence of the collapse has to be determined. The tectonic collapse is located around the inner rim of the caldera. This collapse will be the main tectonic and structural feature in the area. This collapse determines the shape and size of the caldera. But, in this thesis work the actual location of the

tectonic collapse is not determined. Therefore, the structures included here in this work are the other structures comparatively smaller than the big collapse structure.

The major structures are the primary structures like bedding and X-bedding in the lapilli tuff (Fig. 3.8 A, B), flow banding and columnar joint in the rhyolite/trachyte (Fig. 3.2 A, B) and bedding/lamination in the volcanic ash deposit (Fig. 3.8 A).

Most of the beddings are horizontal except some disturbed strata and the volcanic ash fall deposit which is deposited following the existing inclination. The inclined beds, esp. the volcanic ash falls at the top of the ridges, are dipping towards the lake with a maximum inclination angle of 25^0. The volcanic ash that shows lareritization has either a horizontal bed or in some areas a little bit dipping bed. The inclined bed has a general dipping trend of southward direction with an inclination of 10^0. The columnar joints in the rhyolite/trachyte shows a general trend of $70^0 \rightarrow 140^0$.

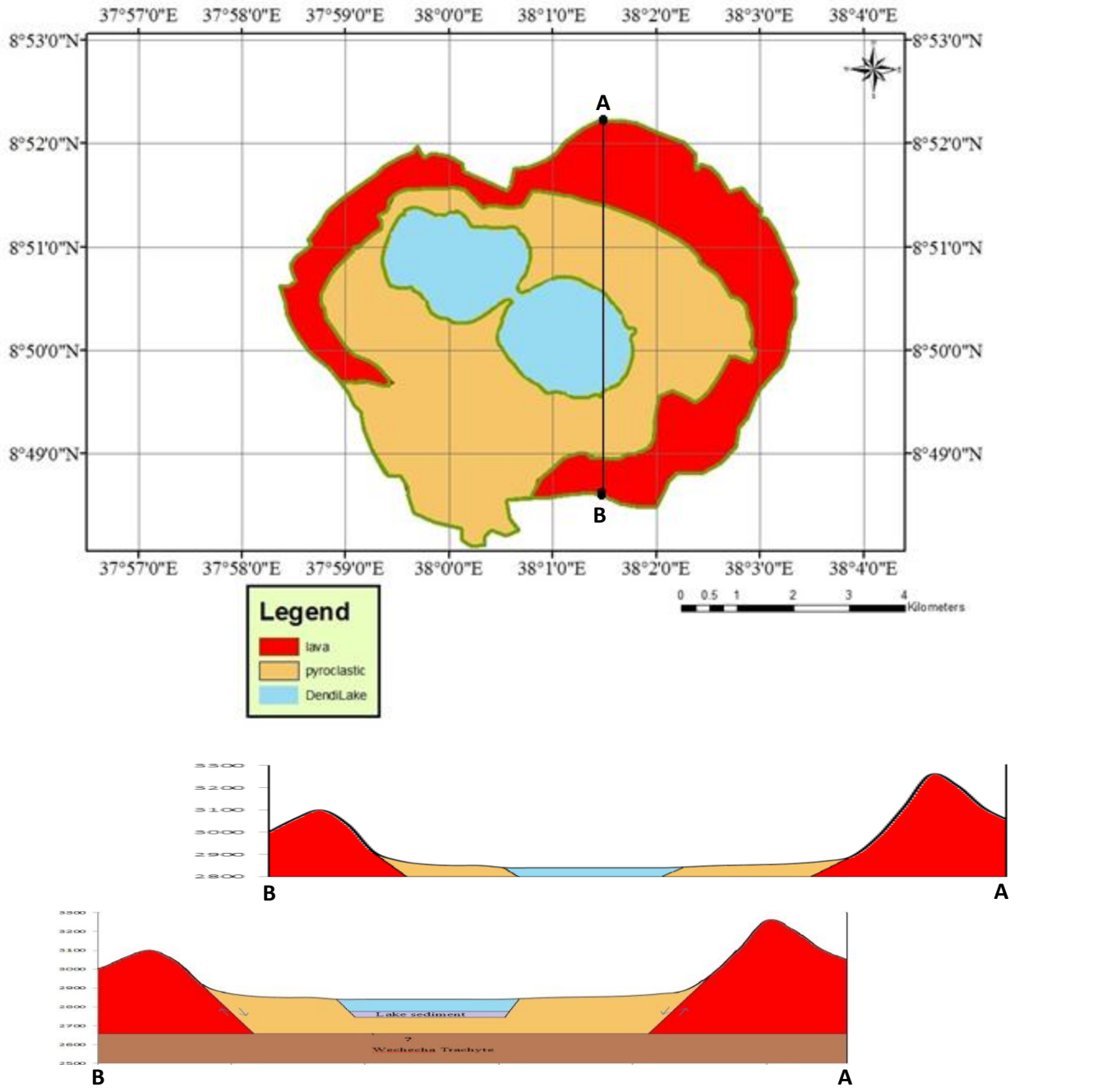

Fig 3.11: Geological map and Cross section of the Dendi Caldera. Vertical scale is exaggerated by 2X over horizontal scale. The bottom cross-section is theoretically extended to locate the bottom unit which is the Wechecha trachyte from literature.

CHAPTER FOUR

4. RESULTS AND DISCUSSIONS

4.1. Classification

There are different methods used for classification of igneous rocks. In volcanic rocks we are more dependent on the chemistry of the rocks because modal composition is difficult to identify and cannot be relied on it. One of the methods used in general classification of igneous rocks is just to use the concentration of SiO2. Depending on the concentration of SiO2, the rocks, then, can be classified into acidic (>63%), intermediate (52-63%), basic (45-52%) and ultrabasic (<45%). If we classify the rocks from Dendi caldera based only on the SiO2 content, most of the lava flows fall in the acidic region while all the pyroclastic fall in the intermediate region.

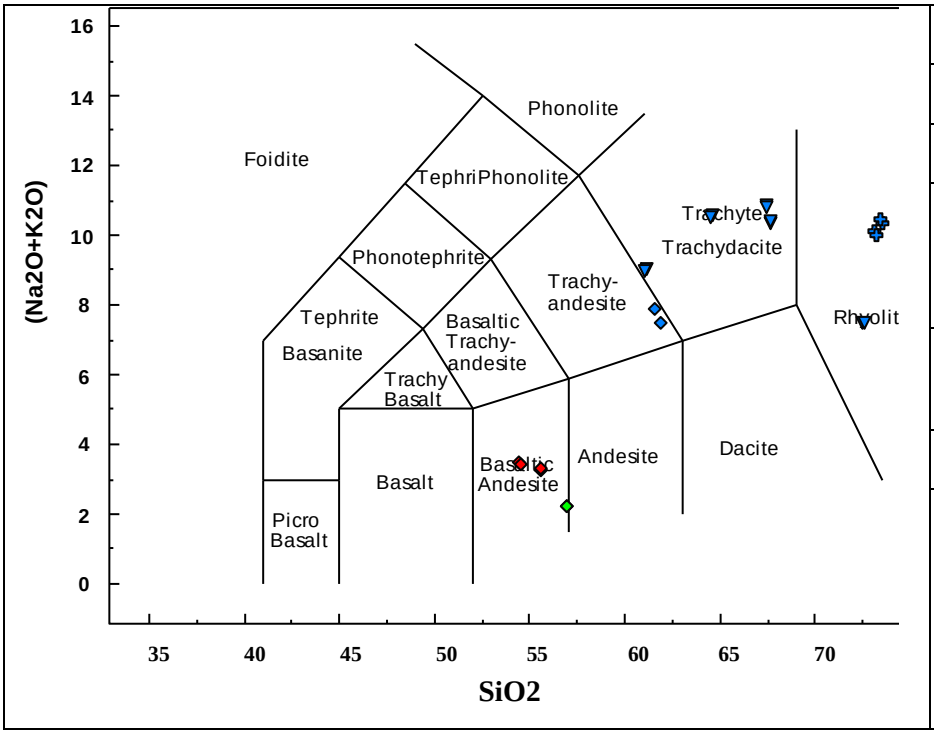

Legend	
+	Obsidian
▼	Rhyolite/trachyte
♦	Volcanic ash/pumice that shows lareritization
♦	Volcanic ash/pumice at the top of the ridges
♦	The lapilli tuff

Fig. 4.1A: TAS classification for Volcanic rocks. All values are wt. %.

According to the Total Alkali–Silica (K20+Na20 Vs. SiO2) classification diagram (after LeBas et.al. 1986), all the obsidians (cross shapes) are compositionally rhyolitic with another rock unit formed from an effusive magma (the rhyolite) crop out in the area is also rhyolitic. But, most of the remaining lavas (triangular shapes) are trachytes/trachydacite. The pyroclastics (diamond shapes) have different composition. For example the volcanic ash (blue colored) that shows lareritization is more of trachyandesite. While, the lapilli tuff (red) in the flat land area is

compositionally basaltic andesite. The volcanic ash (green) at the top of the ridges is on the line that separates andesite and basaltic andesite.

This shows all the lava flows/domes are compositionally either rhyolitic or trachytes/trachydacites. But, the pyroclastic deposits have considerably differing composition which ranges from trachy-andesite, andesite to basaltic andesite. This might be due to contamination from the previously existing materials during the explosion and deposition or they might have different source magma. For example the geochemistry of an inclusion (included layer of dark brownish material within the lapilli tuff) in the lapilli tuff falls in Tephrite-Basanite area. If this unit intercalate with a rhyolitic material the composition of the new mixture will be between the rhyolite and Tephrite-Basanite region which is most probably the Basaltic Andesite. And also the composition of the lateritic soil at the top of and within lareritization showing volcanic ash has a basaltic and basaltic-andesitic composition.

The per alkalinity index (PAI) (Na2O+K2O/Al2O3) of the dendi volcanics show variability due to either initial composition or later alteration where the highly mobile elements Na & K are easily washed away. This is especially seen in the volcanic ash. The less altered obsidian is peralkaline showing an average value of 1.22 whereas the rhyolite/trachyte 0.73 and the pyroclastics 0.23. As it's seen in Fig 4.1B, the Dendi obsidian is Pantellerite peralkaline rhyolite which shows it has higher Fe than Al.

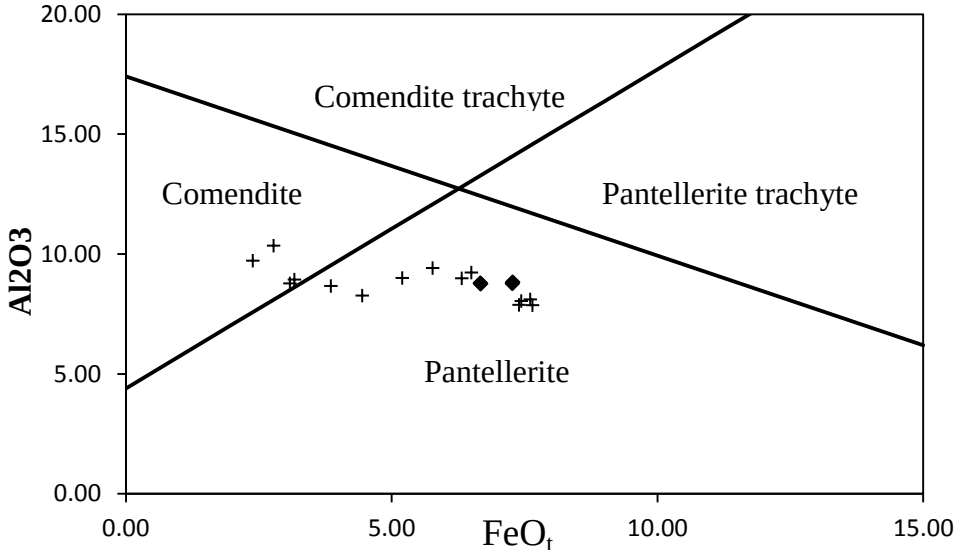

Fig 4.1 B: FeOt vs Al2O3 classification diagram for peralkaline volcanic rocks. Diamond shapes are obsidian from dendi and the cross shapes are from literature in the MER. (Datas are from Boccaleti et.al. 1999; Mazzarini et. al., 1999; Yirgu et. al., 1999)

4.2. Major Element Variations

The obsidian has a very high amount of Si02 (70-75 %), K2O and Na2O than the others while the lappiili tuff and the volcanic ash at the top of the ridges has low amount of Si02 (~55±2%), K2O and Na2O compared to the others. The rhyolite/trachyte shows SiO2 content between 61-72.5% and the volcanic ash that shows lateratization has SiO2 content of ~ 61 % which is more or less similar with that of the rhyolite/trachyte samples. This shows that the volcanic ash in this area has a composition that differs from the other pyroclastic deposits and they might have different source.

The lappili tuff has a higher concentration of MgO (~3.7%), CaO (~8.4%) and TiO2 (~2%) while the obsidian shows a very low concentrations for these oxides with the total absence of MgO (0%) and CaO and TiO2 values are 0.18% and 0.28% respectively. The rhyolite/trachyte MgO values range from 0.02-0.45% with an average value of 0.16% while the CaO and TiO2 has average values of 0.41% and 0.54% respectively. An inclusion in the lapilli tuff which has a darker color has the highest concentration of these elements. 7.7% MgO, 16.8% CaO and 2.39% TiO2. This composition and the color of this inclusion show that the inclusion is compositionally mafic. The legend for all the plots in this chapter is identical to that of Fig.4.1.

The volcanic ash at the top of the rhyolite/trachyte ridges has a very high concentration of MnO (~0.45%) and FeO (13.5%) and Al2O3 (25%) compared to the others. The obsidian and the rhyolite/trachyte have the lowest concentration in Al2O3 and FeO and also P2O5 (~0.05%). The lappili tuff has higher P2O5 concentration (0.49%) and the inclusion in this unit also has higher concentration of P2O5 (0.58%).

Harker's variation diagram for these oxides as a function of silica is presented in Fig. 4.2. On this diagram the oxides with different properties correlate with the SiO2 differently. The K2O and Na2O show a positive correlation with SiO2, i.e. they show an increasing pattern when the amount of SiO2 increases. But, FeO, Al2O3, TiO2 generally have a negative correlation with SiO2, i.e. When the SiO2 concentration increase their concentration decreases and vice versa.

The pattern of SiO2 vs MnO is not that much clear while the pattern of SiO2 vs MgO and CaO seems a little bit negatively correlated but generally it is constant. When the concentration of SiO2 increases their concentration generally doesn't change except their very high value with low silica in the lapilli tuff.

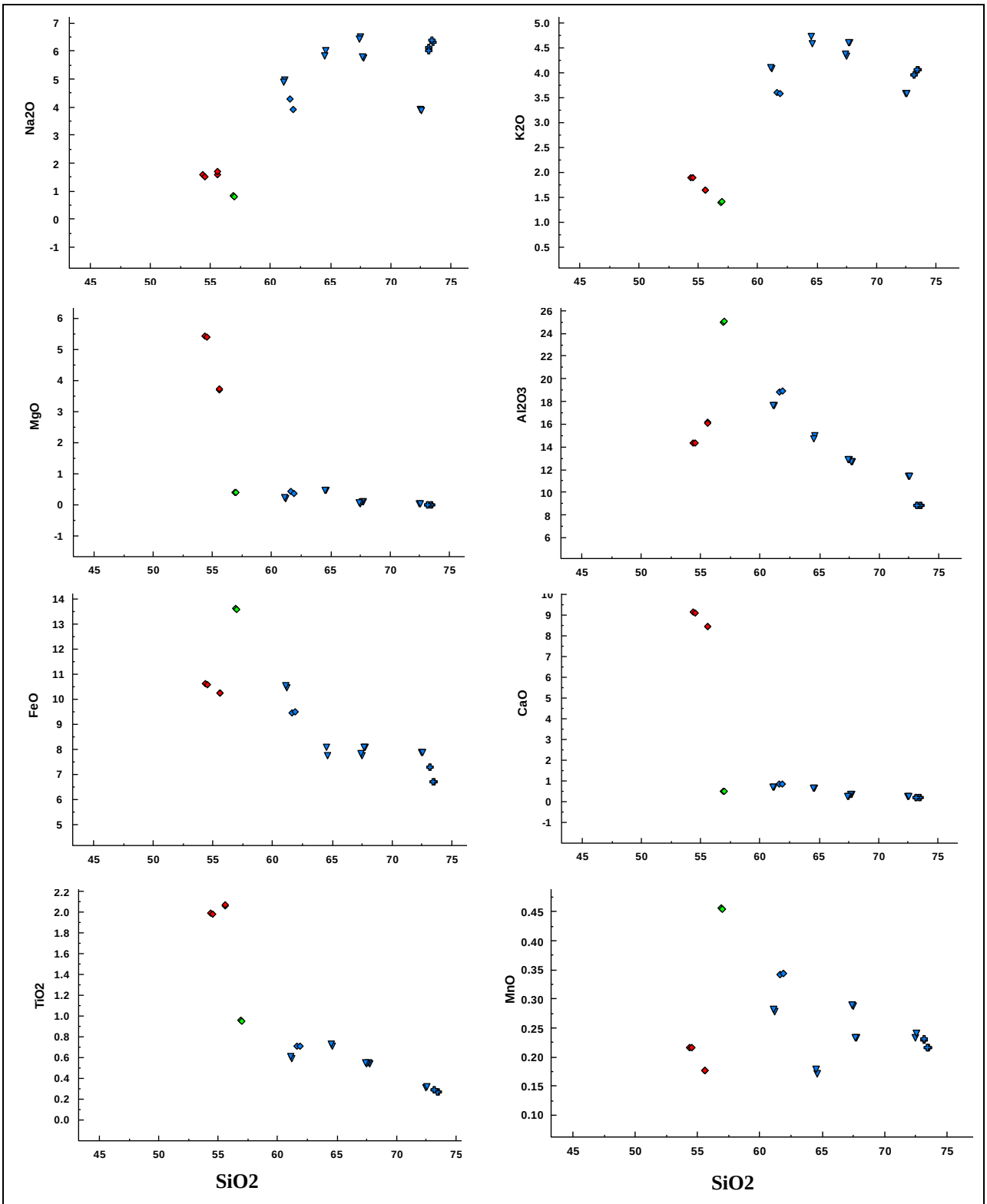

Fig 4.2: Harker variation diagram for Major elements (in the form of oxides) as a function of silica. All values are wt%. Iron is presented as FeO (total)

4.3.Trace Element Variations

Trace and minor elements are often more sensitive indicators of petrogenesis than are major elements. In other words, those rocks, which share a common source, should plot similarly. Note that all of the Dendi volcanic fields look quite similar to one other especially in the spidergram variation diagram.

4.3.1. Trace Element Vs Silica

Harker's variation diagram for trace elements as a function of silica is presented in Fig. 4.3. On this diagram the trends of the trace elements with increasing SiO2 is well visible. Some elements show strong correlation with an increasing SiO2 while the others show weak correlation. The correlation also could be either positive (increases with an increase in SiO2) or negative (decreases with an increase in SiO2).

Variation of Rb has a strong positive correlation with increasing value of the SiO2 with a value ranging from 50ppm (in the lapilli tuff) to 300 ppm (in the obsidian). Similarly, Zr, Nb, Th, (High Field Strength Elements, HFSE) La, Ce, Nd (Rare Earth Elements, REE) and Pb generally shows a positive correlation with increasing SiO2 but the correlation is not as strong as the Rb and their distribution is widespread. The concentration of Zr varies greatly from ~400ppm to ~3750ppm. La and Ce also are widely spread with concentration ranging from 0 to 400 (for La) and 700 ppm (for Ce). The variation range of the other trace elements which shows positive correlation with the SiO2 in the Harker's diagram in ppm is: Nb (50-450), Nd (100-400), Th and Pb (10-70).

More or less strong negative correlation is shown by Sr and Ba. Both are Large Ion Lithophile Elements (LILE) with more or less similar property. The Sr has a higher value in the lapilli tuff reaching 480ppm but in the remaining rocks its value ranges between 3.2 ppm (for the obsidian) - 42.9ppm (for the volcanic ash). This very low concentration of Sr in combination with the positive correlation and relatively higher concentration of Rb, results in a very high value of Rb/Sr ratio. The average concentration of Ba shows distinct values between the pyroclastics and the lava flows/domes. Ba concentration in the rhyolite/trachyte and obsidian samples is 19.5 ppm, in the lateritic volcanic ash is 146.5 ppm and in the lapilli tuff and the volcanic ash at the top of the ridges is 395.17 ppm.

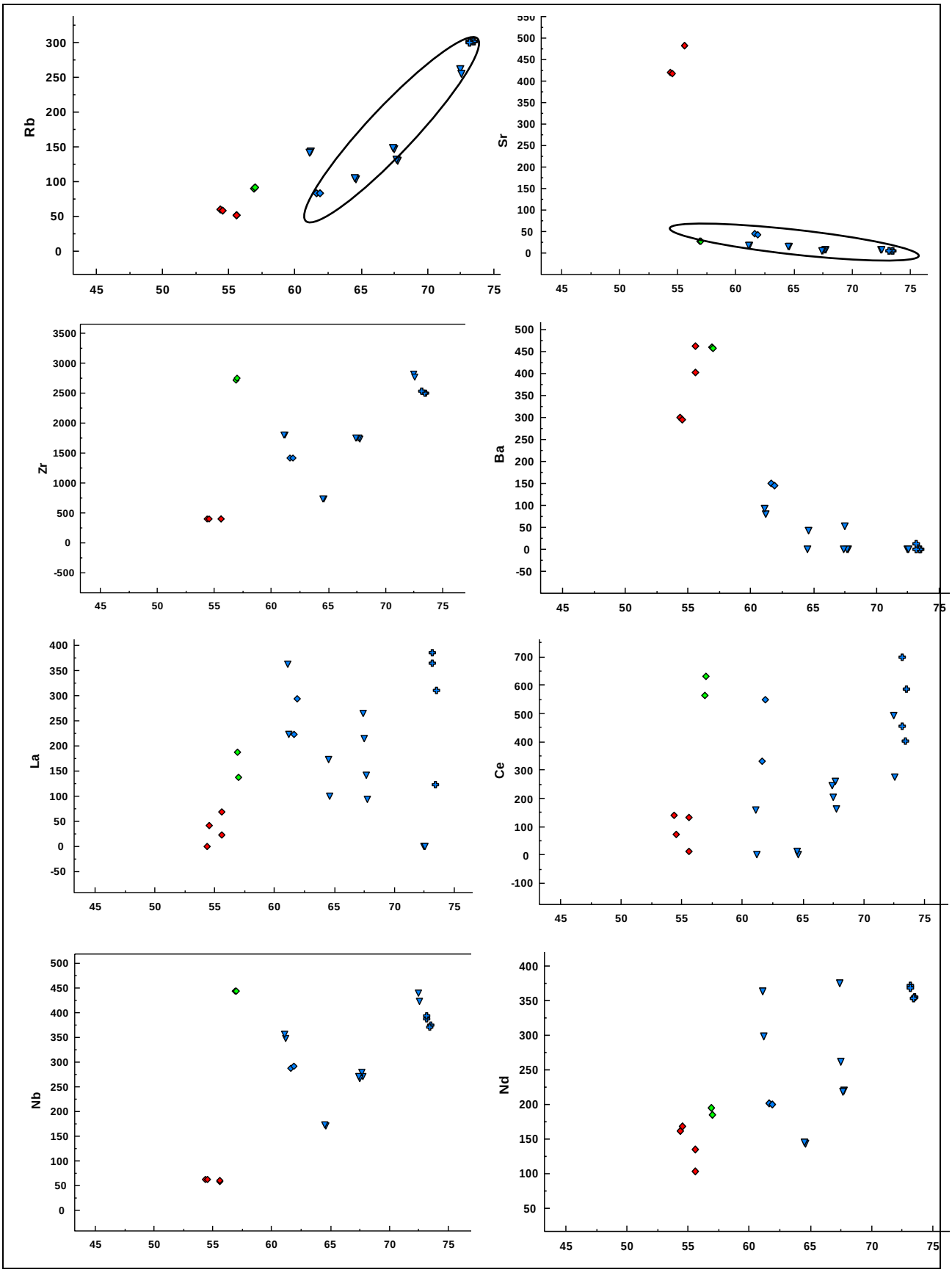
Rb
Sr
Zr
Ba
La
Ce
Nb
Nd

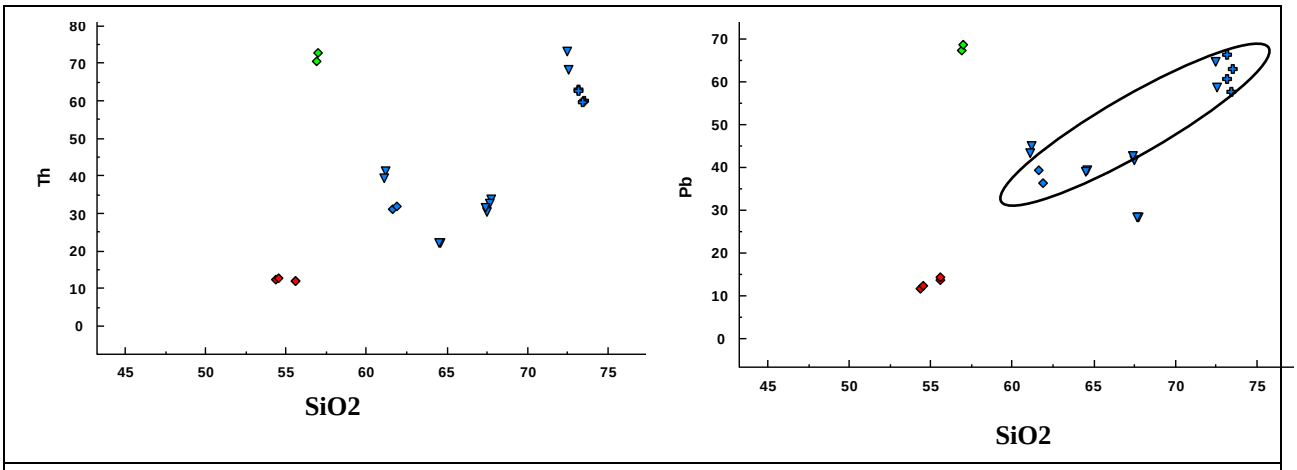

Fig 4.3: Harker variation diagram for Trace elements (in ppm) as a function of silica (SiO2). SiO2 values are in wt%.

4.3.2. Trace element Vs Trace element

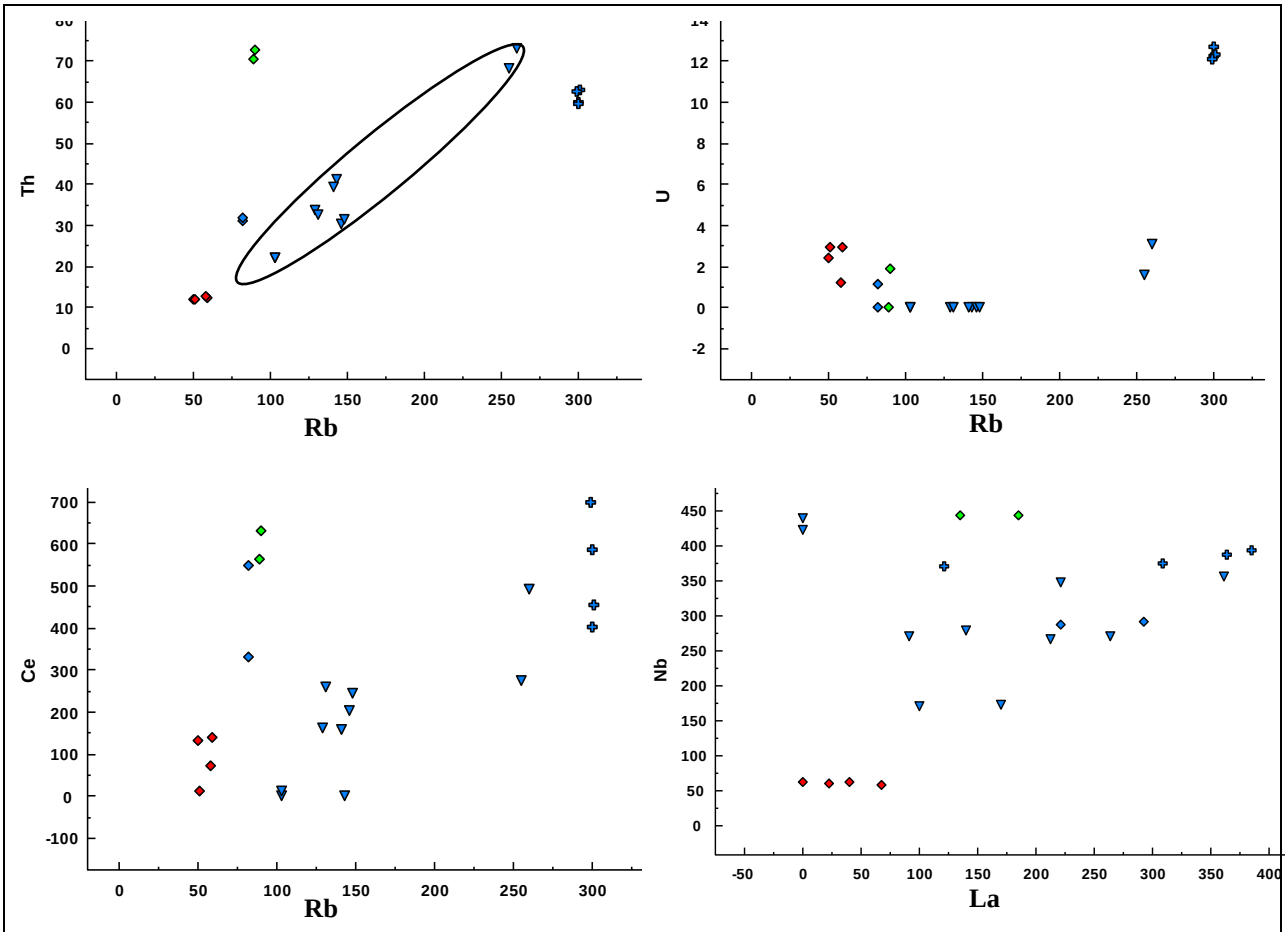

Fig 4.4: Trace element Vs Trace element (both in ppm) variation diagram

A series of lavas related by crystal fractionation usually will plot on a straight line on incompatible element – incompatible element scatter plots. Scattered values in these diagrams might show either alteration in the samples or the weakness of detecting low concentration elements in the analysis employed.

On trace- trace elements scatter plots Fig. 4.5: Rb versus (Th, U and Ce) and La versus Nb shows more or less a positive linear correlation especially for the effusive rocks. These linear positive correlations possibly explain the fact that the two highly incompatible elements are fractionated through extended amounts of crystal fractionation. It may also indicate that the Dendi Caldera products are from the same source related by crystal fractionation.

4.3.3. Trace element Ratios

Table 4.1 shows selected trace element ratios for the Dendi volcanics. The linear enrichments of incompatible element ratios plotted against traces elements are less diagnostic compared with element - element plots. In the ratios, some values are missed. This is due to their denominator value which is zero and dividing a number by zero is impossible. The zero values might be due to detection limits of the instrumentation used during the geochemical analysis.

Although, in the Dendi caldera, they also support that the lava series in the study area are resulted from single magmatic source. The trace versus trace ratio (Nb/Y, Rb/Ba, Rb/Sr, Rb/Nb, Zr/Nb and Nb/Th against Rb) plots of the Dendi Caldera (Fig 4.6) shows a general positive linear correlation interpreted as the lavas are from same magmatic source and differs as a result of fractionation.

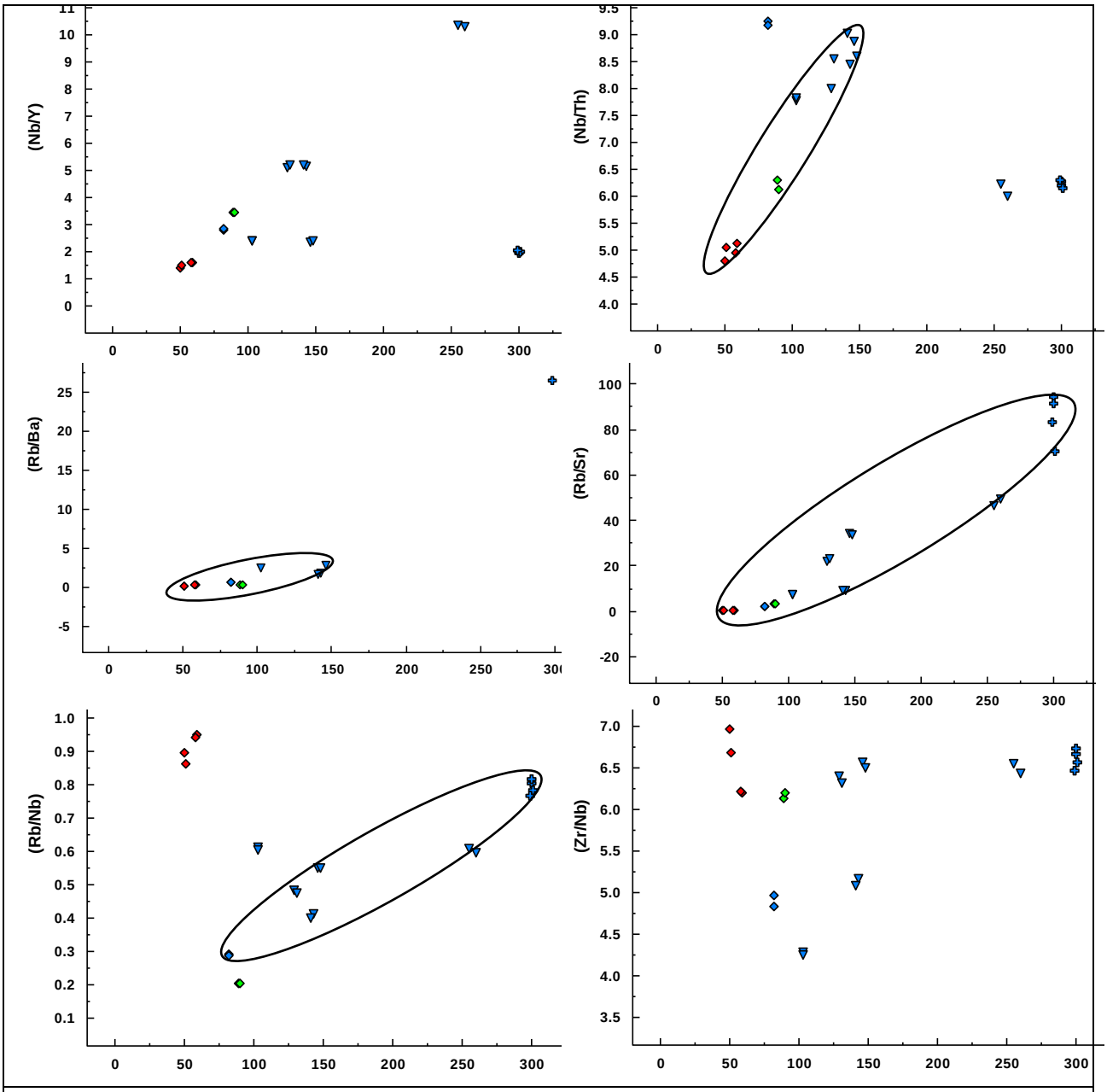

Fig 4.5: Trace element (Rb) Vs Trace element ratios (both in ppm) variation diagram

S. No	R. Type	La/Nb	Zr/Nb	Rb/Nb	Nb/Th	Th/La	Rb/Sr	Rb/Ba	Ba/Y	Nb/Y	La/Yb
Ob 01	Obsidian	0.83	6.66	0.8	6.26	0.19	93.97	-	-	1.97	41.2
Ob 01	Obsidian	0.33	6.73	0.81	6.2	0.49	91.18	-	-	1.95	10.61
Ob 02	Obsidian	0.94	6.56	0.78	6.13	0.17	70.12	-	-	2	26.38
Ob 02	Obsidian	0.98	6.45	0.76	6.28	0.16	83.11	26.48	0.06	2.05	57.46
PM 00A	Volcanic ash	0.78	4.95	0.29	9.25	0.14	1.92	0.55	1.46	2.78	38.95
PM 00A	Volcanic ash	1.01	4.82	0.28	9.16	0.11	1.95	0.58	1.4	2.85	94.52
PM 00B	lapilli tuff	1.2	6.96	0.89	4.78	0.18	0.11	0.11	11.22	1.38	-
PM 00B	lapilli tuff	0.38	6.67	0.86	5.03	0.52	0.11	0.13	9.95	1.48	-
PM 02	rhyolite/trachyte	0.59	4.28	0.61	7.77	0.22	7.1	2.45	0.59	2.37	-
PM 02	rhyolite/trachyte	0.99	4.24	0.6	7.82	0.13	6.97	-	-	2.37	-
Pu 01	Volcanic ash	0.42	6.12	0.2	6.29	0.38	3.24	0.19	3.53	3.41	22.68
Pu 01	Volcanic ash	0.31	6.18	0.2	6.11	0.53	3.32	0.2	3.51	3.41	13.47
Tuff 02	lapilli tuff	-	6.19	0.95	5.11	-	0.14	0.2	7.69	1.6	-
Tuff 02	lapilli tuff	0.65	6.21	0.94	4.94	0.31	0.14	0.2	7.53	1.59	-
Tuff 02in	inclusion within the lapilli tuff	1.23	5.47	0.8	4.9	0.17	0.05	0.1	12.35	1.51	-
Tuff 02in	inclusion within the lapilli tuff	1.17	5.46	0.79	5.3	0.16	0.04	0.1	11.68	1.52	-
Rh 02	rhyolite/trachyte	0.64	5.16	0.41	8.44	0.19	8.77	1.81	1.17	5.12	-
Rh 02	rhyolite/trachyte	1.02	5.08	0.4	9.02	0.11	8.73	1.55	1.33	5.18	-
Rh 04	rhyolite/trachyte	-	6.42	0.59	5.99	-	49.15	-	-	10.29	-
Rh 04	rhyolite/trachyte	-	6.54	0.61	6.21	-	46.36	-	-	10.3	-
Rh 05	rhyolite/trachyte	0.34	6.39	0.48	8	0.37	22	-	-	5.06	-
Rh 05	rhyolite/trachyte	0.51	6.31	0.47	8.53	0.23	22.98	-	-	5.15	-
Rh 06	rhyolite/trachyte	0.8	6.55	0.55	8.85	0.14	34	2.81	0.46	2.34	-
Rh 06	rhyolite/trachyte	0.98	6.49	0.55	8.58	0.12	33.64	-	-	2.37	29.33

Table 4.1: Trace element ratios

4.4. Spidergram

This spider diagram shows selected trace element content and pattern of the Dendi volcanics. Essentially, it plots trace and minor element contents from Dendi caldera rock units normalized to MORB. The MORB standard values are from Bevins et al. (1984).

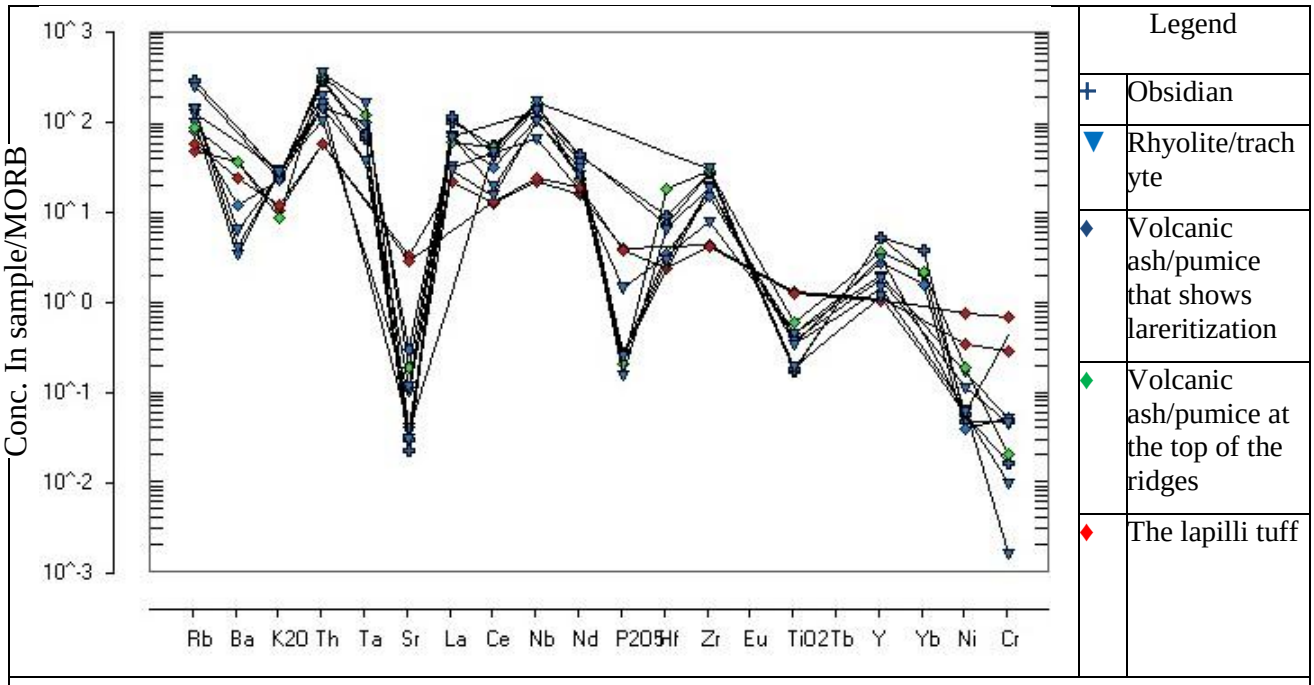

Fig. 4.6: Spider diagram (MORB normalized) showing trace element content of the Dendi volcanics. Standards are those of Bevins et al. (1984).

The spidergram shows a general decrease from left to right. In other words, it has higher concentration of incompatible elements than compatible elements which is the actual case of such more of acidic rocks. The main reason behind this is, during fractionation the compatible elements incorporate with the solid residue while the incompatible elements incorporate with the liquid which remains with the acidic rocks and have the highest concentration in the last stage of the fractionation. The negative anomalies are usually due to fractionation (removal) of some minerals.

The Dendi volcanics show strong negative anomaly in Barium, Strontium, Phosphorus, Titanium and Chromium. This means the Dendi volcanics fractionates those minerals that consist the elements listed above including Apatite (P) and Fe-Ti oxides. The negative anomaly of Cr/Ni shows there might be fractionation of mafic minerals which finally results in such

compositionally felsic rock. Strontium negative anomaly is usually due to fractionation of Ca bearing plagioclase while the Barium negative anomaly probably is due to fractionation of alkali feldspar which is well visible in the thin-section of the rocks as a phenocryst assemblage.

The spider diagram above also shows positive anomaly in Thorium, Niobium, Zircon and Yttrium. These elements are incompatible elements (they incorporate with the liquid). That's why their concentration is high in the most evolved rock (i.e. rhyolite) thus they show a positive anomaly in the spidergram.

4.5. Discussion

4.5.1. Petrogenesis

In Ethiopian igneous province during Miocene –Pliocene there was uplift, rifting and building of basaltic shields with associated rhyolites and phonolites. About 10ma is marked by one of the major episodes of rifting (Kazmin et al., 1980).

The presence of rift – related volcanics on the plateaus can be explained by the possibility that the Afar plume material may have been channeled to adjacent favorable fracture systems allowing 'fissure type' volcanic eruption to take place away from hotspot.

Several models have been proposed to explain the origin of silicic magmas in the Ethiopian volcanics (Barberio et. al. 1999 and references therein). These include:

- Fractional crystallization of mantle derived basaltic magma with or without (limited) crustal contamination
- Partial Melting of the continental crust (anatexis) or partial melting of under plated basic igneous rocks/cumulates followed by crystal fractionation of the resulting magma.

The origin of huge volumes of silicic extrusive rocks (usually ignimbrites) in the Afar depression and the main Ethiopian rift (MER) is attributed to fractional crystallization of basaltic magmas with limited crustal contamination. For example, previous studies in the silicic centers at DebreZeyit found that most silicic magmas are the result of fractional crystallization from parental basaltic liquids (Gasparon et al., 1993) and studies for the origin of rhyolites throughout the MER suggests similar interpretation of fractional crystallization (e.g., Ayalew 2011; Ayalew and Ishiwatari, 2011).

In addition, two-stage model has been proposed for the genesis of the Asela – Ziway pantellerites in the Main Ethiopian Rift (Tura et al., 1999). It involves small degrees of partial melting of a basaltic under plate to produce the least differentiated silicic magmas, which in turn undergo moderate degrees of fractional crystallization to generate the most evolved silicic rocks.

In this thesis work the Dendi volcanic area and the rock samples from the caldera are geochemically and petrographically analyzed. These geochemical and petrographic results from the present work will be more profitably examined for evidence of fractional crystallization model rather than the other options mentioned earlier.

The fractionating mineral assemblage is normally indicated by the phenocrysts present. But, the early crystallized mineral might successfully be removed from the melt and we might not get the fractionated minerals as a phenocryst assemblage. The petrographic investigation indicates that the major phenocryst phases in the lavas are alkali feldspars (sanidine/orthoclase) and opaque minerals (Fe-Ti oxides).

Major elements chemistry displays features that agree with fractionation of the mafic mineral assemblage that is also supported by trace element variation plots.

The Mid Oceanic Ridge Basalt (MORB) normalized trace element variation diagram (Spidergram) (Figure 4.4) displays enriched highly incompatible elements and a lower concentration in the less incompatible elements. It also shows a sharp falls in Sr, Ba, TiO2 and P2O5 and Cr which verifies fractionation of feldspar, plagioclase, apatite and titano - magnetite. Strong depletions in Sr, Ba, and Ti in the more felsic rocks obviously produced by fractional crystallization of some combination of plagioclase, alkali feldspar, apatite, Fe-Ti oxides, and titanaugite (Barker, 1996 and references there in)

The lavas also have high concentration of Nb content i.e. 369- 392 ppm for the obsidian, ~298.5 ppm for the rhyolite/trachyte, for the lapilli tuff ~ 60.2 and for the other volcanic ashes ~300. Similarly, the Th concentration for these rocks is higher, which is: 61.2 ppm for the obsidian, ~39.3 ppm for the rhyolite/trachyte, for the lapilli tuff ~ 12.1 and for the other volcanic ashes ~51.4. Both Nb and Th also show a positive anomaly on the Mid Oceanic Ridge Basalt (MORB) normalized trace element variation diagram (Spidergram).

A very high Rb/Nb and La/Nb ratios characterize crustal rocks and the partial melts derived from these crustal rocks (Pearce et al., 1973). In the table 4.1 below trace element ratio characteristics of Dendi volcanics are compared with rhyolite formed by partial melting of the crust (1-3) and the WegelTena rhyolite (4), Guna volcanics (5-7), and Chefe-Donsa Pumice (9) which are mantle derived and that show a limited crustal contamination.

No	**Lavas**	**Rb/Nb**	**La/Nb**
1	Malusni, peru rhyolite	22-45	0.8-1.7
2	Loch saridain UK rhyolite	7-9	2.6-2.7
3	Yellow stone rhyolite	2-5	0.8-2.3
4	WegelTena rhyolite	0.8-1.3	0.8-1.2
5	Guna Rhyolite	0.93-1.31	0.76-1.03
6	Guna Trachyte	0.40-0.57	0.37-0.84
7	GunaPhonolite	0.31-0.89	0.34-0.70
8	ChefeDonsa pumice	<1.34	<1.1
9	Dendi obsidian	<0.81 (~0.79)	<0.98 (~0.77)
10	Dendi Rhyolite/trachyte	<0.61 (~0.53)	<1.02 (~0.73)
11	Dendi Pyroclastics	<0.95 (~0.62)	<1.23 (~0.79)

Table 4.2: Comparison of trace element ratios (Rb/Nb and La/Nb) in different volcanic provinces. (Data sources are; No 1-4: Ayalew D. and Yirgu G. (2003) and references there in; No 5-7: Adise Mekonnen (2006); No 8: T. O. Rooney et.al. (2012))

The comparison shows that the Dendi volcanic incompatible trace element ratios are different from those of typical crustal melts and similar with the WegelTena rhyolite, ChefeDonsa Pumice and the Guna volcanics implying that they did not originate by partial melting of the crust. Instead, the geochemical features are consistent with their derivation from mantle derived basaltic magma by low pressure fractionation.

Partial melting vs. fractional crystallization

Trace-element behavior as a result of silicate-melt equilibria is described in a number of familiar equations (e.g., Shaw, 1970; Arth, 1976). Partial melting is generally modeled by an equilibrium batch melting equation such as:

$$C^i/C_0^i = 1/F + D^i - FD^i$$

Whereas fractional crystallization is described by the Rayleigh equation:

$$C^i/C_0^i = F^{D^i-1}$$

(In which C^i=concentration of element (i) in the liquid, C_0^i=concentration of element i in the starting mineral-melt assemblage, F=fraction of liquid).

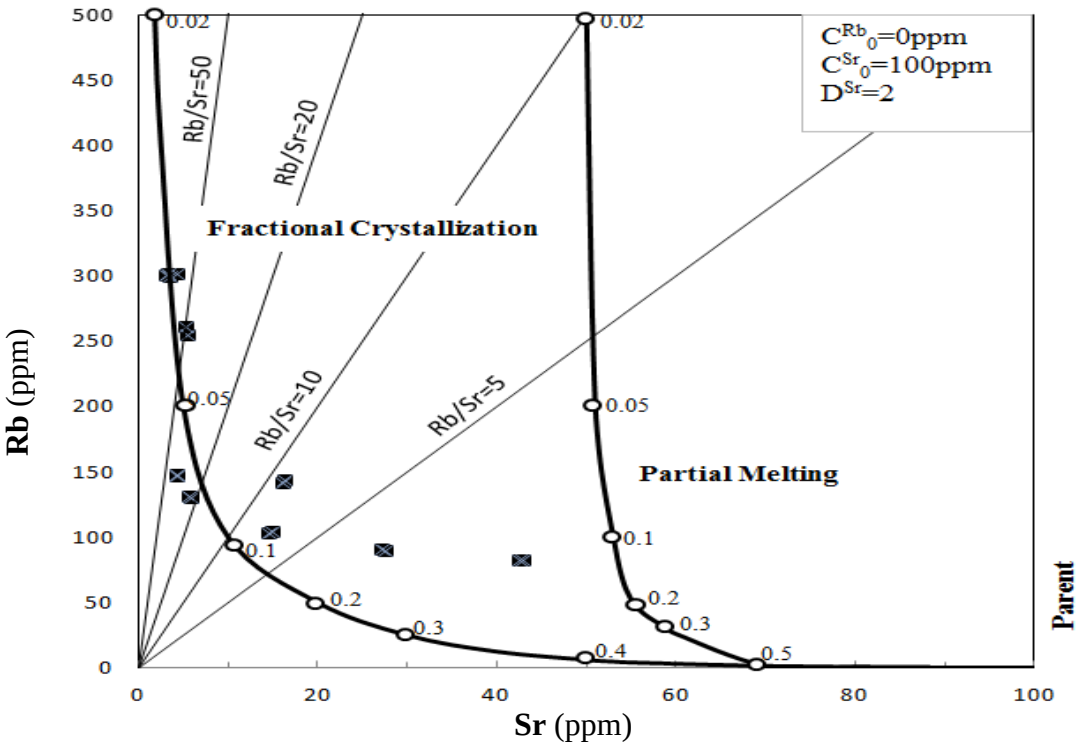

Fig 4.7: Model Sr vs. Rb concentrations (1) expected as a result of differing degrees of partial melting as opposed to Rayleigh fractional crystallization for the same parent composition (modified after Halliday et.al. 1991)

As seen in Fig 4.7, Strontium is depleted much more rapidly during crystal fractionation than in melting. Thus, it is almost impossible to achieve low Sr concentrations (and correspondingly very high Rb/Sr) through equilibrium partial melting. Therefore it's concluded that the only closed system model capable of generating such very high Rb/Sr characteristics in rhyolites is fractional crystallization (Halliday, 1989). In addition to this, such very high Rb/Sr characteristics also show the presence of a significant crustal magma chamber at the time of eruption. Many pre-caldera rhyolites with low Sr concentrations like that of the Dendi caldera are therefore likely to reflect the presence of a large magma system, rather than small pockets of

unrelated melt (Arzi, 1978; Bacon et al., 1981; McKenzie, 1985; Metz and Mahood, 1985; Wickham, 1987; Huppert and Sparks, 1988; Sparks et al., 1990);.

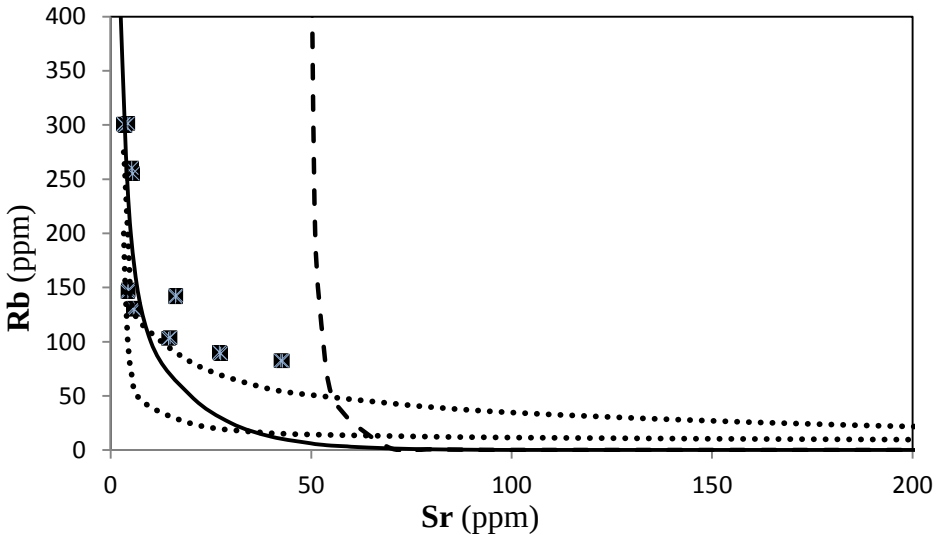

Fig 4.8: Model Sr vs. Rb concentrations (2) expected as a result of differing degrees of partial melting (broken line) fractional crystallization (solid line) for the same parent composition (modified after Halliday et.al. 1991) and calculated assimilation fractional crystallization from basaltic crustal magmas where the Precambrian basement rocks are considered as assimilant (modified after Barberio et. al. 1999)

As it's seen in fig 4.8 above in modeled Rb-Sr concentration diagram, assimilation might be occurred during the formation of the dendi volcanics especiallt for the pyroclastics. But, alteration might be the reason for such values since the unweathered obsidian values clearly shows pure fractional crystallization with limited contamination.

Sr shows a very low concentration and strong negative anomaly on the spidergram (the Mid Oceanic Ridge Basalt (MORB) normalized trace element variation diagram). Note that contamination cannot be responsible for the very low observed Sr concentrations. In fact, exceedingly low Sr concentrations in a rhyolite are inconsistent with post-fractionation crustal contamination (Halliday et al., 1989). The observed low Sr concentration also ruled out the hypothesis that suggests partial melting of underplated basaltic magma. Since basalts are enriched in Sr, their product will not give such a very low Sr values in rhyolite/trachte (Barberio et. al. 1999).

4.5.2. Caldera Formation

Collapse calderas are sub-circular depressions, in volcanic areas, whose diameter is considered to be larger than that of explosive vents and craters (Williams, 1941), possibly reaching many tens of km, as La Garita, USA (Lipman, 2003). Calderas may be characterized by a variable amount of subsidence, ranging from few meters to few kilometers. Their shape may be subcircular, or more commonly elliptical, possibly reflecting the influence of a regional tectonic control (Holohan et al., 2005, and references there in).

Calderas are formed under various tectono-magmatic conditions, as along felsic (or silicic) volcanic arcs in convergent settings (De Silva, 1989; Cole, 1990; Yoshida, 2001), mafic and felsic oceanic and continental divergent settings (Mohr and Wood, 1976; Gudmundsson, 1998; Bosworth et al., 2003), felsic strike-slip settings (Bellier and Sebrier, 1994) and mafic hot spots (Newhall and Dzurisin, 1988, and references therein). Despite this variability, there is a tendency for felsic explosive eruptions to be related to calderas formed in a shorter time span (hours to days), triggering catastrophic events. Conversely, moderate effusive mafic activity is usually associated with calderas formed over broader time spans (days to years) (Newhall and Dzurisin, 1988, and references therein).

Two mechanisms have been proposed to explain caldera formation. In the most popular model, calderas are the surface expression of the emptying of the magma chamber during effusive or explosive eruptions. As a result of an underpressure within the magma chamber at some point before the collapse, the roof of the reservoir yields, forming a depression at surface (Williams, 1941; Druitt and Sparks, 1984; Branney, 1995; Lipman, 1997). The amount of magma that must be erupted to induce collapse varies between a few percent to 40%. Almost all of the volatile rich magma will be forced out from the magma chamber after the collapse is induced. (Martì et al., 2000). The alternative mechanism explains caldera collapse as a result of an overpressure within the chamber; the overpressure induces doming and subsequent apical tensile stresses, which may lead to the initiation of collapse (Gudmundsson, 1988; Gudmundsson et al.,1997; Burov and Guillou-Frottier, 1999; Guillou Frottier et al., 2000).

Primarily based on field data, five end-member caldera geometries or styles (piston, piecemeal, trapdoor, downsag, funnel) have been proposed (Fig. 3.11; e.g. Lipman, 1997) and commonly referred to in the literature (e.g. Cole et al., 2005, and references therein).

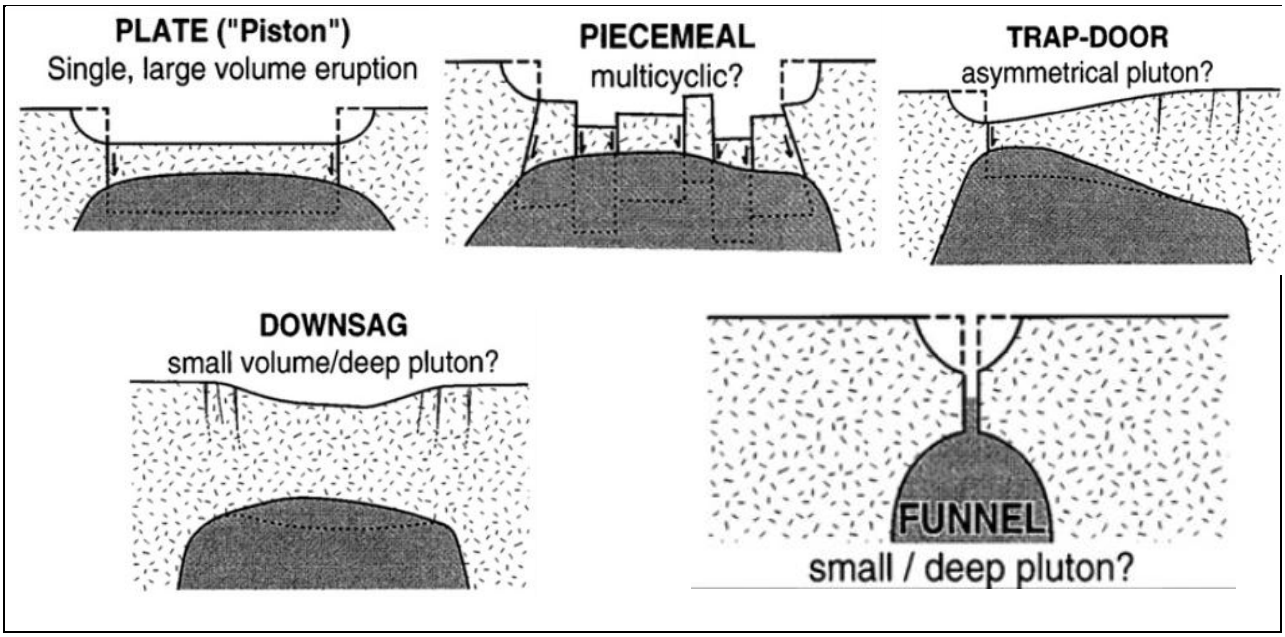

Fig. 4.9: Established caldera end-members proposed in the literature (after Lipman, 1997; Cole et al., 2005).

Piston-type calderas are bordered by a ring fault, delimiting the sinking central block; piecemeal collapses result from the differential vertical movement of multiple independent blocks; trapdoor collapses area symmetric depressions, with an unfaulted hinge; downsag calderas are broad depressions characterized by inward tilted margins; funnel calderas are narrow and deep cone-shaped depressions, often associated with gravitational slumping.

A study by Acocella V. (2007) on the analogue models of calderas identifies the following points which clearly show the main mechanisms by which most of the natural calderas are formed.

- ✓ The experiments simulating an overpressure within the reservoir, even if in agreement, require unrealistic uplifts to develop depressions; therefore, they do not explain most natural calderas.
- ✓ All experiments simulating calderas resulting from underpressure within the reservoir point to a consistent scenario defining the evolution and structure of calderas, regardless of any experimental boundary condition (materials, apparatus, scaling, volcanic edifices, regional stresses). These models may constitute a suitable analogue.
- ✓ In underpressure experiments, caldera collapse develops in 4 stages, proportional to the amount of subsidence, progressively characterized by: a) downsag, b) reverse ring fault, c) peripheral downsag and d) peripheral normal ring fault.

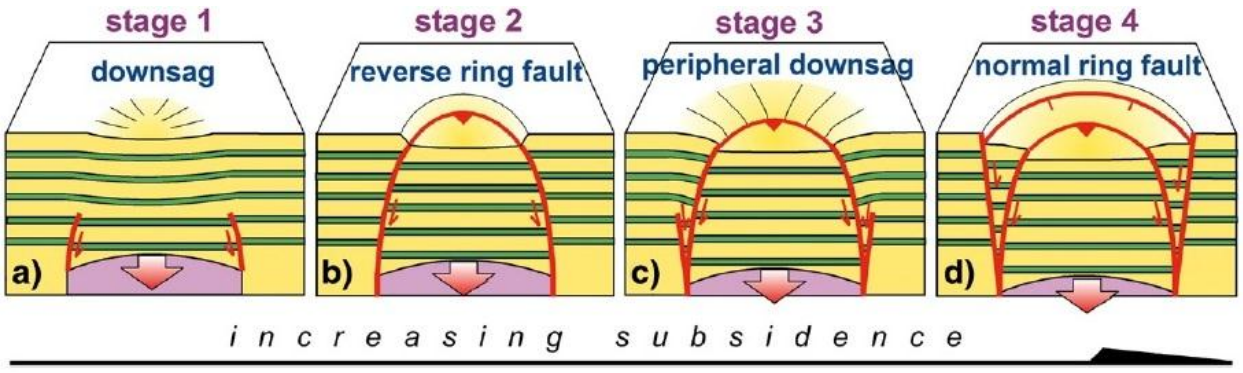

Fig. 4.10: Schematic representation of the four stages of evolution of caldera collapse, obtained in all the underpressure experiments, as a function of the amount of subsidence. (after Acocella V., 2007)

Most of the available geological and geophysical data at known calderas are consistent with the experimental structural features, as well as with their progression. This consistency between experiments and geological - geophysical data has two main implications: (a) the experiments allow an understanding of the subsurface structure of natural calderas by knowing their surface structure; (b) considering the surface structure of calderas it may be possible to discriminate their deeper structure and belonging to any of the four experimental stages.

Several calderas, with a defined overall structure, maybe suitable natural examples of these four stages, defining caldera types along a subsidence continuum. Many other natural calderas, when their surface structure is sufficiently known, may be reconciled with any of the four evolutionary stages, to infer their subsurface structure.

The obtained relationship between the evolutionary stage of a caldera and its d/s (diameter/subsidence) ratio shows that stage1 calderas are characterized by $d/s>40$, stage2 by $18<d/s<40$, stage3 by $14<d/s<18$ and stage4 by $d/s<14$. The consistency between experiments and nature suggests that, in principle, the d/s ratio may permit to evaluate the overall structure and evolutionary stage of a caldera even when its surface structure is poorly known.

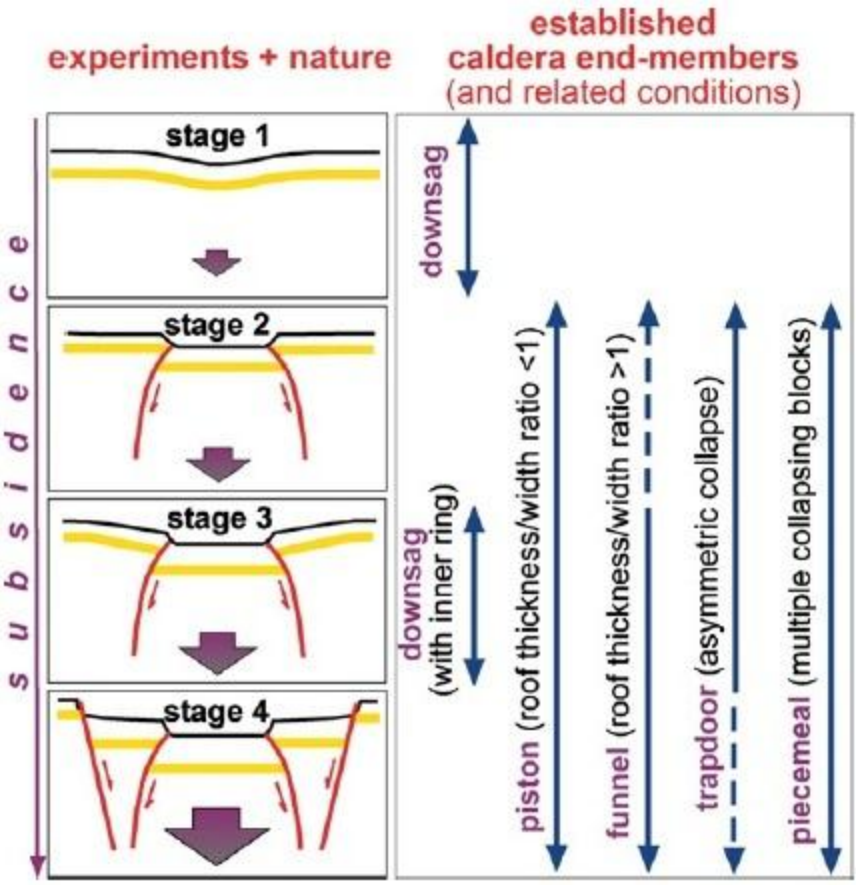

Fig. 4.11: Evolution of natural calderas geometries, summarized in four stages from a combination of experimental data and actual examples. To the right: caldera end-members and related conditions to form. (after Acocella V., 2007 and references there in)

The d/s values of the Dendi caldera falls in the stage2 and/or stage3 range of this category where the actual value falls around 18. The stage2 evolution of the caldera suggests that it is a reverse ring fault and stage3 is peripheral downsag.

While the d/s ratio has an overall relation with the evolutionary stage of a caldera, it may be independent of the volume of erupted magma. However, the location of syn- and post-collapse volcanism may depend not only upon the amount of collapse, but also on the roof aspect ratio.

The evolutionary stages explain the architecture and development of the established caldera end-members along a continuum, where one or more end-members may correspond to a specific stage. While such a continuum is defined by precise structural features, controlled by progressive subsidence, specific geometries result from secondary factors (roof aspect ratio, collapse symmetry, pre-existing faults), not diagnostic of the collapse stage. These considerations allow

proposing an original classification of calderas, incorporating their structural and genetic features.

Different experiments may explain the ellipticity of a part of natural calderas elongated parallel to the regional extension, while the control of pre-existing structures, though not simulated, may explain the elongation of elliptic calderas oblique or parallel to the regional structures. In the case of the Dendi caldera, it has a general elongation of NW-SE direction which is almost orthogonal to the NNE-SSW trending regional structure of the Main Ethiopian Rift. This shows the influence of the MER might affect it orthogonally or the rift totally doesn't have any influence on the ellipticity of the caldera.

The main sequences included for the formation of the Dendi caldera are as follows. The first to form is the doming by rhyolite/Trachyte lava and subsequently followed by the rhyolite trachyte lava flow forming an elevated area (the Dendi Mountains) and leaving the magma chamber empty/near empty/. Then, cracks are initiated due to an empty magma chamber on the lava dominated Dendi Mountains. These cracks might be forced by regional tectonics or pre-existing structures. The subsidence of the caldera is followed when the empty magma chamber cannot support the overlying body anymore which is accompanied by energetic pyroclastic eruptions during and/or after the collapse forming pyroclastic deposits in the caldera and might also out of the caldera.

The Crater Lake is the vent through which all the volcanic products from the magma chamber forced out prior, during or after the formation of the collapse. The other option might be, after the formation of the Dendi caldera a secondary eruption takes place which leaves its vents now as the Dendi Crater Lake.

The volcanic surge deposit in the caldera might also be the result of a later eruption where there has been water body during its deposition. This is clarified when we see that the lapilli tuff is a surge deposit with different sedimentary structures. But the time gap between these eruptions, i.e. the eruption that form the lava flows (before/during the caldera formation) and the eruption that form the surge deposit (during/after the caldera formation), is unknown. But there might be a significant gap between these two eruptions as there seems to be a paleosoil developed beneath the lapilli tuff. There exists also leaf casts at the bottom of the lappili tuff (see Fig 3.8 B & C).

CHAPTER FIVE

5. GEOMORPHOLOGY

5.1. Introduction

The Dendi caldera is found partly in the Central Lava Highlands and Massifs within the Western Highland Plateaus. These plateaus are well known for their rugged topography. The study area is featured by varied topography ranging from plain lands and steep slope areas to vertical cliffs. The area is situated in a topographically elevated area with the lowest point, at the lake level with the highest point, at the top of the mountain in the North East side of the caldera.

The Dendi Mountains with the neighborhood Wenchi Mountains are more elevated than the surrounding area. This is evidenced by the presence of outflowing rivers from these mountains to join the Blue Nile basin. There might be many reasons for such topography. The first reason could be either these mountains were uplifted or the eruption from these central volcanoes gives these mountains higher elevation. The other reason might be with the surrounding area where this area has been collapsed or eroded and peneplained sometime in the past. But, the first one gives more sense and it is most probably the main reason why the Dendi and Wenchi mountains stood higher than the surrounding area.

5.2. Geomorphic Units

The study area is featured by varied topography ranging from plain lands and steep slope areas to vertical cliffs. The area is situated in a topographically elevated area with the lowest point, at the lake level, is 2830m above sea level, while the highest point, at the top of the mountain in the North East side of the caldera, is 3270 m above sea level. The geomorphology of the area can be grouped into four geomorphic units: The flat lands at the top of the mountains, the vertical cliffs, the steep slope areas, the gentle slope areas and the flat land surrounding the lake. A brief description of each unit is rendered below.

The flat lands at the top of the mountains: this area is covered by soil and some indigenous vegetation plus small grasses. The bed rock also crops out in some areas. In limited areas the local community uses it for farming purpose. In the western side of the caldera, the people use it as a settlement area. Some pictures of this unit are given below.

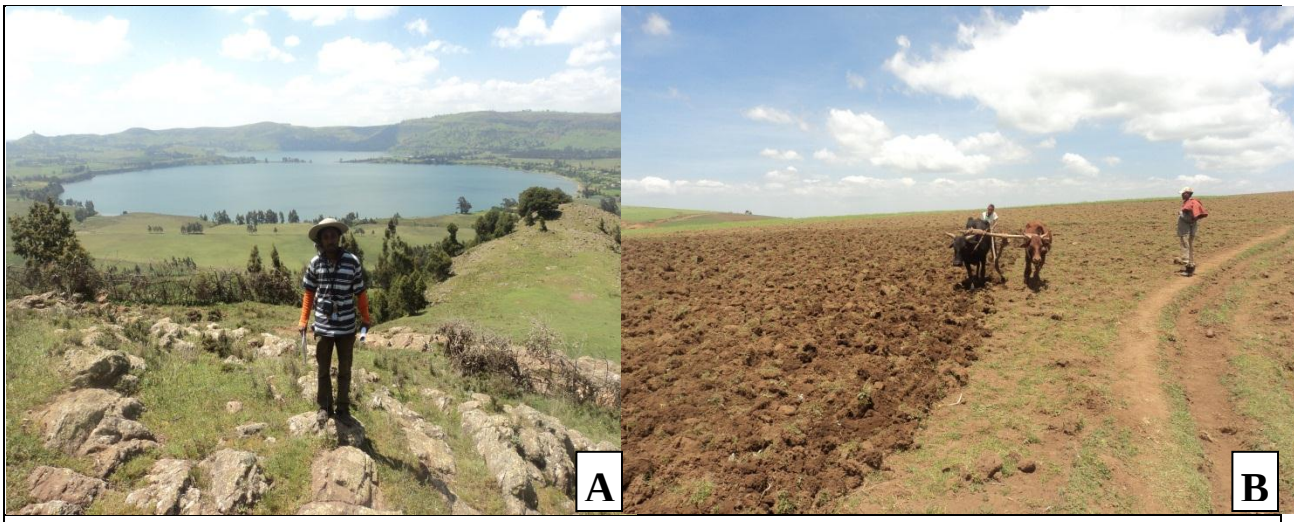

Fig. 5.1: The flat land at the top of the mountains; A, exposed bed rock; behind the lakes from SE to NW direction; B, ploughing activities showing thicker soil.

The vertical cliffs: It is just above the steep slope area where the hard rock is well exposed and climbing becomes impossible. Most of my fresh hard rock samples of rhyolite/trachyte are collected from here. It's a vertical cliff with no vegetation and soil formation. In some places the vertical cliffs have dome shape which is seen in Fig. 5.2 below.

Fig. 5.2: The vertical cliffs; In the right overlying the steep slope areas.

The steep slope areas: This area is just below the cliffs. It's widely used for farming purpose. It's also the source of most of the springs in the caldera. It's subjected to erosion because of its slope and intensive activity of improper farming (Fig 5.3 B, C). Because its slope is steep contour farming and terracing are suggested method of farming to conserve the soil and protect it from erosion. Some big gorges are also present in this area (Fig. 5.3 A).

Fig. 5.3: The steep slope areas; A, big gorge; B, farming land; C, thick vertical soil profile at the boundary between the gentle and steep slope areas.

The gentle slope area: It is located below the steep slope areas, where most of the people living in the Dendi locality settled in this area and also farming is widely practiced here. Even if it has a gentle slope the farming practices has to be changed like the steep slope areas. This unit has thick soil cover. But due to the problems mentioned above Soil erosion also attacks this area. In contrary with the steep slope area, this area has more trees which can potentially conserve some amount of soil (Fig. 5.4 A).

The flat land surrounding the lake: It's a flat land composed of pyroclastic and alluvial deposits, which is widely used by the locals for grazing. Near the natural bridge which separates the two lakes there are settlements and farming activities. The only church in the area is also located here in this area. This area has many gorges through which water and sediment is transported to the lakes. It also consist an area subjected to inundation where during rainy season it will be converted to swamp and no one can go over there even the animals.

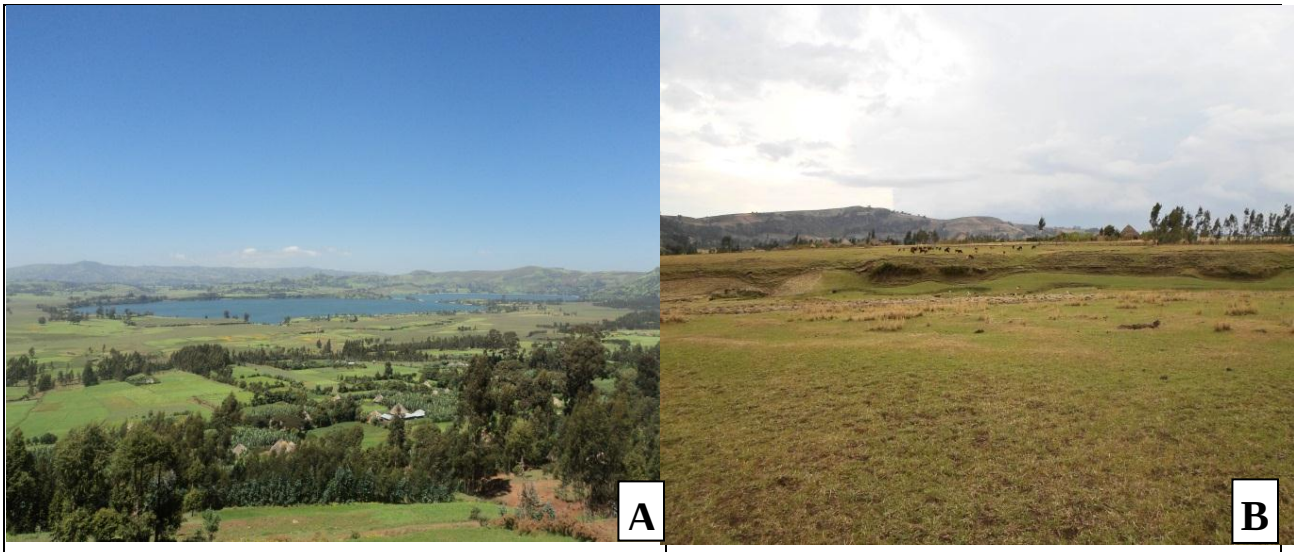

Fig. 5.4: A, settlement and farming in the gentle slope area; B, the flat land surrounding the lake with stream channel; it also uses for grazing.

With the exception of the cliffs, the top of the area is covered by pyroclastic and/or alluvial deposits with varying thickness. There is no natural forest in the area. Different vegetation also covers these areas. Savanna grasses are the most common and widely cover these areas dominantly the flat land surrounding the lake. Bamboo forest, eucalyptus and other varieties are also found here and there. There are several scattered settlements and villages inhabited by the local people who practice rain feed subsistence agriculture. But the ploughing method they are using and the absence of forests and/or many big trees derives the soil to erosion.

Different processes are attributed to the formation of such a rugged landscape. The main reason for these landscapes in the Dendi locality is the tectonic process that forms the caldera. A caldera is a geological feature formed by the near-total eruption of magma from beneath a volcano, leading to collapse of the volcanic structure into the now-empty magma chamber. This collapse

typically leaves a crater or depression where the volcano stood, and later volcanic activity or streams and rivers can fill the caldera with younger lavas, ash, pyroclastic rocks, and sediments. A crater lake can be formed, if the caldera is later filled with water.

5.3. Water bodies

There are many springs located mostly in the steep slope areas and flows as streams towards the lake with the exception of tributaries of Huluka River. Springs can be grouped according to the nature of the water-conducting passages as seepage, tubular, and fissure. As the geology and geochemistry seen in the Dendi Caldera reveals the springs in this area are categorized as fissure. Some of the streams flow throughout the year while the others flow only in rainy seasons.

During rainy seasons the streams are fed mainly by the rainfall. The Dendi locality is among those localities in Ethiopia which gets high amount of precipitation every year, where the average rainfall reaches as high as 1,172mm. Most of the streams within the caldera flow towards the Dendi Lake. While, the streams in the south and south western area of the caldera flows away from the caldera and joins the Blue Nile (Abay) basin. The south eastern lake also flows out through these streams during overflow periods to join the Huluka River.

The two connected lakes forming a shape that looks like the number '8' are the most beautiful features in the area. The location map, the geologic map and Fig 5.1 A and Fig 5.4 show this beautiful scene. Generally the lake level is at 2830m above sea level with a depth around 56m. These lakes are the lowest point in the area and they are volcanic vents. There is no inflow towards the lake from outside of the caldera. While the lakes flow out of the caldera and joins the Blue Nile (Abay) basin. Due to a reason which I don't really know, the lakes give no service to the local community. No one swims on them, the lakes don't have any fish and due to lack of technology and absence of well-trained farmer the lakes are not giving use for irrigation purpose.

The drainage pattern in the study area shows a radial drainage pattern surrounding the remnants of the Dendi volcanic cone. Such patterns typically form around volcanoes, as rainfall has equal potential to move downslope on all sides of the cone and incise channels. Through these channels all the water (both from rain fall and springs) joins the lakes in the center.

5.4. Soil and Erosion

The Dendi caldera is subjected to weathering and erosion. Physical disintegration and chemical

dissolution plus the effect of organisms attribute for the weathering of preexisting rocks in the Dendi caldera. Water erosion is the dominant erosive process in the caldera but due to the slope instability erosion by gravity has also a significant impact in the area.

Formation of soil (Pedogenesis) is a process that is dependent on the combined effects of these soil-forming factors: parent material, climate, living organisms, topography, and time. The combination of any of these factors could produce different types of soils. The amount of soil produced and the final place of deposition is also dependent on one or more of these factors.

The parent material for the soil formation in the Dendi caldera is restricted to the rhyolite/trachyte lavas, the pyroclastic deposits and the vegetation and organisms in the area. In addition to being the parent material, these organisms facilitate the weathering process, for e.g., plant roots can disintegrate the bed rock to varying size of boulder and gravel by creating cracks. In contrary to this, the trees can protect erosion of soil by keeping it by their roots which makes them important for soil conservation.

Due to its high altitude and low latitude location, the caldera receives considerable amount of rain and the dry seasons give elevated temperature with the mean maximum is around 24^0C. This condition, getting high amount of rain water and fluctuating temperature throughout the year, facilitates the weathering of the rocks and soil formation. The topography of the area is much suitable for sediment transport to the lake because of its high elevation difference. The time span during the formation of the soil is also an important factor because soil formation can. The amount of time a soil requires to develop varies widely according to the action of the other soil-forming factors. The soils deposited by the stream may be as young as days to months. The other soils may take hundreds of thousands of years to form. For e.g., the soil formation where the Acheulian artifact has been found is older than 150000 years while in other areas it might be less than 10000 years old.

Different types of soils are found in the study area. Generally, the color ranges from red, reddish brown, dark brown to black while the texture of the well-developed soil (A-horizon) is generally silty clay. But, there are rock fragments and other coarse materials and then the bed rock in the layers below (B, C & D horizons). Above the A horizon, i.e. the O horizon, organic matter dominate which consists of loose organic matter such as fallen leaves and other biomass. For the soil profile see Fig. 5.5.

The thickness of the soil deposits vary from place to place. On top of the cliffs, the thickness might vary between an exposed bed rocks (no soil at all) and might reach as high as 1 meter. The sloppy areas have the thickest soil in the area reaching more than 3 meters with red color soil and the lateritic soil in the volcanic ash with black and dark brown color also located here. The soil profiles are exposed by a road cut and different gorges in the area. The flat land adjacent to the lake has thin soil cover with a maximum thickness of 75cm except the stream channels which accumulates even very new soil with varying thickness.

Geochemical analysis is done on the lateritic soil which is located within and above the lateritic volcanic ash deposit. As the geochemistry reveals these units have very different composition than the surrounding rock units. Among the major elements, these units show higher concentration in Al2O3 (25-27%), TiO2, P2O5, FeO, MgO and CaO while they show lower concentrations in SiO2, Na2O and K2O. HFS elements have lower concentration in the soil while among the LIL elements the Ba and Sr concentration is above the rhyolitic and below the pyroclastic rocks. But, the reverse is true for Rb.

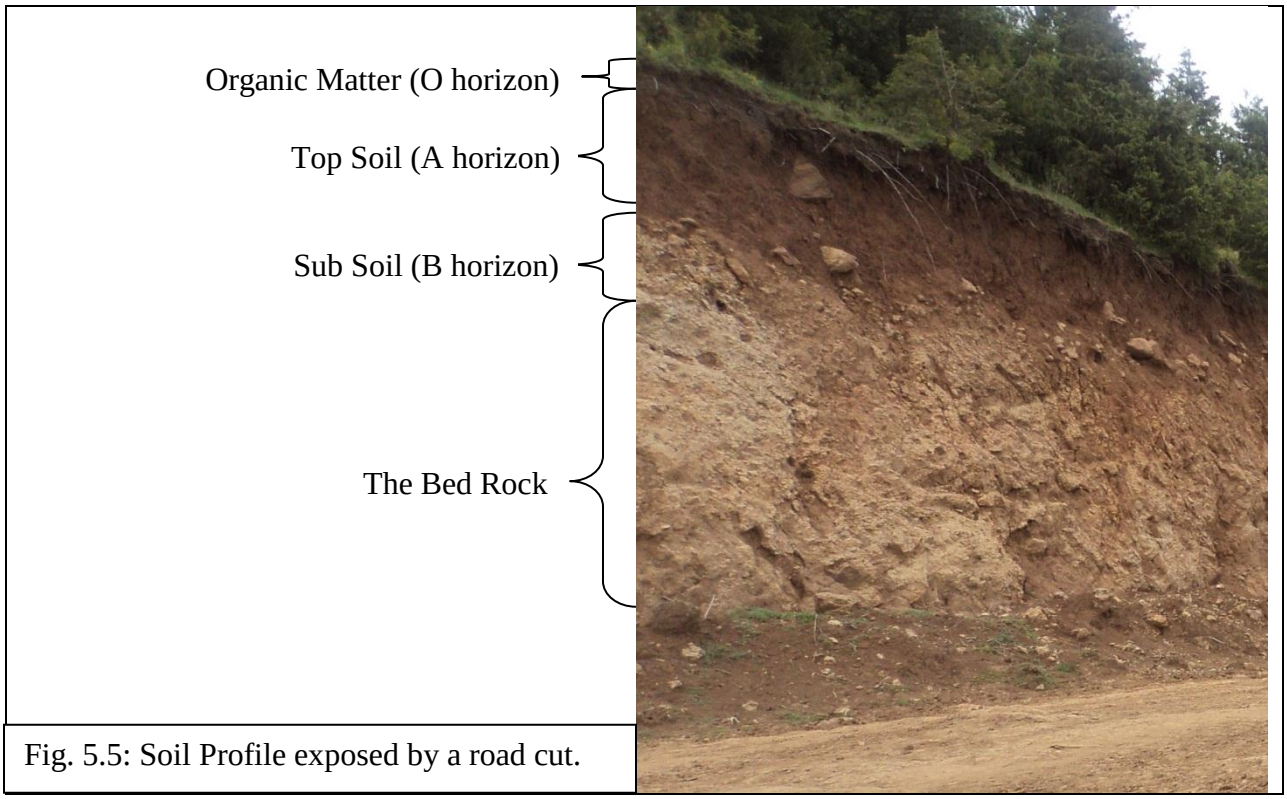

Fig. 5.5: Soil Profile exposed by a road cut.

Soil erosion is one of the major problems in Ethiopia. Human impacts like deforestation,

overgrazing, and poor land management accelerated the rate of erosion. Many farmers in Ethiopia's highlands, such as those in the Dendi locality, cultivate sloped or hilly land, causing topsoil to wash away during the torrential rains of the rainy season. The rains also leach the highland soils of much fertility, particularly those soils overlying crystalline rocks. The volcanic soils of the highland are less readily leached and therefore are more fertile. In order to overcome soil erosion afforestation, terracing, contour farming and proper land management has to be implemented extensively. To prevent exposure of bare soil, farmers can use techniques such as leaving crop residue in the soil after harvesting or planting temporary growths, such as grasses or vegetables, to protect the soil from rain between crop-growing seasons.

CHAPTER SIX
6. GEOCHEMISTRY OF THE CORE SEDIMENT

6.1. Introduction

Two long cores, Dendi 1 (10.2m) and Dendi 2 (8.5m), were recovered from the center of one of the Dendi Lake in May 2010. All the analysis and interpretation here in this research is only for the Dendi 1 core. Eight overlapping cores are taken to form the Dendi 1 long core, each with a 2 meter length except the short core which is only 63 cm long. The field overlaps between each cores and the general outline for the Dendi 1 sediment core is given in Fig 6.1 and Table 6.1. After the recovery of the sediment cores, all the cores starting from run1 to run7 are bisected for the ease of transportation and each half is noted as A and B.

After opening the core, the analysis started from description of the sediment core followed by high resolution photography, which allows seeing the sediment color and structure at any time. XRF scanning is followed for the geochemical variation and it's taken every two millimeter for detailed scanning while the MS scanning is taken every centimeter. The unit for all XRF values is cps (counts per second) and for the MS is Instrument Unit

The initial correlation between each core is generally based on the field description as shown above, in Fig 6.1 and Table 6.1, which is susceptible for error. Additionally, color, grain size, MS and geochemical data are used to confirm the field description and to come up with a different correlation trend as discussed in Correlation section below. Most of the core boundaries show similar trend and there is no significant gap or overlap more than the mentioned value between each sediment cores. But, in two areas there exists a missing gap. The first one is the missing of the contact between run 3B and run 4A. According to the field description there has to be a 50 cm overlap. The distribution shows an anomaly around 460cm and the manual description also reveals the presence of coarse material at the top of run 4A which is totally missed at the bottom of D 3B. This shows that the two cores run 3 and run 4 are not overlapping and the gap between them is unknown. The second one is between run 6 and run 7. According to the field description the cores run 6B and run 7A are almost overlapping. Instead run 7A starts overlapping from run 6A and the sandy layer at the bottom of run 6B is not found in the whole run 7 (7A and 7B). There is a similar depression (negative anomaly in Fe, Ti, Si, Ca) at run 6A 800cm mark and run 7A 855 cm mark. The manual description doesn't show any change in color

or grain size in both cores. The field note also doesn't show any correlation between these two points. They are about 50 cm away each other.

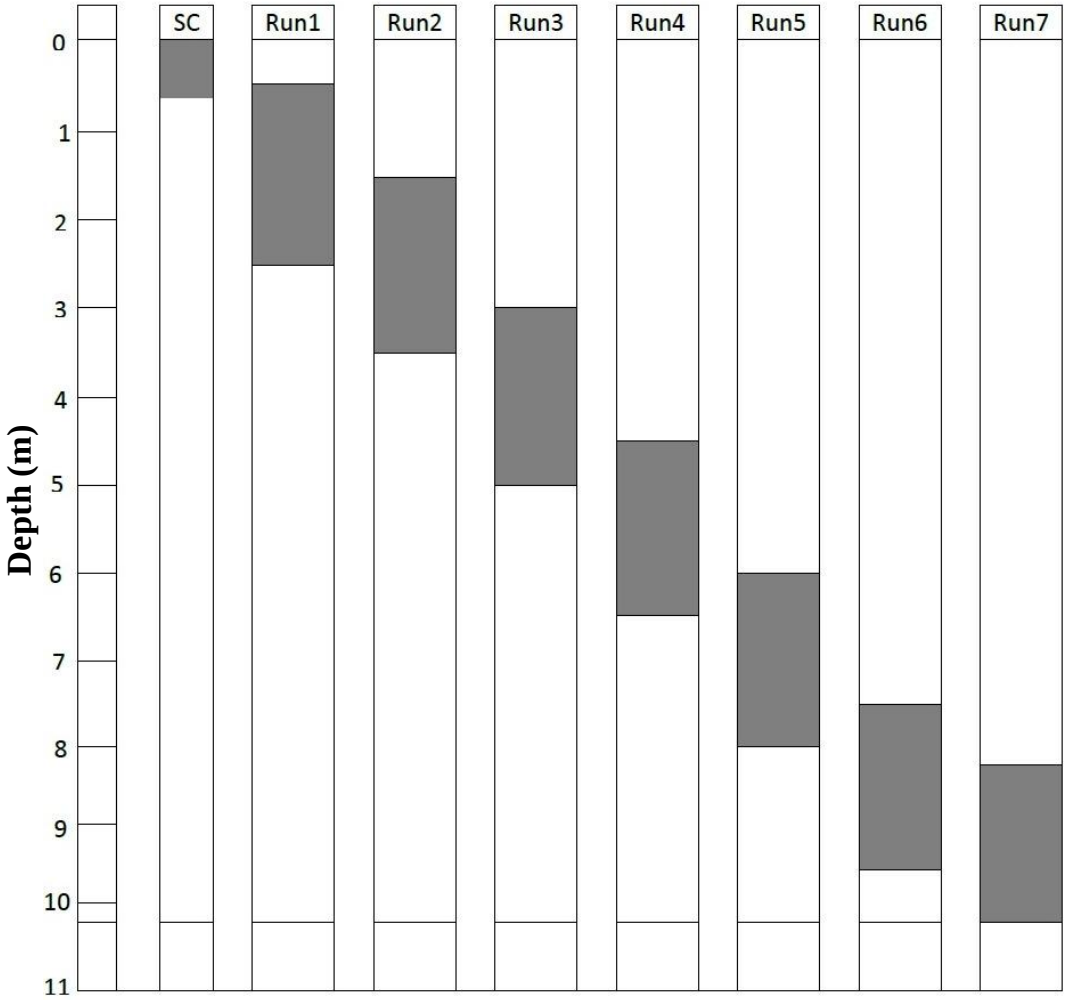

Fig. 6.1: The Dendi-1 sediment core outline showing the field overlap.

Run	SC	run 1	run 2	run 3	run 4	run 5	run 6	run 7
Top	0	0.5	1.5	3	4.5	6	7.5	8.2
Bottom	0.63	2.5	3.5	5	6.5	8	9.5	10.2

Table 6.1: The general outline of Dendi-1 sediment core.

6.2. Color, Grain size and Sediment structure

The Dendi core shows various color changes. Generally, the sediment color at the top is light to dark brownish and light grayish at the bottom. Munsell color chart was used during description of the sediment core. The first short core (SC-01) shows a light brownish color (10 YR 4/3) at the top 14 cm and the bottom 12cm and the middle 32 cm shows a very dark brownish color

(2.5Y 2.5/1). The range of cores from Dendi 1A to Dendi 4Aexcept Dendi 2B has a v. dark brown color (2.5 Y 2.5/1 and 2.5 Y 3/1), while the Dendi 2B has a dark brown color (7.5YR 3/2). There are two thin coarser layers at the top of Dendi 4A has a light and yellowish gray color (5 Y 5/1 and 2.5Y 7/4). Dendi 4B and the top 86cm of Dendi 5A is generally a v. dark grayish brown with ranging color in the Munsell chart (2.5Y 4/2, 2.5Y 3/1, 2.5Y 2.5/1, 2.5Y 4/1, 2.5Y 3/1 and 2.5Y 3/2). Starting from the bottom 13cm of Dendi 5A to the top 77cm of Dendi 6B and including the top 68cm of Dendi 7A the color ranges from light gray to light yellowish gray (5 Y 4/1, 5 Y 5/1, 5Y 5/2, 5 Y 6/1, 5 Y 7/3). The bottom 10cm of Dendi 6B is black colored (5Y2.5/1) clay. Overlaying it, a material similar with the previous light gray material is intercalated with a v. coarse material where every grains color is well visible dominantly gray material with some white, black and light green grains. Between this unit and the top light gray unit there is a 6 cm thick dark brown (2.5 3/1) material. The coarse material also intercalates with this layer. The bottom of Dendi 7A is similar with the bottom of Dendi 6B. Dendi 7B contains several materials with both vertical and horizontal boundaries with color ranging from light gray, dark gray and black (2.5Y 2.5/1, 2.5Y 3/1, 5Y 5/2, 5Y 5/3).

Most of the dark brown sediment material is composed of silty-clay material. In different places its texture shows a little bit change from clayey silty-clay to more silty silty-clay. Intercalation of sandy material is also present which might be a result of volcanic product. The light gray material has generally silty texture which ranges from fine silt to coarse silt. Intercalation of a very coarse material (coarse sand) is also present.

Most of the deposits are consolidated and dried out. The short core and Dendi 7A are very wet and Dendi 1A, 1B, 2A and 2B are wetter than the remaining cores. The dark gray materials are highly consolidated and dried out which makes them difficult to split. Cracks and surface loss characterize some parts of the core. Most of them occur connected with the dark brown layer. There is no crack present in the white layer. Lamination is present in different parts of the core. But, the white layers didn't show any lamination. Fine laminations are found here and there in the dark layer. In some places they are highly concentrated while in other places they are totally absent.

6.3. Correlation

The field overlap, in some cases, is inconsistent with the core description (color, texture and grain size), MS and XRF data. The main reason behind this is that the sediment core segments are taken from different trials and/or spots. Therefore a correlation has to be done on the sediment core to come up with a single master core. Due to the absence of dated materials from the sediment core, any correlation might not be perfect. A correlation and a single master core that seems closer to the actual sediment layer have been given by Dr. Tamrat Endale based on Lithology, Magnetic Susceptibility, Magnetic Intensity and Declination (Fig. 6.2). This correlation is also supported by the XRF results. There are three main problems with this correlation. The first one is lack of overlap between the first short core (DEN1_SC 01) and the second short core (DEN1_1A) where the actual size of this gap is not known but assumed to be 38cm for the sake of easiness. The other two problems are the missing overlaps among [(DEN1_3B) and (DEN1_4A)] and [(DEN1_6B) and (DEN1_7A)]. Similar with the previous, the gap between these units is also unknown, while in the correlation this gap is totally ignored.

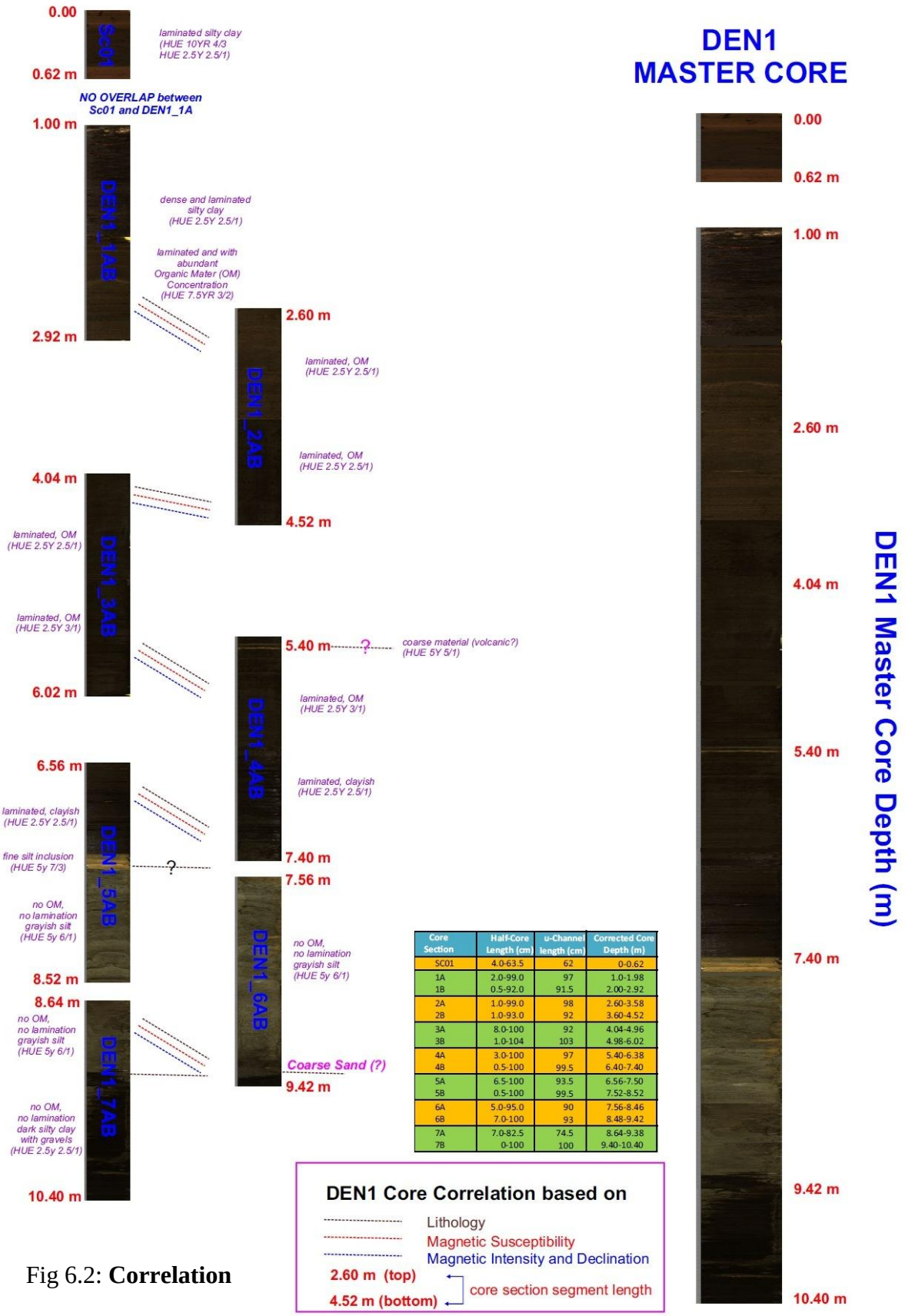

Core Section	Half-Core Length (cm)	u-Channel length (cm)	Corrected Core Depth (m)
SC01	4.0-63.5	62	0-0.62
1A	2.0-99.0	97	1.0-1.98
1B	0.5-92.0	91.5	2.00-2.92
2A	1.0-99.0	98	2.60-3.58
2B	1.0-93.0	92	3.60-4.52
3A	8.0-100	92	4.04-4.96
3B	1.0-104	103	4.98-6.02
4A	3.0-100	97	5.40-6.38
4B	0.5-100	99.5	6.40-7.40
5A	6.5-100	93.5	6.56-7.50
5B	0.5-100	99.5	7.52-8.52
6A	5.0-95.0	90	7.56-8.46
6B	7.0-100	93	8.48-9.42
7A	7.0-82.5	74.5	8.64-9.38
7B	0-100	100	9.40-10.40

Fig 6.2: **Correlation**

6.4. Sediment Geochemistry

Finally the distribution of the elements Ca, Ti, K, Fe and Mn as well as the ratios Si/Ti, and Rb/K was calculated along the sediment record. Furthermore, the MS values and the grain size distribution indicate changes in the sedimentation type during the past. In this section the distribution of the elements and element ratios mentioned above are given and the MS values are given in the next section while the distribution graph for both is given in Fig 6.3 below.

6.4.1. Calcium

The Ca distribution graph shows several peaks. Generally there is a big shift at 687 cm mark where the Ca starts to increase and this high calcium level starts to decrease around 900 cm mark. The Caconcentration in the top 140cm is more or less flat except two negative anomalies at 22cm and 46cm mark. The Concentration decreases a little bit around 140 cm mark and continue up to 450cm mark. This section is more or less flat and has a little bit smaller amounts of Ca than the previous. There are smaller positive anomalies at 325cm and 403cm mark whereas a negative anomaly is encountered around 318 cm marks. The high negative anomalies at 150, 250 and 400 cm mark are values of either the start or end of a core, therefore they are considered as noises. A bit elevated value is encountered between 450 and 500cm mark with a moderate peak at 460 cm and high peaks at 463 and 485 cm mark. Between 500 and 555 cm mark it has a similar trend with that of 140-460 cm. The distribution shows an elevated value in the range b/n 555-690 cm. here the calcium value is highly fluctuating with many positive and negative anomalies. There is one recognizable positive anomaly at 682 cm mark. Another fluctuating value, where the values are more elevated than the sediment cores above, is encountered between 690 and 940 cm marks. There is a high peak at 775cm and a negative anomaly at 800cm mark. The 940cm mark is marked by a sharp decrease in Ca then the low Ca value continues up to the 996cm mark. At the 996cm mark the calcium value shows a very sharp increase and continues till the end of the core with very highly fluctuating values which shows a clear positive anomalies at 1004 and 1010cm mark.

6.4.2. Potassium

The K distribution graph also shows a rapid increase around the 687 cm mark. There are more than five comparatively small peaks before the 450cm mark where negative anomalies at 55cm and 250cm mark and positive anomalies at 55, 202, 275, 338cm marks are well visible. Several

peaks are present after 450 cm mark to 690 cm where the K concentration is higher than the previous section. The significant one is the very high peak at 460cm mark. The others are at 450, 485, 503, 532, 555, 587, 602 and 617 cm mark. At the 690cm mark there is a sharp increase in K concentration from below 1000 cps (in average <300cps) reaches up to 3500cps. This very fluctuating and a very high K value layer continue up to the 940 cm mark. There exist many positive and negative anomalies, where the negative anomalies at 698, 798, 826, 845, 857, 920 cm mark are more prominent than the others. A sharp decrease in K concentration follows after the 940 cm mark which continues up to the end of the sediment core. There are two important positive anomalies with a very high value of K present at/ around 984cm and 995cm mark. Negative anomalies are also seen at the 974, 1012 and 1017cm marks.

6.4.3. Titanium

The top 150cm has a more elevated value with a slight decreasing in the last 20cm. There is a positive anomaly at the 22 cm mark while the positive anomaly is at 54cm mark. Starting from 150cm mark to 450 cm mark, the K concentration shows an elevated value than the previous and it's more or less flat value. There are two clear positive anomalies at 250cm and 400cm mark and negative anomalies at 250, 318 and 387 cm marks. After the 450cm mark till the end of the core the distribution is more or less similar with very fluctuating values. The most important positive anomaly is at the 681cm mark. The others are at 645, 700, 984 cm mark and there several anomalies b/n 480-610 cm marks. Between the 700 and the 910cm mark, the K distribution has values <1000 lacking positive anomalies. But there are negative anomalies at 800, 845, 856 cm mark.

6.4.4. Iron

The Fe distribution graph shows several peaks. Generally, it shows lower and more or less flat values between 150 and 450cm mark and elevated fluctuating value starting from the 550 cm mark to the end. The top 125 cm has a bit elevated value with negative anomaly at 22cm mark and two main anomalies at 53 and 85cm mark. Starting from 125cm mark to 450cm mark the Fe has lower concentration and more or less flat value with a positive anomaly at 353cm mark and negative anomalies at 250, 318, and 400 cm marks. Starting from 450 to 550 cm mark the Fe distribution has similar trend with the top 125 cm with a significant positive anomaly at 463cm mark. A very fluctuating value continues after 550cm mark till the end of the core with a very

significant positive anomaly at 696cm mark and negative anomalies at 798 and 856 cm marks. After 950 cm mark the distribution decreases a little bit with positive anomalies at 980 and 995cm mark and a negative anomaly at 1011 cm mark.

6.4.5. Manganese

The Mn distribution has more or less similar trend with the Fe distribution. Two positive anomalies at 7 and 49cm marks and negative anomaly at 21cm mark then continues being flat till 121 cm mark which in turn is a point of slight decrease in Mn values and continues up to 450cm mark. The area between 120-220 and 275-365 cm marks show a slight fluctuation and a bit elevated values. Starting from 450 to 625 it's a more elevated and fluctuating layer with positive anomalies at 459-462, 565 and 615 cm marks and negative anomalies at 546 and 574 cm marks. The layer between 625 and 685 cm mark is similar with that of the layer between 121 and 450 with a positive anomaly at 661 cm mark. Starting from 685cm to 942cm mark, the Mn distribution curve is characterized by a very fluctuating and elevated value with many positive and negative anomalies. The two positive anomalies at 696cm and 700cm mark and a negative anomaly between them are highly exaggerated value. The other important negative anomalies are at 800 & 856cm marks. The layer continuing from this to the end of the core has smaller value like that of 121 to 450cm mark with very important positive anomalies in the range between 982-997cm marks.

6.4.6. Silicon/Titanium

The Si/Ti distribution graph shows a highly fluctuating curve generally showing two big shifts at 150cm and 687 cm marks where the Si\Ti distribution curve shifts to a more elevated and fluctuating value. The top 150 cm distribution curve of Si/Ti shows lesser fluctuation than the remaining core with no anomalies at all. Starting from the 150cm mark to 545 cm mark, it shows a more elevated and fluctuating value with many minor anomalies. It starts decreasing from this point on wards to 685cm mark and reaches a level which is similar to but a bit elevated than the first 150cm of this core. The big shift in this curve starts at the 685cm mark where the Si/Ti reaches higher value and more fluctuating with prominent positive anomaly at the 800cm mark and negative anomaly at the 700cm mark. These anomalies might be noises because they are at the end of cores. This unit starts decreasing around the 900 cm mark to the end of the core to reach a level that is similar to the layer preceding the 685cm mark. There are two positive

anomalies in this unit right at 985cm and 995cm marks.

6.4.7. Rubidium/Potassium

The Rb/K distribution graph shows a different trend than that of Si/Ti curve. It starts from a higher and more fluctuating value to a flat lower value for the last 300cm of the core. The fluctuating curve of the Rb/K shows a strong positive anomaly at 23cm mark and smaller anomalies at 69,100 and 137 cm marks and at 150cm mark it shifts to a more fluctuating condition where the Rb/K value shows many up and downs having a peak value at 166cm mark. This unit has positive anomalies at 319cm and 399cm mark and also a smaller anomaly at 452cm mark then it continues to the 500cm mark where it shifts to a lower Rb/K value and flatter curve with more or less small anomalies. Another unit starts from the 678cm mark and continues up to 925 cm mark with a very low Rb/K value and a totally flat curve. There are three important anomalies at 700cm, 845cm and 857cm marks and one minor anomaly at 800cm mark. The final unit has a similar trend with the unit between the 500cm and 678cm mark with two big positive anomalies at 950cm mark and the end of the core.

6.5. Magnetic Susceptibility

The MS distribution graph starts with a lower value and more or less flat trend up to the 450cm mark. There are about four positive anomalies at the starting point, 53cm, 188cm and 403cm marks. The MS value for the first 130cm is higher than the next 320cm sediment but the value following this unit starting from 450cm mark to 660 cm mark has a similar value with the first 130cm but it shows more fluctuation especially the positive anomalies at 460cm, 485cmand 587cm mark. The significant shift towards a higher and more fluctuating value starts around the 660cm mark. This area is more pronounced by so many ups and downs with an average value ~25. This unit drops down to a lower value unit around 940 cm mark after a very elevated value (234). From this point to the end is similar with the first 450cm sediment with little/no fluctuation up to 970cm mark and a more or less fluctuating value starts here and continues to the end with one peak value at 984cm mark.

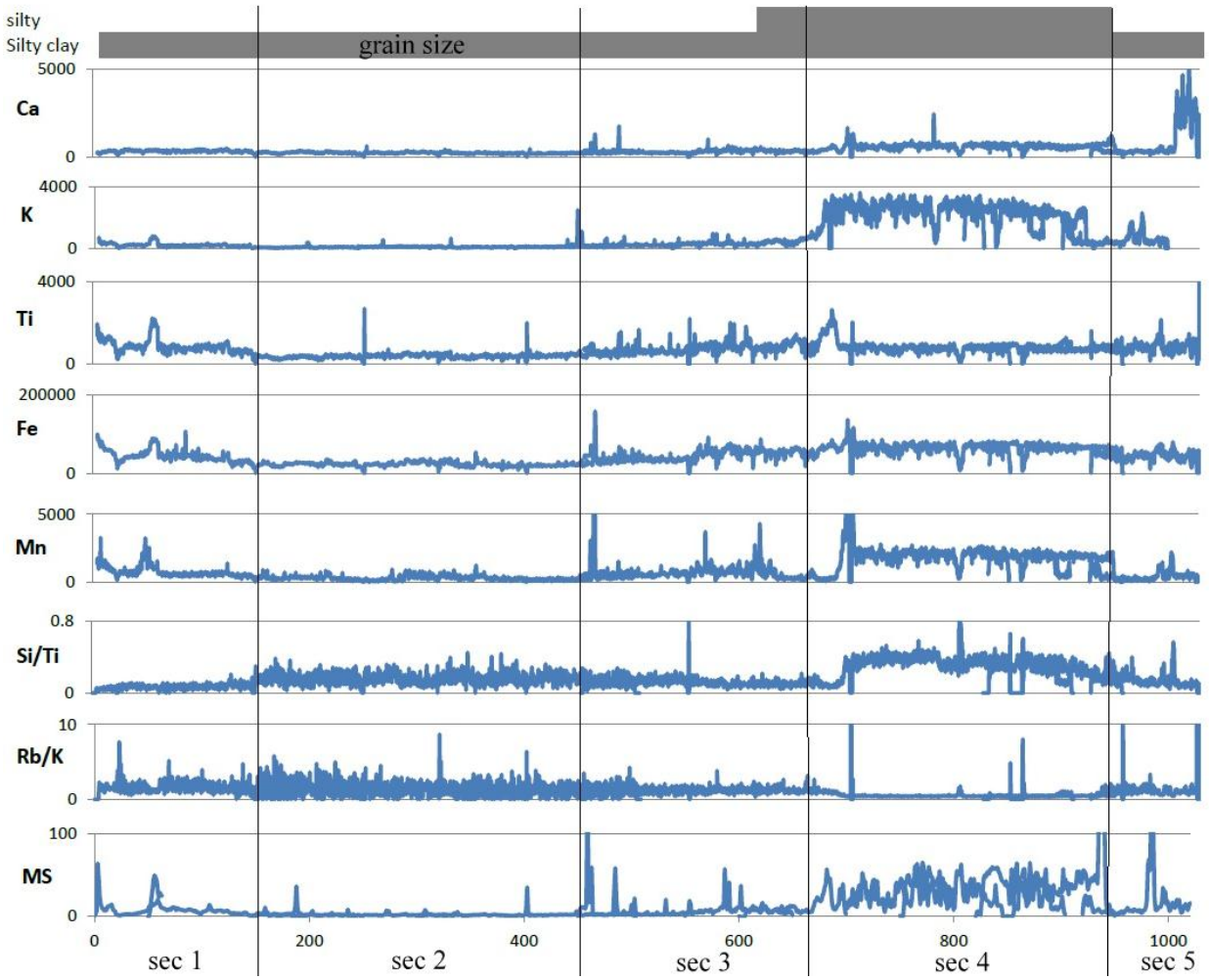

Fig. 6.3: The Distribution graph for depth (in cm) vs. grain size, MS and different elements/ element ratios (in cps)

6.6. Discussion

6.6.1. Introduction

The geology of the Dendi caldera shows two physically different materials, i.e. results of effusive and explosive eruptions, with different and unrelated resistance of weathering. The pyroclastics, with the help of a very rugged topography, can easily be washed away with little rain even in arid condition and can be deposited in the Dendi Lake. While the effusive ones (rhyolite and trachyte), which are among weathering resistant geologic materials, need more of erosive condition to be weathered and washed away. But, chemical weathering can affect both to erode the highly mobile elements such as K.

The physiography of the area favors both erosional and depositional settings in the area. The Dendi Lake is the best depositional area for the weathered sediments from the rim or the sloppy area of the caldera. The wide flat land adjacent to the lake can also be depositional area where the transporting agent doesn't have the power to bring the sediments to the lake. In situ weathering and deposition characterizes the flat land at the top of the ridge, but with the help of intensive weathering and strong rain fall in the absence of vegetation cover the sediment accumulated here can easily be transported into the lower areas, i.e. the Dendi Lake and the flat land next to it. Most of the pyroclastic deposits are deposited in these flat lands, which helps them to stay without being eroded for longer period of time.

The cliffs are the surfaces for the eroded material from the top to be transported through them and deposited into the Lake basin and the surrounding. Due to its slope instability any material cannot be deposited there and there is no sediment overlaying this unit. It has little or no vegetation cover. These cliffs are formed from acidic/felsic/ (the feldspar and silica rich) rocks rhyolite and trachyte which makes the cliff to be strong and it can withstand with higher level of weathering. But, its slope favors erosion even during arid times which lacks water. Gravity and wind plays an important role for such transportations of materials in such sloppy surfaces.

The soil samples show very low concentration of the highly mobile elements K and Ca compared to the lithologic units in the area. While the concentration of the immobile elements Al and Mg is very high in the soil. This shows the mobile elements are being eroded and deposited to the basin with little weathering whereas the immobile elements need strong weathering and high chemical activity with the presence of water for their weathering and erosion to be deposited in the depositional basin.

Since the Dendi caldera is far from the Main Ethiopian rift and any volcanic activity it's not that much affected by hydrothermal activity. There is no reported hydrothermal activity in the area during the near past. Therefore, the effect of hydrothermal input of different elements into the lake sediment deposit is ignored.

The core sediment lithologic unit is divided in to five different sections based on the distribution graph trend of the different proxies used (Fig. 6.3). This subdivision helps to easily interpret the paleoclimate based on the sediment core geochemical distribution graph. The first section is the top 150cm followed by section 2 up to the 450cm mark. From the 450cm mark to 660cm mark is

the third section followed by the fourth section which continues up to the 942cm mark. The final and the fifth section follow the fourth section and continue up to the end of the core.

6.6.2. Paleoclimate

The geochemical results supported with physical/geophysical indicators of the lacustrine sediments recovered from the Dendi lake core sediment reflect a highly variable environment in East Africa, specifically in West Central Ethiopia. The geochemical values of different elements and/or element ratios interpreted as a proxy for aridity/wetter condition in the Dendi caldera catchment are the most important paleoenvironmental indicators, which are supported by the physical/geophysical indicators.

During arid conditions and when there is a sparse vegetation cover, the rocks (rhyolite and trachyte with the pyroclastics) containing potassium-rich mineral (k-feldspar, orthoclase) are eroded with difficulty especially the silica rich minerals, and then washed and deposited in the Dendi Lake. These events are expressed by sharp increases of K and decrease of Rb/K in the record. Increased sediment supply into the Dendi Lake during dry conditions into a shallower lake level is also reflected by coarse grained material rather than the fine grained clay in the stratigraphy, which is washed in during strong rain events. The K in the record can be attributed exclusively to terrigenous and allochthonous input, because there is no process in the lake that can change the concentration of K. And after deposition no further processes, like diagenesis and organic activity, increase or decrease the amount of K.

During humid conditions with a higher lake water level and denser vegetation cover, evenly distributed rains result in the more or less continuous discharge of all streams, transporting more diverse and generally finer material. This causes all the lithologic units constituting the caldera to be easily washed away and deposited in the lake. This causes the Si rich minerals (mainly from rhyolite) and also Ca (feldspars), Fe, Mn, and Ti-rich material (the opaque minerals and the intermediate/mafic pyroclastic rocks) from the surrounding lithologic unit and organic matter to be deposited in the lake basin. This input firstly dilutes the already decreased potassium input via the alluvial fan and secondly mixes in an array of sediments from the entire catchment. Thus, the K record visibly decreases and potentially provides a clear signal of climatic change.

In support of this dry/wet interpretation, magnetic susceptibility, Ca, Fe, Mn, Ti, Si/Ti, largely parallels the potassium record. The Ca distribution doesn’t show strong variation like the others

except for the last 20 cm where the calcium value shows extreme enrichment comparing it to the whole sediment core stratigraphy. The Ti, Fe and Mn distribution curve and the MS value shows more or less similar pattern except they have a more elevated value in the first section and lower elevation in the fourth section where the K curve shows more elevation and the sediment core has silty texture.

The Rb/K ratio has totally an opposite curve compared with the others. It reaches the highest point in the second section and the lowest point in the fourth section. The Si/Ti ratio also has a bit different pattern from the others. This section reaches its maximum in the fourth section like the others but, its lowest point is the first section. This is not seen in any of the other sections.

Section 5:

The Ca and Sr concentration is very high with low Rb and Zr concentration in the last 20cm of the DEN1 sediment core, which could be interpreted as a shift to an extreme dry condition (Burnett et al., 2011) where the increase of these elements is due to precipitation following increased evaporation (Felton et al., 2007). But, physical conditions doesn't show any shift towards a dryer condition.

While, above this unit both the Ca and Sr shows lower values. The K record in this section shows intermediate values comparing it with its record in other sections with two positive anomalies corresponding to a coarser (sandy) grayish material. The positive anomalies are also shown by Si, Zr, Rb and Mn and a slight anomaly by Ca while inc/coh shows negative anomaly and Sr also shows negative anomaly in the bottom layer. The record for the bottom sandy white layer is especially well preserved. These conditions might be indicators of volcanic ash deposit within the lake sediment. Besides the sandy materials, the remaining sediment shows intermediate values of Rb/K, Si/Ti, inc/coh and MS which has similar trends. The interpreted climate condition is intermediately humid.

Section 4:

The very coarse sandy material with in this section that is located near the boundary of this section and the bottom section doesn't show any significant geochemical change in the distribution. It might be result of a flash flood event following a relatively humid period during the deposition of the previous section. The sediment changes its texture upward to coarse silt and

silty.

The whitish layer with silty texture showing very high value of K, MS, Si/Ti and Mn characterizes this section. The Si, Rb, Zr, Fe, Ca and Mn, graph also shows an increasing trend. While the inc/coh, Sr/Ca, Zr/Rb and Rb/K graph shows decreasing trend and low values. These results show arid condition during the time of sedimentation of this section. The increase in K is the main indicator of dry condition (Forster et. al., 2012). Increase in Ca, Si/Ti and high lithogenic fraction (larger grain size) and decrease in inc/coh and Rb/K are also indicators of dry condition (Burnett et. al., 2011). Increase in MS, Si, Mn suggests more terrigneous input into the lake while decreased Sr/Ca suggests less evaporation and precipitation of Sr-Aragonite.

Negative anomaly in K, Ca, Zr, Rb, Si, Sr and Ti and positive anomaly of Rb/K, Sr/Ca, Si/Ti around the 800cm mark is not supported by the sediment description (i.e. no change in grain size and color). It might be a sudden change in climatic conditions to a wetter condition and immediately reversed back to the dry condition.

Section 3:

Very low K concentration compared to the previous section characterizes this section. It's a dark silty clay material with colors varying between light brown, dark brown to black. There are many laminations in different locations which generally have brighter color (brownish, yellowish and whitish) where some of them have more silty texture. Terrigneous organic matter is also present in different locations. This might show more terrigenous input of sediments to the lake basin. But, low Ti and Zr/Rb values show the opposite.

Intermediate humid condition better characterizes this section. Decreased K value, Ca and Si/Ti, fine texture, high allochtonous organic matter and increased inc/coh and Si/Ti helps a lot for this interpretation (Forster et. al., 2012, Burnett et. al., 2011). Minor fluctuations might indicate some fluctuating drier and wetter conditions in-between this longer intermediate moisture dominated period.

Most of the laminations with brighter color show positive anomalies in Ca and Sr which in some case coincide with positive Ti anomaly and negative anomalies in Zr with limited anomalies of Si and Rb. This shows those layers are resulted from the precipitation of Ca and Sr-aragonite which needs much drier condition. Therefore, within this long wet period there were small drier

periods. But, the white sandy material at the top of Den1_4A (located on 5.4m of the correlation in Fig. 6.2) shows strong positive anomaly in Zr, Si, MS and K while it shows small positive anomaly in Fe, Ca and no anomaly in Sr. These characteristics are more interpreted as a volcanic ash deposit. The other brighter (more yellowish) sandy layer immediately below the volcanic ash shows strong positive anomaly in Ca, Sr and Fe while it shows negative anomaly in Zr and K with no anomaly for Si. Due to these conditions it is interpreted as a drier period which is formed due to precipitation of Ca and Sr.

Section 2:

With low Ca and the lowest K record in the whole stratigraphy, this section represents an era of a highly humid condition. Lower Ca value also suggests a higher lake level. This section has more or less similar characteristics with the previous section in terms of color and sediment structure. Darker silty clay sediment with the presence of organic matter and brighter color laminations (sometimes coarser) also characterizes this section. The brighter laminations represent drier conditions within the long generally wet period.

Low Fe and Ti values show decreased runoff and limited allochthonous input, as Ti is not sensitive to dissolution through weathering (Haberzettl, 2006). Very low MS values and increased in Si/Ti might show a higher nutrient supply and production of Biogenic Silica (Rothwell et al., 2006 and Burnett et al., 2011). Increase in delivery of chemically weathered material to the lake basin is shown by increase in Rb/K.

Section 1:

Silty clay texture, increased artificial crack, limited laminations and absence of organic matter characterizes this section. The color is generally dark brown to black with limited light brown sediment and lamination. The lack of overlap between the short core SC_01 and the first long core DEN-1A is shown by the light brown material at the bottom 10 cm of SC_01 is not continues in the long core.

The K concentration is more or less elevated than the previous section showing a change from highly humid condition to intermediate humid condition (Forster et. al., 2012). Elevated Fe and Ti values show increased runoff and higher allochthonous input into the lake basin. Increase in MS, Si, Mn suggests more terrigneous input into the lake. Lower values of Ca and Si/Ti and low

lithogenic fraction (smaller grain size) and increase in inc/coh and Rb/K are also indicators of dry condition (Burnett et. al., 2011). The light brown material at the bottom 10 cm of SC_01 shows elevated K, Ti, Si, Fe, Mn and Rb suggesting a more or less drier episode within the long wetter period.

CHAPTER SEVEN

7. CONCLUSION AND RECOMMENDATIONS

7.1. Conclusion

The Dendi Caldera is composed of both effusive (rhyolite, trachyte and obsidian) and explosive (volcanic ash, surge deposit and ignimbrite) felsic volcanic rocks. The effusive ones are the oldest whereas the pyroclastic ones are the youngest.

The geochemical and petrographic results show that the lithologic units that compose the Dendi caldera are formed by fractional crystallization of basaltic magma with limited or no crustal contamination.

Calderas are the surface expression of the emptying of the magma chamber during effusive or explosive eruptions. The diameter/subsidence (d/s) values of the Dendi caldera falls in the stage2 and/or stage3 range of the Acocella V., (2007) category of natural calderas where the actual value falls around 18. The stage2 evolution of the caldera suggests that it is a reverse ring fault and stage3 is peripheral downsag.

The Dendi caldera is characterized by different geomorphic units which are mainly formed due to the subsidence that form the caldera. These are the flat lands both at the top of the ridges and surrounding the lakes, the vertical cliffs, the steep and gentle slope areas and the lake which is a result of an eruption after the formation of the caldera.

The altitude of the Dendi area varies between 2,830 and 3,270 meters above sea level. The whole area, lying in a tropical climate, classified as wet, humid region with a mean annual rainfall of 1137.35mm. There are two seasons of rainfall. The mean maximum temperature is 19.6^0C and the mean minimum temperature is 17.2^0C.

The sediment core from the lake is analyzed based on physical parameters (color grain size and MS) and chemical parameters (element and element ratio distribution) to help to interprete the paleaoclimate of the area.

Five different sections have been identified based on the variation of different parameters applied. Section 4 shows the driest period in the stratigraphy while section 2 shows the most humid period in the stratigraphy. The remaining sections spans between these two extremes.

7.2. Recommendations

Additional whole rock geochemistry analysis and isotope geochemistry studies are recommended to adequately understand the magma source characteristics and the geochemical processes involved to produce the Dendi caldera and to compare it with other volcanic centers. Dating is also recommended to give a clear stratigraphy of the area in the whole volcanic episodes of the central Ethiopia.

Dating, isotope studies and biological studies in the sediment core are also recommended to reconstruct both the paleoclimate and paleoenvironment of the area and to compare and correlate it with Global events.

REFERENCES and BIBLIOGRAPHY

Abebe T., F. Mazzarini, F. Innocenti and P. Manetti (1998): The Yerer-TulluWellel volcano tectonic lineament: a transtensional structure in central Ethiopia and the associated magmatic activity Journal of African Earth Sciences, Vol. 26, No. 1, pp. 135-150.

Abebe T., Manetti, P., Bonini, M., Cort, G., Innocenti, F., Mazzarini, F. and Pecksay, Z. (2005): Geological Map (Scale 1:200,000) of the Northern Main Ethiopian Rift and Implications for the Volcano-tectonic evolution of the rift: Geological Society of America, Map and Chart Series MC H094, 20P.

Abenezer Kefeni (2007): Hydrogeochemical evolution in the ambo-woliso area; unpublished MSc Thesis; Addis Ababa University, Addis Ababa, Ethiopia, 123pp.

Acocella, V., (2007): Understanding caldera structure and development: An overview of analogue models compared to natural calderas. Earth-Science Reviews, 85 (2007), 125–160.

Alene, M., Ruffini, R., and Sacchi, R. (2000): Geochemistry and Geotectonic setting of the Neoproterozoic rocks from Northern Ethiopia (Arabian-Nubian Shield). Gondwana Research 3:333-347

Allègre, C. J. & Minster, J. F. (1978): Quantitative models of trace element behavior in magmatic processes. Earth and Planetary Science Letters 38, 1–25.

Allen, S. R. (2001). Reconstruction of a major caldera-forming eruption from pyroclastic deposit characteristics: Kos Plateau Tuff, eastern Aegean Sea. Journal of Volcanology and Geothermal Research 105, 141–162.

Arzi, A.A., (1978): Critical phenomena in the rheology of partially melted rocks. Tectonophysics, 44:173-184.

Arth, J.G., (1976): Behavior of trace elements during magmatic processes--a summary of theoretical models and their applications. J. Res. U.S. Geol. Surv., 4: 41-47.

Asnani G. (2005): Tropical Meteorology, revised edn; Vol. 1. Praveen Printing Press: Pune, India.

Asrat, A., Barbey, P., and Gleizes, G. (2001): The Precambrian geology of Ethiopia: a review. Africa Geoscience Review 8, 271-288.

Ayalew D., (2011): The relations between felsic and mafic volcanic rocks in continental flood basalts of Ethiopia: implication for the thermal weakening of the crust. In: Van Hinsbergen DJJ, Buiter SJH, Torsvik TH, Gaina C, Webb SJ (eds) The formation and evolution of Africa: a synopsis of 3.8 Ga of earth history. Geological Society, London, Special Publication, London, pp 253–264

Ayalew D., Ishiwatari A. (2011): Comparison of rhyolites from continental rift, continental arc and oceanic island arc: implication for the mechanism of silicic magma generation. Island Arc 20:78–93

Ayalew. D., and Yirgu G. (2003): crustal contribution to the genesis of Ethiopian Plateau rhyolitic ignimbrites, basalt and rhyolite geochemical provinciality. J. of the Geo. soc., 160, 47-56.

Ayalew, T., Bell, K., Moore, J.M., Parish, R.R. (1990): U-Pb and Rb-Sr geochemistry of the western Ethiopian Shield. Geol. Soc. Am. Bull. 102: 1309-1316

Bacon, C.R., Macdonald, R., Smith, Ri. And Baedecker, P.R., (1981): Pleistocene high-silica rhyolites of the Coso volcanic field, Inyo County, California. J. Geophys.Res., 86: 10223-10241.

Baker, J., Snee, L. & Menzies, M. A. (1996): A brief Oligocene period of flood volcanism in Yemen: implications for the duration and rate of continental flood basalt volcanism at the Afro-Arabian triple junction. Earth and Planetary Science Letters 138, 39-55.

Barberio, M.R., Donati, C., Donato, P., Yirgu, G., Peccerillo, A., Wu, T.W. (1999): Petrology and geochemistry of Quaternary magmatism in the northern sector of the Ethiopian Rift between Debre Zeit and Awash Park. Acta Vulanologica 11(1): 69-81.

Bekele Abebe, Mario Boccaletti, Marco Bonini, Roberto Mazzuoli, Luigi Piccardi & Luigi Tortorici, (1998): Quaternary Oblique Extensional Tectonics in the Ethiopian Rift (Horn of Africa).

Bekele F. (1997): Ethiopian use of ENSO information in its seasonal forecasts. Internet Journal of African Studies **2**: (in press).

Bellier, O., & Sebrier, M., (1994): Relationship between tectonism and volcanism along the Great Sumatran fault Zone deduced by spot image analyses. Tectonophysics 233, 215–231.

Berhe, S. M., Desta, B., Nicoletti, M. and Teferra, M, (1987): Geology, Geochronology and Geodynamic implications of the Cenozoic Magmatic province in W and SE Ethiopia. Journal Geological Society, London 144, 213-226.

Boccaletti, M., Bonini, M., Mazzuoli, R., Tura, T., (1999): Pliocene-Quaternary volcanism and faulting in the northern Main Ethiopian Rift (with two geological maps at scale 1:50000). Acta Vulanologica 11(1): 83-97.

Bosworth, W., Burke, K., Strecker, M., (2003): Effect of stress fields on magma chamber stability and the formation of collapse calderas. Tectonics: 22 (4), 1042.

Bradley R.S., (1999): Paleoclimatology – Reconstructing Climates of the Quaternary. - San Diego, Academic Press.

Branney, M.J., (1995): Downsag and extension at calderas: new prospective on collapse geometries from ice-melt, mining, and volcanic subsidence. Bulletin of Volcanology 57, 303–318.

Bruno K., Nicholas A., Henriette L., Florence B., Delphine B., Arnaud P., Gezahegn Y., Dereje A., Domo-nique W., Dougalg A. J., Francine K., Claudine M. (2004), Flood and Shield Basalts from Ethiopia: Magmas from the African Super swell, J. of Petrology, Vol. 45 No. 4, Pages 793–834

Camberlin P., (1995): June-September rainfall in northeastern Africa and atmospheric signals over the tropics: a zonal perspective. International Journal of Climatology 15: 773–783.

Camberlin P, Philippon N. (2002): The East African March-May Rainy season: associated atmospheric dynamics and predictibility over the 1968–97 periods. J. of Climate 15: 1002–1019.

Cohen, A.S., (2003): Paleolimnology - The History and Evolution of Lake Systems. New York, Oxford University Press.

Cole, J.W., (1990): Structural control and origin of volcanism in the Taupovolcanic zone, New Zealand. Bulletin of Volcanology 52, 445–459.

Cole, J.W., Milner, D.M. and Spinks, K.D., (2005): Calderas and caldera structures: a review. Earth Science Reviews 69, 1–96.

De Silva, S.L., (1989): Altiplano-Puna volcanic complex of the central Andes. Geo. 17, 1102–1106.

Degefu W. (1987): Some aspects of meteorological droughts in Ethiopia. In Drought and Hunger in Africa: Denying Famine a Future, Glantz M (ed.). Cambridge Univ. Press: Cambridge; 23–36.

Diro, G. T., Grimes, D. I. F., Black, E., O'Neilla, A. and Pardo-Iguzquizab, E. (2009): Evaluation of reanalysis rainfall estimates over Ethiopia; Int. J. Climatol. V.29: 67–78.

Dow D.B., Beyth N. and Tsegaye Hailu (1971): Paleozoic glacial rocks recently discovered in northern Ethiopia; Geol. Mag. V. 108.1.

Druitt, T.H. & Sparks, R.S., (1984): On the formation of calderas during ignimbrite eruptions. Nature 310, 679–681.

Felton, A.A., Russell, J.M., Cohen, A.S., Baker, M.E., Chesley, J.T., Lezzar, K.E., Mcglue, M.M., Pigati, J.S., Quade, J., Stager, J.C. and Tiercelin, J.J. (2007): Paleolimnological evidence for the onset and termination of glacial aridity from Lake Tanganyika, Tropical East Africa. - Palaeogeography, Palaeoclimatology, Palaeoecology, 252: 405- 423.

Foerster V., Junginger A., Langkamp O., Gebru T., Asrat A., Umer M., Lamb H.F., Wennrich V., Rethemeyer J., Nowaczyk N., Trauth M.H., Schaebitz F., (2012): Climatic change recorded in the sediments of the Chew Bahir basin, southern Ethiopia, during the last 45,000 years; Quaternary International 274: 25 – 37

Francisa, P. W., Sparksa, R. S. J., Hawkeswortha, C. J., Thorpea, R. S., Pylea, D. M., Taita, S. R., Mantovania, M. S. and McDermotta, F. (1989): Petrology and geochemistry of volcanic rocks of the Cerro Galan caldera, northwest Argentina

Gasparon M, Innocenti F, Manetti P, Peccerillo A&Tsegaye A., (1993): Genesis of the Pliocene to Recent bimodal mafic-felsic volcanismin the DebreZeyit area, central Ethiopia; volcanologicaland geochemical constraints. J Afr. Earth Sci. 17(2):145–165

Getaneh Assefa (1991): Lithostratigraphy and Environment of deposition of the Late Jurassic–Early Cretaceous sequence of the central part of northwestern plateau, Ethiopia. Neues Jahrb. Geol. Paleontol. Abhandubglen 182, 255–284.

Gudmundsson, A., (1988): Formation of collapse calderas. Geology 16, 808–810.

Gudmundsson, A., (1998): Magma chambers modeled as cavities explain the formation of rift zone central volcanoes and their eruption and intrusion statistics. Journal of Geophysical Research, 103, 7401–7412.

Gudmundsson, A., Marti, J., Turon, E., (1997): Stress fields generating ring faults in volcanoes. Geophysical Research Letters 24, 1559–1562.

Guillou-Frottier, L., and Burov, E.B., (1999): Thermo mechanical behavior of large ash flow calderas. Journal of Geophysical Research 104, 23081–23109.

GuillouFrottier, L., Burov, E.B., and Milesi, J. P., (2000): Genetic links between ash flow calderas and associated ore deposits as revealed by large-scale thermo-mechanical modeling. Journal of Volcanology and Geothermal Research 102, 339–361.

Haberzettl, T. (2006): Late Quaternary hydrological variability in southeastern Patagonia: 45,000 years of terrestrial evidence from Laguna Potrok Aike: Unpublished PhD thesis: University of Bremen, Bremen.

Halliday, A.N., Mahood, G., Holden, P., Metz, J.M., Dempster, T.J. and Davidson, J.P., (1989): Evidence for long residence times of rhyolite magma in the LongValley magma system; the isotopic record in the precaldera rhyolite lavas of Glass Mountain. Earth Planet.Sci. Lett., 94: 274-290.

Halliday, A.N., Davidson, J.P., Hildreth, W.and Holden, P. (1991): Modelling the petrogenesis of high Rb/Sr silicic magmas. Chemical Geology, 92:107-114

Hassen Shube (2011): Carbon dioxide-water-rock interaction and hydrogeochemical evolution of thermal and cold ground waters in Wenchi Crater Lake and Ambo-Woliso area. Unpublished MSc thesis: Addis Ababa University, Addis Ababa, Ethiopia, 119pp.

Heiken, G. & McCoy, F. J. (1984): Caldera development during the Minoan eruption, Thira, Cyclades, Greece. Journal of Geophysical Research: 89(B10), 8441–8462.

Hofmann, C., Courtillot, V., Feraud, G., Rochette, P., Yirgu, G., Ketefo, E. & Pik, R. (1997): Timing of the Ethiopian flood basalt event and implications for plume birth and global change. Nature 389, 338-341.

Holohan, E.P., Troll, V.R., Walter, T.R., Munn, S., McDonnell, S., Shipton, Z.K., (2005): Elliptical calderas in active tectonic settings: an experimental approach. Journal of Volcanology and Geothermal Research, 144, 119–135.

Huppert, H.E. and Sparks, R.S.J., (1988): The generation of granitic magmas by intrusion of basalt into continental crust. J. Petrol., 29: 599-624.

Ininda J, Desalegn B, Befikadu A. (1987): The characteristics of rainfall in Ethiopia and its relationship to el-nino southern oscillation. Proceedings of First Technical Conference on Meteorological Research in Eastern and Southern Africa, Kenya Meteorological Department: Nairobi; 133–135.

Kassahun B. (1987): Weather systems over Ethiopia. Proceedings of First Technical Conferences on Meteorological Research in Eastern and Southern Africa, Kenya Meteorological Department: Nairobi; 53–57.

Kazmin, V., (1972): Geological Map of Ethiopia, 1:2,000,000 Scale, with explanatory note (1975), 14 p, Geological Survey of Ethiopia.

Kazmin, V. Shiferaw A., Balcha T., (1978): The Ethiopian basement: Stratigraphy and possible manner of evolution, Geol. Rdsch. V.67, p.531-546.

Kazmin V., Berhe S.M., Nicolitti M. and Petruccian C., (1980): Evolution of Northern part of the Ethiopian Rift, in Geodynamic Evolution of the Afro-Arabian Rift System, Accademia Nazionale deiLincei, Roma, v.47, p.275-291.

Lipman, P.W., (1997): Subsidence of ash-flow calderas: relation to calderasize and magma-chamber geometry. Bulletin of Volcanology: 59,198–218.

Lipman, P.W., (2003): Geometrically complex calderas and underlying magma chambers in the Western USA. Proceedings of the IUGG XXIII Assembly, Sapporo, Japan, pp. 526–527.

Martì, J., Folch, A., Neri, A., Macedonio, G., (2000): Pressure evolution during explosive caldera-forming eruptions. Earth and Planetary Science Letters 175, 275–287.

Mazzarini, F., Abebe, T., Innocenti, F., Manetti, P., Pareschi M.T., (1999): Geology of the Debre Zeyt area (Ethiopia) (with a geologic map at scale 1:100,000). Acta Vulanologica 11(1): 131-141.

McKenzie, D., (1985): The extraction of magma from the crust and mantle. Earth and Planetary Sci. Lett., 74:81-91.

Metz, J.M. and Mahood, G.A., (1985): Precursors to the Bishop Tuff eruption: Glass Mountain, Long Valley, California. J. Geophys. Res., 90:11121-11126.

Mohr P., (1983): Ethiopian flood basalt province. Nature 303, 577-584.

Mohr P. (1971): Geology of Ethiopia: Haile Selassie I university press, Addis Ababa, pp 268.

Mohr, P.A. and Wood, C.A., (1976): Volcano spacing and lithospheric attenuation in the Eastern Rift of Africa. Earth and Planetary Science Letters 33, 126–144.

Mohr, P. & Zanettin, B. (1988): The Ethiopian flood basalt province. In: Macdougall, J. D. (ed.) Continental Flood Basalts. Dordrecht: Kluwer Academic, pp. 63-110.

Newhall, C.G., Dzurisin, D., (1988): Historical unrest at large calderas of the world, U.S. Geological Survey, 1109 pp.

Nicholson S, Grist J. (2003): The seasonal evolution of the atmospheric circulation over West Africa and equatorial Africa. Journal of Climate 16(7): 1013–1030.

Oliver L., (2011): XRF-core-scanner element distribution indicating paleoenvironmental changes in South Ethiopia during the late Quaternary. Unpublished M.Sc. Thesis: University of Cologne, Cologne, Germany 81pp.

Pearce, J.A. and Cann, J.R. (1973): Tectonic setting of basic volcanic rocks determined using trace elements analyses. Earth and Planetary Science Letters, 19, 290-300.

Reubi, O., and Nicholls, I. A., (2005): Structure and Dynamics of a Silicic Magmatic System Associated with Caldera-Forming Eruptions at Batur Volcanic Field, Bali, Indonesia

Rothwell, R.G., H00gakker, B., Thomson, J., Croudance, I.W. and Frenz, M. (2006): Turbidite emplacement on the southern Balearic Abyssal Plain (western Mediterranean Sea) during Marine Isotope Stages 1-3: an application of ITRAX XRF scanning of sediment cores to lithostratigraphic analysis. In: Rothwell, R.G. (ed.) New Techniques in Sediment Core Analysis: London, Geological Society Special Publications, 267: 79- 98.

Segele ZT and Lamb P. (2005): Characterization and variability of Kiremt rainy season over Ethiopia. Meteorology and Atmospheric Physics 89: 153–180.

Shaw, D.M., (1970): Trace element fractionation during anatexis. Geochim.Cosmochim.Acta, 34: 237-243.

Sparks, R.S.J., Huppert, H.E. and Wilson, C.J.N., (1990):Discussion of "'Evidence for long residence times ofrhyolitic magma in the Long Valley magmatic system:the isotopic record in precaldera lavas of Glass Mountain"by A.N. Halliday, G.A. Mahood, P. Holden, J.M.Metz, T,J. Dempster and J.P. Davidson. Earth Planet.Sci. Lett., 99:387-389

Tefera, M., Chernet, T., Workeneh H. (1996): Geological map of Ethiopia and Explanation to Geological map of Ethiopia. Scale 1:2,000,000. 2nd ed, Eth. Inst. Geol. Surv. Addis Ababa

Teklay, M., Kroner A., Metzger, K., Oberhansli, R. (1998): Geochemistry Pb-Pb single zircon ages and Nd-Sr isotope composition of Precambrian rocks from southern and eastern Ethiopia: implications for crustal evolution in East Africa. J. Afr. Earth Sci. 26:207-227

Tura, T., Deniel,C., Mazzuoli, R.(1999): Crustal controls in the genesis of Plio-Quaternay bimodal magmatism of the Main Ethiopian Rift (MER): geochemical and isotopic (Sr, Nd, Pb) evidences. Chemical Geology, 155, 201-231.

Weltje, J.G. and Tjallingii, R. (2008): Calibration of XRF core scanners for quantitative geochemical logging of sediment cores: Theory and application, Earth & Planetary Sci. Let., 274: 423- 438.

Wickham, S.M., (1987): The segregation and emplacement of granitic magmas. J. Geol. Soc. London, 144: 281-297.

Williams, H., (1941): Calderas and their origin. Bulletin of the Department of Geological Sciences, University of California 21, 239–346.

Yirgu, G., Dereje, A., Peccerillo, A., Barberio, M.R., Donati, C., Donato, P., (1999): Fluorine and chlorine distribution in the volcanic rocks from the Gedemsa volcano, Ethiopian Rift Valley. Acta Vulanologica 11(1): 169-176.

Yoshida, T., (2001): The evolution of arc magmatism in the NE Honshun arc, Japan. Tohoku Geophysical Journal 36, 131–249.

http://spaceflight1.nasa.gov/gallery/images/station/crew-16/html/iss016e019239.html: accessed on 30-oct-2012

ANNEXES

Annex 1: Major element concentrations for the Dendi volcanics

s.name	description	SiO2	Na2O	MgO	Al2O3	K2O	CaO	FeO	MnO	P2O5	TiO2	sum
Dendi 12	soil (profile)	51.73	0.44	1.70	27.14	1.12	1.04	15.05	0.30	0.26	1.22	100
Dendi 12	soil (profile)	51.85	0.47	1.65	27.07	1.13	1.03	15.02	0.30	0.26	1.22	100
Lat 01	soil (lateratization)	52.40	0.62	1.86	25.87	1.46	0.98	15.47	0.24	0.08	1.02	100
Lat 01	soil (lateratization)	52.34	0.64	1.84	25.85	1.47	0.99	15.52	0.24	0.09	1.02	100
Ob 01	Obsidian	73.56	6.29	0.00	8.78	4.04	0.18	6.67	0.22	0.00	0.27	100
Ob 01	Obsidian	73.45	6.39	0.00	8.76	4.05	0.19	6.68	0.22	0.00	0.27	100
Ob 02	Obsidian	73.21	6.11	0.00	8.76	3.95	0.17	7.27	0.23	0.00	0.28	100
Ob 02	obsidian	73.24	6.01	0.00	8.82	3.96	0.19	7.28	0.23	0.00	0.28	100
PM 00A	tuff	61.64	4.27	0.41	18.75	3.58	0.81	9.46	0.34	0.03	0.71	100
PM 00A	tuff	61.94	3.88	0.34	18.90	3.58	0.81	9.47	0.34	0.03	0.71	100
PM 00B	tephra	55.62	1.58	3.68	16.12	1.63	8.43	10.22	0.18	0.50	2.06	100
PM 00B	tephra	55.62	1.66	3.70	16.03	1.63	8.42	10.21	0.18	0.48	2.06	100
PM 02	rhyolite/trachyte	64.62	5.99	0.45	14.96	4.57	0.60	7.75	0.17	0.18	0.70	100
PM 02	rhyolite/trachyte	64.56	5.80	0.44	14.70	4.71	0.62	8.08	0.18	0.19	0.73	100
Pu 01	pumice/tuff	56.95	0.81	0.39	24.95	1.39	0.46	13.61	0.46	0.03	0.95	100
Pu 01	pumice/tuff	57.02	0.79	0.38	24.99	1.40	0.45	13.55	0.45	0.03	0.95	100
Tuff 02	tephra	54.44	1.55	5.40	14.29	1.88	9.13	10.62	0.22	0.49	1.98	100
Tuff 02	tephra	54.59	1.50	5.40	14.30	1.88	9.07	10.58	0.21	0.49	1.98	100
Tuff 02 inc	inclusion in z tephra	43.22	2.33	7.70	14.04	1.13	16.77	11.65	0.19	0.58	2.39	100
Tuff 02 inc	inclusion in z tephra	43.11	2.34	7.78	14.04	1.12	16.78	11.67	0.19	0.58	2.38	100
UKN 01	baking/oxidation	45.91	1.05	0.82	16.90	1.45	0.64	30.03	1.43	0.18	1.58	100
UKN 01	baking/oxidation	46.09	1.08	0.83	16.90	1.47	0.64	29.84	1.42	0.18	1.56	100
UKN 02	within the tephra	48.11	1.41	3.82	20.86	0.99	5.08	15.42	0.21	0.90	3.20	100
UKN 02	within the tephra	48.16	1.32	3.93	20.77	0.99	5.09	15.45	0.22	0.90	3.17	100
Rh 02	rhyolite/trachyte	61.21	4.93	0.18	17.60	4.07	0.67	10.44	0.28	0.03	0.59	100
Rh 02	rhyolite/trachyte	61.12	4.86	0.20	17.57	4.10	0.68	10.53	0.28	0.03	0.61	100
Rh 04	rhyolite/trachyte	72.55	3.89	0.02	11.38	3.58	0.20	7.85	0.23	0.00	0.30	100
Rh 04	rhyolite/trachyte	72.60	3.86	0.02	11.33	3.57	0.21	7.85	0.24	0.00	0.31	100
Rh 05	rhyolite/trachyte	67.75	5.72	0.08	12.66	4.60	0.33	8.06	0.23	0.03	0.54	100
Rh 05	rhyolite/trachyte	67.68	5.78	0.09	12.65	4.59	0.33	8.06	0.23	0.03	0.55	100
Rh 06	rhyolite/trachyte	67.52	6.49	0.03	12.86	4.32	0.22	7.73	0.29	0.02	0.53	100
Rh 06	rhyolite/trachyte	67.47	6.40	0.04	12.83	4.37	0.22	7.82	0.29	0.02	0.55	100

Annex 2: Trace element concentrations for the Dendi volcanics

s.name	description	S	Cl	V	Cr	Co	Ni	Cu	Zn	Ga	Ge	As	U
Dendi 12	soil (profile)	142	< 2.0	83.2	67.9	43.3	99.3	81.4	284.4	42.8	2.6	< 0.5	< 1.0
Dendi 12	soil (profile)	146.1	< 2.0	74.6	69.1	43.2	103	86.8	281.7	43.7	2	1.7	< 1.0
Lat 01	soil (lateratization)	93.5	< 2.0	87.2	73.1	26.1	85	62.6	286.7	47.8	2.8	0.9	< 1.0
Lat 01	soil (lateratization)	88	< 2.0	91.9	71.9	39.8	80.9	63.4	286.7	44.4	2.4	0.2	< 1.0
Ob 01	Obsidian	24.2	3699	5	5.1	< 10	8.5	129.3	353	37.3	<	< 0.5	12.2
Ob 01	Obsidian	23.7	3687	0.8	3.6	< 10	5.1	126.9	353.1	36.4	1	5.1	12.7
Ob 02	Obsidian	30.7	3839	6.8	14.8	< 10	7	144.1	370	37.5	<	< 0.5	12.3
Ob 02	obsidian	31.4	3832	4.4	14.7	14.9	9.8	143.5	367.5	38	0.9	4.3	12.1
PM 00A	tuff	11.1	24.9	3.2	16	27.2	5.8	459.6	248.3	37.7	<	< 0.5	1.1
PM 00A	tuff	9.1	12.4	2.6	15.4	25.2	5.8	444.3	248	36.6	1.1	< 0.5	< 1.0
PM 00B	tephra	57.9	274.8	165.9	86.2	32.8	50.3	113.9	108.2	21.2	<	< 0.5	2.4
PM 00B	tephra	61.1	273.9	189.6	90.8	27.2	52.2	123	109.1	23.9	<	< 0.5	2.9
PM 02	rhyolite/trachyte	118.2	40.3	7.3	15.8	283.7	24.2	2244	193.3	32.7	<	5.3	< 1.0
PM 02	rhyolite/trachyte	105.7	35.4	5.7	12.7	290.5	29.8	2195	192.9	29	<	4.1	< 1.0
Pu 01	pumice/tuff	12.4	< 2.0	20.4	6.4	43.2	27.7	10.8	240.2	51.5	2.4	< 0.5	< 1.0
Pu 01	pumice/tuff	17.3	0.4	20	5	42.6	29	10.7	237.5	51.1	0.7	< 0.5	1.9
Tuff 02	tephra	89.8	268.5	203.3	214.7	49	108.4	140.2	118.8	18.6	0.5	0.8	2.9
Tuff 02	tephra	87.1	273.6	197	211.5	44.7	112.3	141.4	117.4	19.2	<	< 0.5	1.2
Tuff 02 inc	inclusion in z tephra	176.4	299.7	273	333.1	41.7	143.1	96	78.2	15.8	<	< 0.5	0.9
Tuff 02 inc	inclusion in z tephra	180.4	300	281	324.5	51.6	145.7	97.2	77.8	17.3	<	< 0.5	1.9
UKN 01	baking/oxidation	< 2.0	< 2.0	177.2	61.9	69.2	81.9	43.9	267.4	30.5	1.2	3.6	< 2.1
UKN 01	baking/oxidation	< 2.0	< 2.0	195	58	56.7	74.8	45.6	265.6	33.2	1.5	2.9	1.5
UKN 02	within the tephra	27.3	236	146	162.3	52.1	96.3	49.4	103.8	20.9	0.5	< 0.5	1.7
UKN 02	within the tephra	32.1	235.4	163	178.1	57.8	102.6	48.8	104.6	20.6	<	< 0.5	2.7
Rh 02	rhyolite/trachyte	9.1	6.2	10.9	13.9	< 9.8	16.3	315.3	375.5	43.8	<	< 0.5	< 0.9
Rh 02	rhyolite/trachyte	< 2.7	4.4	2.5	6.4	19.9	11.4	304.8	372.5	42.1	1.8	0.1	< 0.9
Rh 04	rhyolite/trachyte	74.1	24.9	< 1.0	3	< 3.0	8.5	860.5	372.4	42.9	<	< 0.5	3.1
Rh 04	rhyolite/trachyte	72.4	23.9	< 1.0	6.1	17.6	18.5	809	365.9	38.3	<	< 0.5	1.6
Rh 05	rhyolite/trachyte	< 2.0	19.1	< 1.0	0.5	< 3.0	9.4	21.9	246.7	42.8	0.5	< 0.5	< 1.0
Rh 05	rhyolite/trachyte	< 2.0	8.5	< 1.0	2.6	< 9.7	5.2	20.3	248.2	42.1	0.4	< 0.5	< 1.0
Rh 06	rhyolite/trachyte	8	20.9	< 1.0	< 1.0	21.2	8.9	505.1	255.6	36.9	1.3	< 0.5	< 1.0
Rh 06	rhyolite/trachyte	11.5	18	< 1.0	0.7	22	3.6	498.7	255.1	34.7	1.9	< 0.5	< 1.0

Se	Br	Rb	Sr	Y	Zr	Nb	Mo	Ag	Cd	Sn	Sb	Te	I	Cs
< 0.5	25	109.6	52.9	232.7	998	141.6	< 1.0	< 2.0	1.1	7.2	< 3.0	< 3.0	3.3	6
< 0.5	23.6	109.6	53.3	232.5	995.4	144.7	< 1.0	< 2.0	3.4	10.9	1	< 3.0	< 3.0	< 4.0
< 0.5	29.2	115.3	52.3	130.2	1002	142.4	< 1.0	< 2.0	0.2	5.8	< 3.0	< 3.0	3.1	< 4.0
< 0.5	29.1	116.4	52.5	129.3	1001	145.6	< 1.0	6.7	< 2.0	4	< 3.0	< 3.0	4.5	< 4.0
< 0.5	10.6	300.7	3.2	190.2	2490	374	< 1.0	< 2.0	1.1	23.3	< 3.0	< 3.0	< 3.0	< 4.0
< 0.5	11.2	300.9	3.3	189.6	2487	369.4	< 1.0	< 2.0	2	21	< 3.0	< 3.0	< 3.0	11.1
< 0.5	12.3	301.5	4.3	193.2	2529	385.8	< 1.0	< 2.0	1.8	22.2	1.8	< 3.0	< 3.0	< 4.0
< 0.5	13.2	299.2	3.6	191.5	2529	392	< 1.0	7.2	< 2.0	19.2	< 3.0	< 3.0	< 3.0	< 4.0
< 0.5	< 0.5	82.4	42.9	102.7	1415	285.8	< 1.0	6	< 2.0	6.1	< 3.0	< 3.0	< 3.0	< 4.0
< 0.5	0.2	82.7	42.5	102	1401	290.4	< 1.0	5.7	0.6	6.3	< 3.0	< 3.0	< 3.0	< 4.0
< 0.5	2.7	50.9	480.8	41.1	396.1	56.9	< 1.0	< 2.0	0.5	2.1	< 3.0	< 3.0	< 3.0	7.4
< 0.5	2.2	51.5	481.8	40.4	399.8	59.9	< 1.0	< 2.0	0.3	1.3	< 3.0	< 3.0	< 3.0	< 4.0
4.6	< 0.5	103	14.5	71.5	724.3	169.3	< 1.0	5.7	1.8	2	< 3.0	< 3.0	< 3.0	< 4.0
< 0.5	< 0.5	103.9	14.9	72.6	729.5	172.1	< 1.0	3.2	< 2.0	4.5	< 3.0	< 3.0	< 3.0	< 4.0
< 0.5	1.1	89.2	27.5	130.2	2715	443.4	< 1.0	< 2.0	4.1	24.3	1.6	< 3.0	< 3.0	< 4.0
< 0.5	< 0.5	90.3	27.2	130	2738	442.7	< 1.0	12	< 2.0	18.8	< 3.0	< 3.0	< 3.0	7
< 0.5	1.9	59	420	39	385.4	62.3	< 1.0	< 2.0	< 2.0	< 3.0	< 3.0	< 3.0	< 3.0	< 4.0
< 0.5	1.4	58.1	415.6	38.9	383.4	61.7	0.4	< 2.0	0.5	< 3.0	< 3.0	< 3.0	< 3.0	< 4.0
< 0.5	1.2	26.8	586.6	22.1	182	33.3	< 1.0	< 2.0	< 2.0	< 3.0	< 3.0	< 3.0	< 3.0	< 4.0
< 0.5	1.5	26.4	586.8	22	182.5	33.4	< 1.0	< 2.0	3.8	< 3.0	< 3.0	< 3.0	< 3.0	< 4.0
< 0.5	0.5	104.4	48.6	113.1	870.5	136.7	9.2	< 2.0	0.5	1.5	< 3.0	< 3.0	< 3.0	< 4.0
< 0.5	0.6	106.3	49.6	112.6	869.2	133.3	12.2	< 2.0	1	3.3	< 3.0	< 3.0	< 3.0	< 4.0
< 0.5	2.1	26.6	341.2	35.9	325.6	52.3	< 1.0	< 2.0	< 2.0	< 3.0	< 3.0	< 3.0	< 3.0	< 4.0
< 0.5	2.3	26.7	343.6	35.1	323.4	57.3	< 1.0	< 2.0	< 2.0	1.7	< 3.0	< 3.0	< 3.0	< 4.0
< 0.5	< 0.5	143	16.3	67.8	1790	346.8	< 1.0	2.5	1.5	11.4	< 3.0	< 3.0	< 3.0	< 4.0
< 0.5	0.1	141.5	16.2	68.4	1800	354.3	< 1.0	7.2	0.1	10.5	< 3.0	< 3.0	< 3.0	< 4.0
< 0.5	< 0.5	260.5	5.3	42.6	2815	438.2	< 1.0	< 2.0	3.4	16.1	< 3.0	< 3.0	< 3.0	< 4.0
< 0.5	< 0.5	255	5.5	40.9	2754	421.4	< 1.0	3.2	< 2.0	18.4	5.3	< 3.0	< 3.0	< 4.0
< 0.5	< 0.5	129.8	5.9	53.3	1721	269.5	< 1.0	< 2.0	< 2.0	9.7	< 3.0	< 3.0	< 3.0	< 4.0
< 0.5	< 0.5	131	5.7	53.8	1749	277.3	< 1.0	5.5	5.3	12.6	0.1	< 3.0	< 3.0	< 4.0
< 0.5	< 0.5	146.2	4.3	113.7	1746	266.4	< 1.0	< 2.0	0.2	6.3	< 3.0	< 3.0	< 3.0	< 4.0
< 0.5	< 0.5	148	4.4	113.8	1748	269.3	< 1.0	7.8	1.1	8.5	< 3.0	< 3.0	10.2	< 4.0

Ba	La	Ce	Pr	Nd	Er	Yb	Hf	Ta	W	Hg	Tl	Pb	Bi	Th
194	279	222	132	310	26	14.9	16.5	< 1.0	< 1.0	0.1	< 1.0	32.4	< 1.0	27.3
181	228	241	133	298	27	11	13	1.9	< 1.0	1.4	0.4	30.9	< 1.0	25.1
165	88	268	90.8	155.1	36	< 3.4	2.4	< 1.0	< 1.0	1.9	0.2	31.2	< 1.0	24.8
202	190	279	78.3	169.2	11	< 3.4	14.1	< 1.0	< 1.0	1.7	< 1.0	31	< 1.0	25
< 2.0	309	583	72.6	354.2	42	7.5	24.3	11.7	86.6	2.9	0.4	62.8	< 1.0	59.7
< 2.0	122	400	84.7	352.1	35	11.5	33.2	17.6	88.3	0.8	0.5	57.6	< 1.0	59.6
< 2.0	364	452	85.1	370.6	48	13.8	18.9	12.8	159	< 1.0	0.3	66.1	< 1.0	62.9
11.3	385	698	83.9	367.9	37	6.7	28.7	12.1	161.9	< 1.0	0.7	60.6	< 1.0	62.4
150	222	331	82.8	201.2	16	5.7	8.9	17.8	26.5	2.2	0.4	39.1	< 1.0	30.9
143	293	546	79.7	199.4	15	3.1	11.6	17.6	31.8	< 1.0	0.7	36.1	< 1.0	31.7
461	68	129	< 2.0	133.6	14	< 2.0	< 1.0	< 1.0	15.1	1.6	0.5	13.6	< 1.0	11.9
402	22.7	10.4	< 2.0	102.8	15	< 2.0	< 1.0	< 1.0	9.9	1.9	0.3	14.2	< 1.0	11.9
42	100	< 2.0	5.4	142.5	40	< 2.0	< 1.0	< 1.0	4540	< 1.0	2	39.2	< 1.0	21.8
< 2.0	171	10.3	12	144.1	30	< 2.0	< 1.0	< 1.0	4601	< 1.0	2.9	39	< 1.0	22
459	186	562	82	194.4	17	8.2	47.2	21.3	< 1.0	< 1.0	0.9	67.2	< 1.0	70.5
456	136	630	90.5	183.8	13	10.1	49.9	22.6	< 1.0	2.5	1.2	68.4	< 1.0	72.4
300	< 2.0	139	< 2.0	160.3	< 5.1	< 2.0	6.3	< 1.0	13.7	0.1	0.2	11.4	< 1.0	12.2
293	40	69	< 2.0	166.8	< 5.1	< 2.0	9.8	< 1.0	14.9	0.3	0.7	12.3	< 1.0	12.5
273	41	< 2.0	0.6	72.1	< 5.1	< 2.0	< 2.6	< 1.0	13.3	< 1.0	0.6	6.8	< 1.0	6.8
257	39	< 2.0	10.8	67.8	< 5.1	< 2.0	3.9	< 1.0	14.8	1	< 1.0	6.5	< 1.0	6.3
890	< 2.0	528	83.1	83.7	15	< 2.0	5.4	< 1.0	< 1.0	1.2	1.4	37.1	< 1.0	30
911	< 2.0	308	69.4	104.6	19	< 2.0	3.7	< 1.0	< 1.0	0.9	< 1.0	37.6	< 1.0	28.2
521	41	113	10.5	51.5	< 5.1	< 2.0	5.7	< 1.0	2.3	0.2	< 1.0	10.2	< 1.0	10.2
506	< 2.0	< 2.0	< 2.0	98.3	< 5.1	< 2.0	4.1	< 1.0	3.8	1.5	0.7	12.4	< 1.0	12.9
79	222	< 2.0	41	298	42	< 2.0	< 1.0	6.5	15.3	1.7	< 1.0	45	< 1.0	41.1
91	362	157	72	362.1	21	< 3.1	14.9	13	14.6	< 1.0	0.3	43.1	< 1.0	39.3
< 2.0	< 2.0	490	26.7	< 2.0	49	< 2.0	< 1.0	29.2	188.4	< 1.0	0.5	64.5	< 1.0	73.1
< 2.0	< 2.0	272	23.4	< 2.0	< 5.1	< 2.0	48.6	17.6	204.9	< 1.0	0.4	58.6	< 1.0	67.9
< 2.0	92	161	58.7	219.1	35	< 2.0	7.6	< 1.0	< 1.0	2.7	< 1.0	28.3	< 1.0	33.7
< 2.0	141	258	45.4	218.1	30	< 2.0	10.4	< 1.0	< 1.0	0.9	< 1.0	28.3	< 1.0	32.5
52	213	202	88.7	260.9	17	< 2.0	17.2	6.6	5.9	0.2	< 1.0	41.5	< 1.0	30.1
< 2.0	264	244	97.7	373.6	20	9	16	14.5	< 1.0	< 1.0	0.5	42.6	< 1.0	31.4

Declaration

This thesis is my original work and has not been presented for a degree in any other university, and that all sources of material used for the thesis have been duly acknowledged.

_____

Bahru Zinaye

College of Natural Sciences
School of Earth Sciences
Petrology stream

Approved by: _____

Dr. Asfawossen Asrat (Advisor)